LIGAND AND MODULATOR BINDING IN THE SKELETAL MUSCLE RYANODINE RECEPTOR

by

PAOLO ANTONIO LOBO

B.Sc., The University of British Columbia, 2010

A THESIS SUBMITTED IN PARTIAL FULFILLMENT OF THE REQUIREMENTS FOR THE DEGREE OF

MASTER OF SCIENCE

in

THE FACULTY OF GRADUATE STUDIES

(Biochemistry)

THE UNIVERSITY OF BRITISH COLUMBIA
(Vancouver)

December 2012

Abstract

Calcium (Ca^{2+}) is required in the cytoplasm as a potent second messenger for a variety of vital physiological events in the cell. Its supply to the cytoplasm can either be from extracellular sources, or from intracellular sarcoplasmic reticulum stores, predominantly through the ryanodine receptors (RyRs). The latter are large, ~2 MDa homotetrameric channels that sense initial Ca^{2+} blips due to voltage-gated calcium channel influx and respond by opening to result in physiologically significant concentration spikes. This action is known as calcium induced calcium release and is the major process by which an excitation signal is translated to a physical, muscular contraction. Cytoplasmic Ca^{2+} concentrations have to be very well regulated and must return to resting levels for subsequent contractions to occur. The importance of this with regard to the RyR can be seen in two different ways: Firstly, its large cytoplasmic bulk, a huge docking site for modulators, emphasizes the necessity for regulation, and secondly, mutations in the RyR can cause severe genetic diseases as a result of Ca^{2+} mishandling. Presented here, are preliminary structural and binding studies for several different RyR regulators, both physiological and pharmacological.

Skeletal muscle RyR (RyR1) 1-617 that contains the drug dantrolene's supposed binding site was crystallized and its structure determined. Isothermal Titration Calorimetry (ITC) and co-crystallization attempts have not confirmed the binding of dantrolene. The structure does however shed light on the physical involvement of phosphatases as modulators of the channel.

Caffeine binding was detected successfully by ITC and attributed to RyR1 217-536. A co-crystal structure yielded a binding site in the construct that could not be knocked out by site-directed mutagenesis according to ITC.

Three types of modulators were shown to bind RyR1 4071-4128 by ITC. 1) Ca^{2+}, which affects the channel both positively and negatively, 2) magnesium ions, which inhibit the channel, and 3) an intrinsic ligand in RyR1: residues 4295-4325; a peptide that shows affinity for Calmodulin, yet another modulator of RyR.

The results provide insight into allosteric reactions as a result of RyR ligand or modulator binding.

Preface

Ching-Chieh Tung optimized the purification for skeletal ryanodine receptor (RyR1) residues 1-536 and RyR1 217-536. In addition, for the latter construct, he performed the initial Isothermal Titration Calorimetry (ITC) experiments in Chapter 3.2 and discovered the caffeine co-crystallization condition discussed in Chapter 3.2.1.

Kelvin Lau carried out the ITC experiments on RyR1 1-617 with dantrolene and azumolene (Chapter 3.1.3). He is also responsible for all Mass Spectrometry discussed in this thesis.

Lynn Kimlicka maintains a human mutation database for both RyR1 and the cardiac isoform. The database was referred to several times in this discussion (Chapters 1.3, 3.1.1, 4.1.3, and 4.3.2).

Ulrika Brath completed the NMR experiments on RyR1 4071-4138 to detect calcium ion binding to RyR1 4071-4138 (Chapter 3.3.1).

Table of Contents

List of Tables

NOTE: In tables in which residues have been numbered, the numbering used is denoted at the end of each legend. In general, tables with disease mutations are numbered according to RyR1 or RyR2 *Homo sapiens,* and all others adopt the RyR1 *Oryctolagus cuniculus* numbering.

List of Figures

NOTE: In figures in which residues have been numbered, the numbering used is denoted at the end of each legend. In general, figures with labelled disease mutations are numbered according to RyR1 or RyR2 *Homo sapiens,* and all others adopt the RyR1 *Oryctolagus cuniculus* numbering.

List of Abbreviations

(2/3)D	(Two/three) dimensional
(Apo-/Ca^{2+}-)CaM	(Calcium-free/Calcium-bound) Calmodulin
(d)NTP	(Deoxyribo) Nucleotide triphospate
(n/μ/m)M or l	(nano/micro/milli-) molar or litre
ΔG	Gibb's free energy
ΔH	Change in enthalpy
ΔS	Change in entropy
ACh	Acetylcholine
AD#	Rank number # AutoDock solution
ANSA	8-anilino-1-naphthalenesulfonic acid ammonium
APS	Advanced Photon Source
ARVD2	Arrhythmogenic Right Ventricular Dysplasia Type 2
ATP	Adenosine triphosphate
Ca^{2+}	Calcium ions
CaMBD	Calmodulin Binding Domain
CaMKII	Ca^{2+}/CaM-dependent kinase II
Ca_V	Voltage-Gated Calcium Channel
CCD	Central Core Disease
CICR	Calcium Induced Calcium Release
CLS	Canadian Lightsource
CPVT	Catecholaminergic Polymorphic Ventricular Tachycardia
CSQ	Calsequestrin
CV	Column volume
D#	Rank number # DOCK solution
DAG	1,2-diacylglycerol
DNA	Deoxyribonucleic acid
E-C	Excitation-Contraction
E. coli	*Escherichia coli*

EC_{50}	Half maximal effective concentration
EDTA	Ethylenediaminetetraacetic acid
EM	Electron Microscopy
EMDB	Electron Microscopy Data Bank
ER	Endoplasmic Reticulum
FRET	Förster Resonance Energy Transfer
GFP	Green Fluorescent Protein
GST	Glutathione S-Transferase
GUI	Graphical User Interface
HEPES	4-(2-hydroxyethyl)-1-piperazineethanesulfonic acid
IP_3	Inositol 1,4,5-triphosphate
IP_3R[#](A,B,C)	IP3 receptor [isoform 1, 2 or 3](domains A, B and C)
IPTG	Isopropyl-β-D-thiogalactoside
ITC	Isothermal Titration Calorimetry
K^+	Potassium ions
kDa	Kilodalton
LIC	Ligation Independent Cloning
LZ (1,2, or 3)	Leucine/Isoleucine/Valine zipper (1, 2 or 3)
MBP	Maltose Binding Protein
MDa	Megadalton
MH	Malignant Hyperthermia
Na^+	Sodium ions
Na_V	Voltage-Gated Sodium Channel
NCX	Sodium-Calcium Exchanger
OD_{600}	Optical density at 600 nm
P or S/N	Pellet or Supernatant
PAC	Phosphatase Access Channel
PCR	Polymerase Chain Reaction
PIP_2	Phosphatidylinositol 4,5-triphosphate
RyR[#](A,B,C)	Ryanodine Receptor [isoform 1, 2 or 3] (domains A, B and C)
RyR1ABC	RyR1 1-532 (structure, the construct is longer)

RyR1ABCd	RyR1 1-577 (structure, the construct is longer)
SDS PAGE	Sodium dodecyl sulphate polyacrylamide gel electrophoresis
SERCA	Sarcoplasmic/Endoplasmic Reticulum Calcium ATPase
SOICR	Store overload-induced Ca^{2+} release
SR	Sarcoplasmic Reticulum
SSRL	Stanford Synchrotron Radiation Lightsource
TEV	Tobacco Etch Virus
Tris	tris(hydroxymethyl)aminomethane
βME	β-mercaptoethanol

Acknowledgements

I would like to thank Dr. Filip Van Petegem for several years of patient teaching and leading in his laboratory. All of the Van Petegem lab members have been a pleasure to work with. Special appreciation goes to Dr. Michael Yuchi, Kelvin Lau, Jett (C-C.) Tung and Lynn Kimlicka for their valuable input and discussions. From neighbouring labs, Sarah Chow and Maen Sarhan attended lab meetings have always been keen to provide useful insight.

I am very grateful for the PyMOL Molecular Graphics System (Version 1.5.0.4 Schrödinger, LLC), which was used to create all structural figures and in addition carry out some manual docking (Figure 34).

With regard to crystallographic data collection I would like to thank all of the staff at APS 23-ID-D-GM/CA and CLS 08-ID1, as well as Gunnar Olovsson and Anson Chan at UBC homesources.

Finally, thank you to my committee members Dr. Joerg Gsponer and Dr. Calvin Yip for their input and general approachability.

Dedication

To my parents in Kenya, who from thousands of miles away, have lovingly provided the support I have needed to succeed. To my sister Ariana, who inspires me with her confidence and her independence. And in Canada, to Julio and Debbie, the strongest pillars in my life. I strive to make you all proud!

1 Introduction

1.1 Calcium Release and Regulation

Extracellular signals such as membrane depolarization or adrenaline binding have to be relayed from receptors at the cell surface to intracellular target molecules. To do this second messengers are required, which act via signal transduction and amplify the signal. One of the most potent second messengers is calcium (Ca^{2+}), which is required for a large variety of physiological functions. As a result, the demand for Ca^{2+} in the cell can be substantial and although extracellular concentrations are high, the main supply of the ions for these physiological functions are intracellular stores: namely the Sarcoplasmic and Endoplasmic Reticula (SR and ER). Here the main sentinels of these stores are Ryanodine Receptors (RyR), which are activated by, and conduct Ca^{2+} (Endo et al. 1970, Fabiato, 1983).

RyRs are large homotetrameric ion channels located in the SR/ER membranes of the cell. With each monomer measuring ~565 kDa, a complete structure exceeds 2.2 MDa. Despite its main function in controlling calcium release into the cell, it gets its name from the observed high affinity binding of the plant toxin Ryanodine, which locks the channel in a subconductance state at lower (nanomolar) concentrations and completely blocks it at higher (micromolar) concentrations (Meissner 1986). There are three identified isoforms in mammalian organisms: RyR1, which is predominantly expressed in skeletal muscle (Takeshima 1989), RyR2, mostly in cardiac muscle (Otsu et al. 1990), and the more ubiquitously expressed RyR3, which was first discovered in the brain (Hakamata et al. 1992). Although they do generally follow the this trend in expression, all three types are found in other tissues as well, and are close to 70% identical with only a few divergent regions (Sorrentino and Volpe 1993). Here, the focus will be predominantly on RyR1.

In proof of the reliance on intracellular stores, it has been demonstrated that an extracellular influx of Ca^{2+} through voltage-gated Ca^{2+} channels (Ca_Vs) is not necessary for contraction in skeletal muscle. Both twitches (Armstrong et al. 1972) and sarcoplasmic Ca^{2+} release (Miledi et al. 1984) can still occur in muscle cells exposed to Ca^{2+}-free solutions. Instead there is thought to be a direct physical link between RyR1 and L-type Ca_V ($Ca_V1.1$) (Rios and Brum 1987, Block et al. 1988, Tanabe et al. 1988, Tanabe et al. 1990). Here Ca_Vs are recruited as voltage sensors and in turn cause Ca^{2+} release through RyRs. This initial spike in concentration would then trigger further Ca^{2+} release via neighbouring RyRs that are physiologically clustered, corner-to-corner, in 'chessboard' arrays (Saito et al. 1984, Ferguson et al. 1988, Saito et al. 1988). Evidently then, Ca^{2+}-binding is sufficient, but not necessary to activate RyR1.

1.1.1 Calcium Induced Calcium Release and E-C Coupling

As stated, RyR is both triggered by and conducts Ca^{2+} in a process known as Calcium Induced Calcium Release (CICR) (Endo et al. 1970, Fabiato, 1983). This seems to set up a positive feedback loop that would completely deplete the SR of Ca^{2+}, but Meissner et al. (1986) have shown that higher concentrations of Ca^{2+} decrease the open probability of RyR. This means that there must be at least two binding sites for Ca^{2+} in the RyR, one for activation and one for inhibition. In addition, they showed that another divalent cation, Mg^{2+}, binds and inhibits the channel by two proposed mechanisms: direct competition with Ca^{2+} at the activation site, or by binding to a low affinity inhibitory site that can accept either Ca^{2+} or Mg^{2+}. Consequently RyR is activated by micromolar (μM) concentrations of Ca^{2+} and inhibited by millimolar (mM) concentrations of Ca^{2+} or Mg^{2+} (Laver et al. 1997). The subsequent amplification of the Ca^{2+} signal upon activation is a necessary requirement for all muscle contraction.

60 years ago, Sandow (1952) described the relationship between an excitation signal and the consequent activation of muscular contraction. It occurs in a process now known as excitation-contraction (E-C) coupling, which heavily relies on Ca^{2+}. Already mentioned, it was later understood that this process involved a physical $Ca_V1.1$-RyR1 link near transverse tubules (T-tubules), invaginations in the sarcolemma or plasma membrane of muscle cells, and the terminal cisternae of SR (Rios and Brum 1987, Block et al. 1988, Tanabe et al. 1988, Tanabe et al. 1990).

According to the sliding filament model of muscle contraction (Huxley and Niedergerke, 1954, Huxley and Hanson, 1954), shortening of sarcomeres occurs by interactions between thin actin and thick myosin filaments. Melzer et al. (1995) describe the role of Ca^{2+} in binding to troponin C, located on actin filaments. This causes the troponin complex to pull tropomyosin away from the myosin binding sites on these actin filaments. Once free to bind, myosin heads can attach and cause sarcomere shortening by pulling actin filaments and induce contraction of the muscle cell as a whole. Following this, binding of adenosine triphosphate (ATP) to myosin returns the heads to their resting state, primed for re-attachment to actin and thereby causing further sarcomere contraction as long as Ca^{2+} is still present. Sarcoplasmic/Endoplasmic Reticulum Calcium ATPases (SERCAs) must then pump Ca^{2+} back into the SR to re-establish normal concentrations (Carafoli 1987, MacLennan et al. 2002, Dulhunty, 1992, Stephenson et al. 1998). This costs a lot of energy provided by ATP hydrolysis. Other Ca^{2+} concentration restorers include Plasma Membrane Ca^{2+} ATPases, which work in a similar way but pump ions out of the cell, and Na^+/Ca^{2+} exchangers (NCX), which swap three sodium ions (Na^+) into the cell for every Ca^{2+} that they take out.

Ca^{2+} is also involved prior to T-Tubule excitation by an action potential, at the neuromuscular junction. At the presynaptic neuron terminal, Ca^{2+} causes vesicles filled with acetylcholine (ACh) to fuse with the cell membrane and release the neurotransmitter into the synaptic cleft. Receptors on the postsynaptic membrane recognize ACh and open to allow the influx of sodium ions (Na^+)); this initiates the action potential. Being a vital part of both the excitation and contraction, Ca^{2+} can be considered to be the major force behind E-C coupling. Its cytoplasmic concentration

in the cell is controlled by a variety of Ca^{2+}-conductors, most importantly RyR with SERCA, NCX and PMCA (Figure 1).

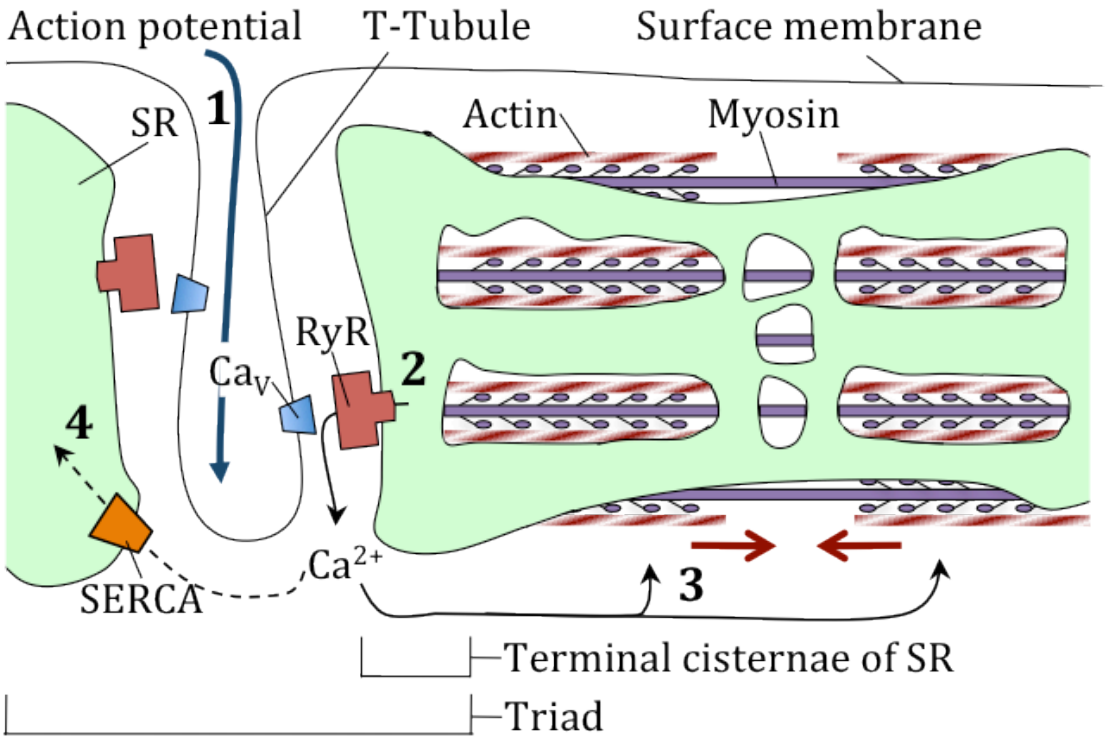

FIGURE 1. **RyR, Ca^{2+} and muscle contraction.** 1) An action potential reaches the T-Tubules. 2) RyR recruits Ca_V as a voltage sensor and releases Ca^{2+} from SR. Nearby RyRs respond by CICR to amplify the Ca^{2+} signal (not shown). 3) Myoplasmic Ca^{2+} causes sliding of actin filaments in the direction of the red arrows. 4) SERCA pumps use ATP to return Ca^{2+} to the SR.

1.1.2 Calmodulin and Calmodulin Binding Domains

The large size of the RyR, with ~4/5ths of its volume in the cytoplasm, provides a huge area for different, smaller proteins to bind. The channels even exhibit corner-to-corner interactions with themselves, resulting in a two-dimensional (2D) RyR 'checkerboard' (Saito et al. 1984, Ferguson et al. 1988, Saito et al. 1988). This

emphasizes the essential requirement for Ca^{2+} concentrations to be well regulated. Understandably then, a plethora of protein chess pieces have been shown to bind these RyR chessboard arrangements. The immunosuppressant FK-506 binding proteins (FKBP12 and 12.6) attach and stabilize the channel in the closed state (Brilliantes et al. 1994, Ma et al. 1995, Timerman et al. 1996). Oligomers of calsequestrin (CSQ), which can hold over 60 ions per monomer (Park et al. 2004) are responsible for the high concentration of Ca^{2+} in SR. CSQ-bound Ca^{2+} is released in communication with RyR1, but whether it activates or inhibits the channel depends on which CSQ isoform is involved (Beard et al. 2004). Other examples include the SR anchoring proteins triadin and junctin (Beard et al. 2009) and more relevant for this discussion, calmodulin (CaM) (Chen and MacLennan, 1994, Yang et al. 1994, Tripathy et al. 1995). Together, and among many others, they form the core of a RyR macrocomplex that defines the release of Ca^{2+}.

Using lipid bilayer studies, CaM in fact was the first protein to be identified as an interacting partner with single RyR channels (Smith et al. 1989). It binds stoichiometrically, with four CaMs binding one tetramer (Tripathy et al. 1995, Moore et al. 1999, Balshaw et al. 2001) even though there are thought to be multiple Calmodulin Binding Domains (CaMBDs) (Zorzatto et al. 1990, Menegazzi et al. 1994, Chen and MacLennan 1995). Cryo-electron Microscopy (cryo-EM) and Förster Resonance Energy Transfer (FRET) experiments further confirmed the 4:1 stoichiometry (Wagenknecht et al. 1994; Wagenknecht et al. 1997; Samsó and Wagenknecht 2002). It is clear that the binding of CaM to RyR is far from simple and is yet to be fully understood. Keeping with the theme, CaM was also part of the first RyR crystal structure as part of a complex with residues 3614-3643 in RyR1 (Maximciuc et al. 2006). The structure unearthed an unusual, novel mode of binding, even for the promiscuous CaM. For the first time CaM was seen to bind two anchoring hydrophobic residues located 17 residues apart (inclusive) along the primary structure of RyR1 in an antiparallel organization.

To further complicate matters, CaM contains two structurally similar lobes, but functionally quite different, each of which can bind Ca^{2+} and change conformation. Their Ca^{2+}-dependent structural changes can have dramatic effects on CaM's

regulatory effect on RyR. Ca^{2+}-free CaM (Apo-CaM) for example has been shown to partially activate RyR1, whereas Ca^{2+}-bound CaM (Ca^{2+}-CaM) has an inhibitory effect on Ca^{2+} release from the SR (Ikemoto et al. 1995, Buratti et al. 1995, Tripathy et al. 1995, Rodney et al. 2000). In addition, Samsó and Wagenknecht (2002) showed by cryo-EM that the centres of bound Ca^{2+}-CaM and Apo-CaM lie ~33 Å apart, and visualized sites that were definitely distinct, but sterically overlapping. This implied that both binding events cannot not occur at the same time and instead that some kind of lobe shifting must occur. This evidence then suggests that CaM must play a role in sensing high Ca^{2+} concentrations achieved after signal amplification by RyR1, and in turn shift to cause the channel to close.

From available crystal structures, we see that its ability to bind Ca^{2+} is due to four EF-hands, two on both lobes, each of which complex a single Ca^{2+} ion resulting in four Ca^{2+} per CaM (Figure 2) (Babu et al. 1988, Chattopadhyaya et al. 1992, Wilson and Brunger 2000). EF-hand domains, consisting of a helix-loop-helix motif, are commonly associated with divalent ions such as Ca^{2+} or Mg^{2+}. S100A, another EF-hand protein, also binds Ca^{2+}, and in addition, can also bind the RyR1 3614-3643 peptide (Wright et al. 2008), suggesting that different EF-hand containing proteins can compete for the same binding sites. Given that RyR itself binds Ca^{2+}, it is reasonable to assume it may contain its own EF-hand domains that could presumably bind CaMBDs as intrinsic ligands. In three-dimensional (3D) space, RyR1 EF-hands could be located close to CaMBDs in the full-length channel. This would put their local, physiological concentrations beyond competitive capabilities. It is therefore possible that *in vivo*, neither CaM, nor S100A bind the RyR1 3614-3643 peptide.

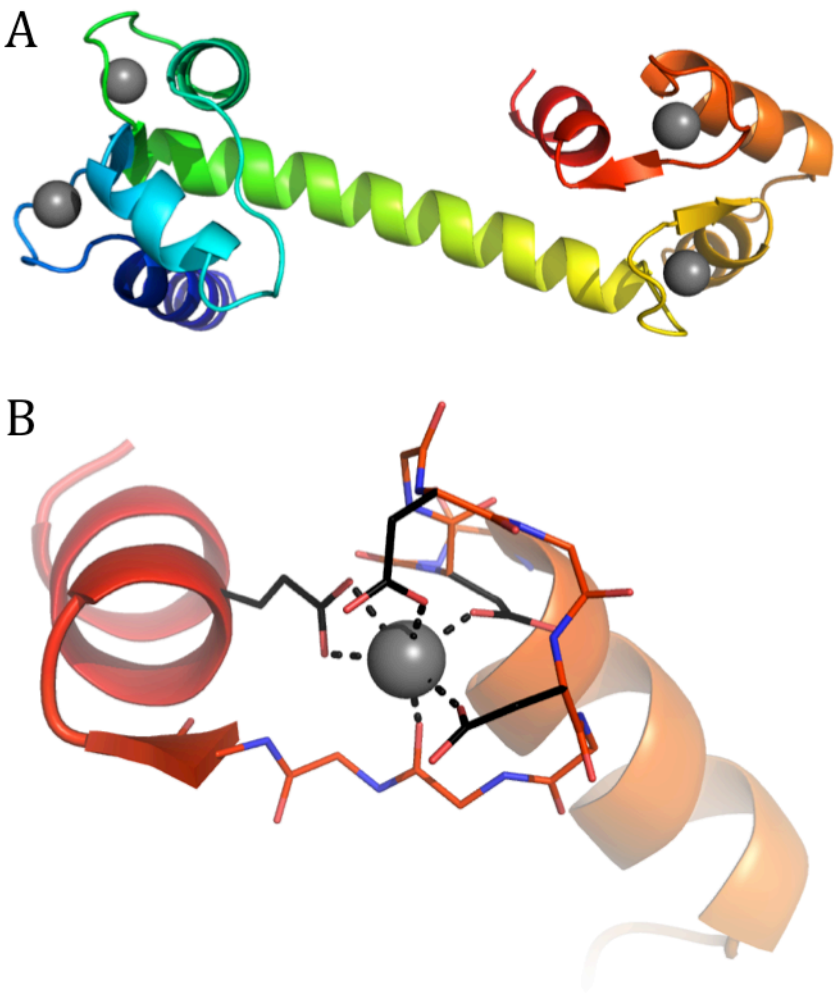

FIGURE 2. **Calmodulin and EF-hands.** (**A**) CaM (PDB 1CLL, Chattopadhyaya et al. 1992) is coloured in a spectrum from its N- (*blue*) to C- (*red*) terminus. Ca^{2+} ions are shown as grey spheres. (**B**) A zoomed in view on the C-terminal helix-loop-helix EF-hand. Highlighted in black are the side-chains of some negatively charged residues involved in binding Ca^{2+}.

Xiong et al. (2006) added serious strength to this argument with their studies on RyR1 4064-4210. Firstly, they used circular dichroism to show that it has α-helical propensity, hinting to the possibility of an EF-hand. Using equilibrium dialysis with $^{45}Ca^{2+}$, they then determined that two Ca^{2+} ions bind the peptide co-operatively with an affinity of ~60 μM and a Hill coefficient of ~1.6. Furthermore, the fluorescent probe 8-anilino-1-naphthalenesulfonic acid ammonium (ANSA), which changes its

fluorescent properties in the company of hydrophobic residues, was used to show binding to a CaMBD binding site in RyR1 3614-3643. Here the affinity was Ca^{2+}-dependent, ranging from ~800 nM in apo conditions to ~180 nM in the presence of 5 mM Ca^{2+}. Lastly, they demonstrated that Histidine-tagged RyR1 4064-4210 pulled down $Ca_V1.1$. Their results hint towards the identification of single RyR1 peptide as a Ca^{2+}-binding site, a CaMBD binding site and the physical link between RyR1 and Ca_V. Care must be taken though, not to interpret too much from experiments on isolated peptides that physiologically could be inaccessible to any or all of the above. Removing such peptides from their folded domains exposes hydrophobic residues that could result in a general 'stickiness'. Interestingly, following lysis, their construct was found almost exclusively in inclusion bodies and had to be refolded in purification.

In addition, as discussed in Chapter 1.3, hundreds of mutations in RyR1 can cause Malignant Hyperthermia (MH). Volatile anaesthetics, for example halothane, trigger the disorder and presumably bind RyR1. Given that CaM has been shown to bind halothane (Streiff et al. 2004), and NMR structures have visualized both the N- and C-lobe bound in solution (PDB 2KUG and 2KUH, Juranic et al. unpublished), it yet again hints that there may not be any discrimination between EF-hands in binding. It would therefore not be too far-fetched to conclude that RyR1 4064-4210 may also interact with the anaesthetic. At present, a binding site for anaesthetics in RyR1 is yet to be established.

1.2 Structural Information

1.2.1 Cryo-Electron Microscopy

Historically, structural studies on RyRs have been dominated by electron microscopy (EM) with their first documented observation in thin-layer or negative stain EM images, as simple protrusions from SR, occurring half a century ago (Revel 1962). With the progress in cryo-EM technology, structures of the full RyR1 channel both in a closed and open state have been made available in the Electron Microscopy Data Bank (EMDB) at resolutions up to ~10 Å determined by fourier shell correlation at cut-offs of either 0.5 or 0.143 (Serysheva et al. 2005, Ludtke et al. 2005, Samsó et al. 2005, Samsó et al. 2009). These reconstructions have extensively been studied and as a result, several globular domains within the channel have been identified. The different cytoplasmic domains or 'subregions' have been assigned arbitrary numbers (Figure 3) (Serysheva et al. 2008). Previously lower resolution images had only allowed larger, more general regions to be named: the 'central rim', 'handles' and 'clamps' (Serysheva et al. 1995).

Comparison between the open and closed states (Samsó et al. 2009) of the channel has also shed some light on the allosteric properties of RyRs (Figure 4). Besides the obvious widening of the central rim in opening, there are clear movements in the handles and clamps, some of which occur more than 100 Å away from the pore. It is then useful to portray the channel as a set of globular gears that can communicate in both directions; opening of the pore can cause structural rearrangements near the periphery of receptor, and conversely, binding of a ligand in a clamp could cause opening or closing at the pore.

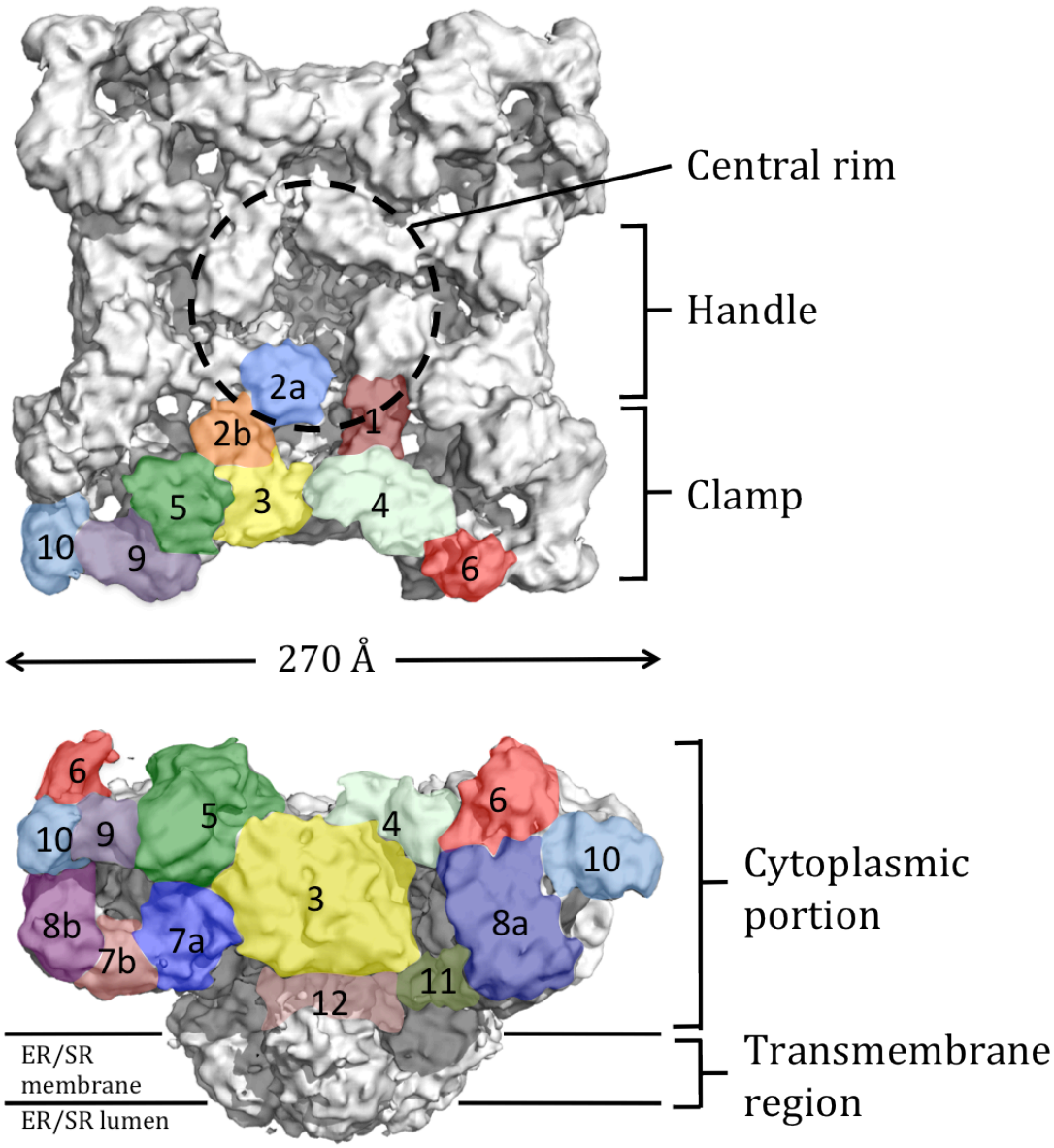

FIGURE 3. **A 9.6 Å cryo-EM reconstruction of RyR1.** Top (*above*) and side (*below*) views of the EMDB 1275 map (Ludtke et al. 2005). Subregions are coloured and numbered (Serysheva et al. 2008). The central rim, a handle and a clamp are also labelled for clarity. (Serysheva et al. 1995). 4/5ths of the channel resides in the cytoplasmic portion of the 'mushroom'-like receptor. As labelled the diameter of the channel measures ~270 Å.

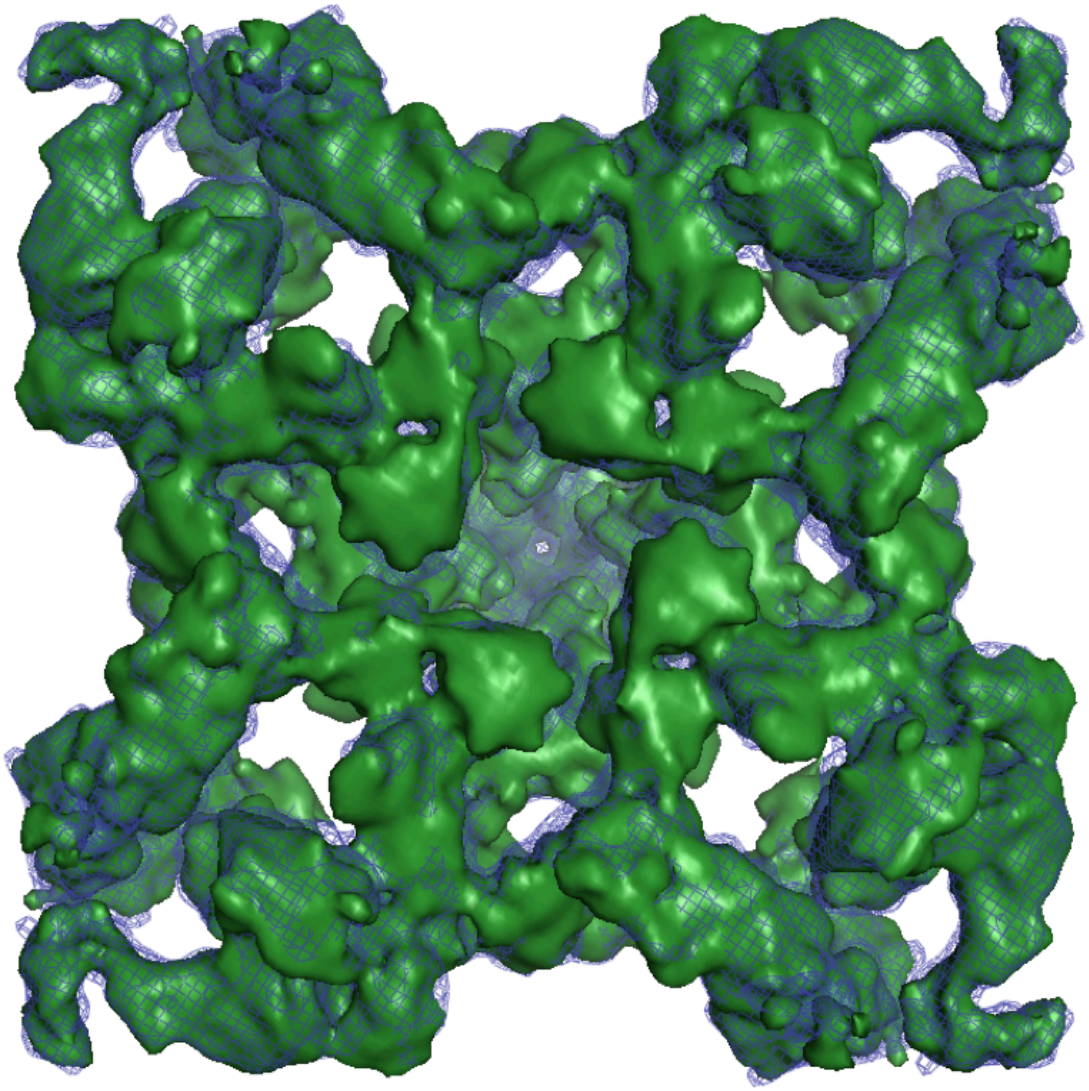

FIGURE 4. **Closed vs open states of RyR.** Comparison of the closed and open cryo-EM reconstructions of RyR1 from Samsó et al. 2009. The closed state (EMDB 1606) is shown as a blue mesh on top of the green surface of the open state (EMDB 1607). The cut-off selection for both maps are set to the same value and chosen so that a clear channel is observed through the open state.

High quality cryo-EM maps have been very useful in looking at the complete ~2.2 MDa structure but pin-pointing the location of individual domains from the primary sequence, has proven to be a little more challenging. To overcome this

barrier, several insertion studies and difference maps with larger protein ligands or antibodies were carried out. Kimlicka and Van Petegem (2011) have reviewed these studies and mapped out each position onto a single reconstruction of RyR1. In each case though, they stress that the exact location of the ligand, insertion or antibody may carry a significant degree of uncertainty due to a combination of factors. Besides the resolution of the EM map, the length of linkers and the size of the insert or ligand must also be taken into account. Longer linkers could result in global differences very far from the true location, and smaller ligands would be difficult to distinguish from noise. Still, the results have proven to be very helpful. The supposed binding location of the drug dantrolene (see Chapter 1.4.1) for example, which resides in RyR1 residues 590-609 (Paul-Pletzer et al. 2002, 2005), could be attributed to subregion 9 due to cryo-EM images of RyR2 in which GFP was inserted at tyrosine 846 (Wang et al. 2011). However, the insertion point is over 200 residues away from the presumed binding site and the observed mass difference could therefore be far from the point of interest. But assuming an average protein domain to be ~200 residues, they could argue this would put the GFP no more than single subregion away. Additionally, an insertion into arginine 626, which could not be expressed well enough for cryo-EM, but was usable for further FRET studies, confirmed that the distant side (from the pore) of subregion 9 might indeed house the dantrolene binding site of RyRs.

1.2.2 Crystallographic Insight

Cryo-EM is without doubt a powerful tool in determining the general structure of RyRs, but falls short when it comes to understanding some of the molecular details involved. The search for the subregion that belonged to the N-terminus in the full-length channel highlighted the limitations of using difference imaging in cryo-EM to unambiguously locate domains. Glutathione S-Transferase (GST) fused at the N-terminus of RyR3 (Liu et al. 2001), a RyR1 416-434 sequence specific antibody (Baker et al. 2002) and a GFP insertion at serine 437 (Wang et al. 2007) all showed major

difference peaks in the clamp regions of the RyR. This corroborating evidence led to a common belief in the field that the N-terminus was localized between subregions 5 and 9. It was not until the crystal structure of the first 3 domains of RyR1 in residues 1-532 (RyR1ABC) was solved that it became clear where the N-terminus really is (Tung et al. 2010). Here we performed extensive docking of RyR1ABC using Laplacian filters, an application that has been shown to be vital in the docking of relatively small crystal structures into large EM maps (Wriggers and Chacón, 2001, Chacón and Wriggers, 2002). In the study we demonstrated that RyR1ABC actually forms the central rim on the cytoplasmic surface of RyR (Figure 5). Following the results, we stressed the need for publishing the docking contrast between the top solution and the remaining ones. A high docking contrast would eliminate false positives and in turn mean a high probability of correctness.

In the study of large membrane proteins like RyR, crystallography though, is definitely not a replacement for, or an upgrade from cryo-EM. With the full channel having so far evaded crystallographic success, viewing atomic detail in 'the bigger picture' can only be achieved in combining the two techniques, done by docking crystal structures into EM maps. Yuchi et al (2012) highlight an example of this in their mapping of phosphorylation domains into RyRs.

Full length RyRs initially intrigued the crystallographic world with their observed formation of 2D 'chessboard' lattices (Saito et al. 1984, Ferguson et al. 1988, Saito et al. 1988). This innate ability of the receptors to network like this meant crystals were easier than thought to obtain. The failure to form 3D lattices though, crippled the progress of determining a full-length structure for several years. Thankfully, high resolution EM images of RyR, showed that as previously mentioned, the complete structure can be broken down into much smaller, globular subregions, each of which provide a much more feasible crystallographic target.

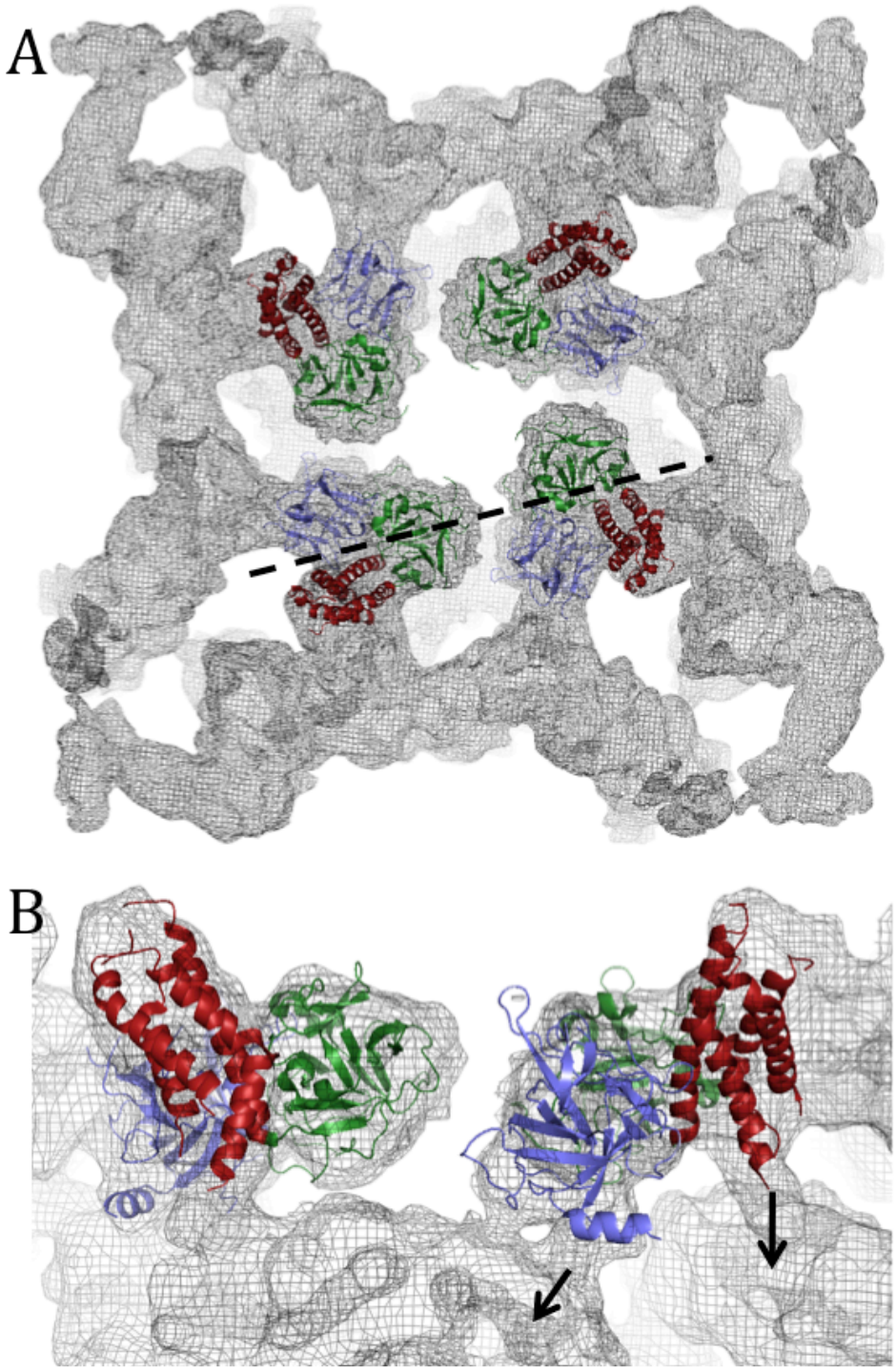

FIGURE 5. **Docking of RyR1ABC.** Docked (EMDB 1275, Ludtke et al. 2005) RyR1 A (blue) B (green) and C (red) are shown from the cytoplasmic top-side (**A**) and from a perpendicular cross-section at the dashed line (**B**). Arrows show the potential for allosteric interactions in the direction of the pore. Distant regions of the EM map (mesh) have been clipped for clarity.

Three years ago, the structures of the N-terminal ~200 residues of RyR1 (Amador et al. 2009, Lobo and Van Petegem 2009) as well as RyR2 (Lobo and Van Petegem 2009) were solved (RyR1A and RyR2A respectively). Since then several wild-type large domains have been solved and docked including the confusingly named Ryanodine Receptor (RYR) domain (Sharma et al. 2012), the aforementioned RyR1ABC domains (Tung et al. 2010) and the phosphorylation domains in all three isoforms (Yuchi et al. 2012, Sharma et al. 2012). Mutations in some of these domains have been shown to cause severe disorders, and crystal structures of some of these mutants have enlightened some of the mechanistic effects (discussed in Chapter 1.3.2). Part of the work described in this thesis aims to increase the number of high-resolution structures of RyR domains.

1.2.3 The IP_3 Receptor

RyRs are not the only Ca^{2+} release channels located in the ER or SR. Another powerful second messenger, inositol 1,4,5-triphosphate (IP_3), and its receptor (IP_3R) have been studied extensively as well. The IP_3 molecule is the result of cleavage of phosphatidylinositol 4,5-bisphosphate (PIP_2) by phospholipase C. An additional by-product of the separation is 1,2-diacylglycerol (DAG), which is another second messenger that activates Protein Kinase C. DAG, like its precursor PIP_2, is membrane-bound whereas IP_3 is water-soluble and diffuses in the cytoplasm to trigger opening of IP_3Rs.

IP3Rs also have three isoforms in vertebrates. Most cell-types express more than one of these isoforms but IP_3R1 is enriched in neurons and smooth muscle, IP_3R2 in the brain, heart and secretory organs, and IP_3R3 is also found in secretory organs, but is more ubiquitously expressed (Newton et al. 1994, De Smedt et al. 1994, Wojcikiewicz, 1995). At ~ 1 MDa, it is less than half the size of RyR, due mostly to its much smaller cytoplasmic portion. Similar to RyR though, it was thought to have the same 'thumb-tack' structure with four-fold, tetrameric symmetry. Ludtke et al (2011)

provided a 9.5 Å cryo-EM structure that confirmed this. The crystal structure of the N-terminal three domains of IP3R was initially solved in two segments: the latter two forming an IP3 binding domain (Bosanac et al. 2002) and the former domain, which suppressed IP3 binding (Serysheva et al. 2003, Bosanac et al. 2005). Later, structures of the first three domains together (IP_3R1ABC) were solved (Lin et al. 2011, Seo et al. 2012), but to lower resolutions.

A detailed comparison of RyR1ABC to the corresponding domains in IP_3R1 shows that their overall structures are conserved, suggesting that the channels must rely on similar allosteric mechanisms in regulation (Yuchi and Van Petegem, 2011). In both cases, a pair of beta-trefoil domains followed by a third helical domain can describe the structure (Figure 6). However, two notable differences can be observed. The first domain of IP_3R1 (IP_3R1A) contains two large helices in comparison with RyR1A that has only one, and the construct length of IP_3R1ABC, which results in a 35-residue extension in the third, helical domain. Despite these differences, Seo et al. (2012) used some intricate chimera studies to show that RyR1A can functionally replace the suppressor domain in IP_3R1.

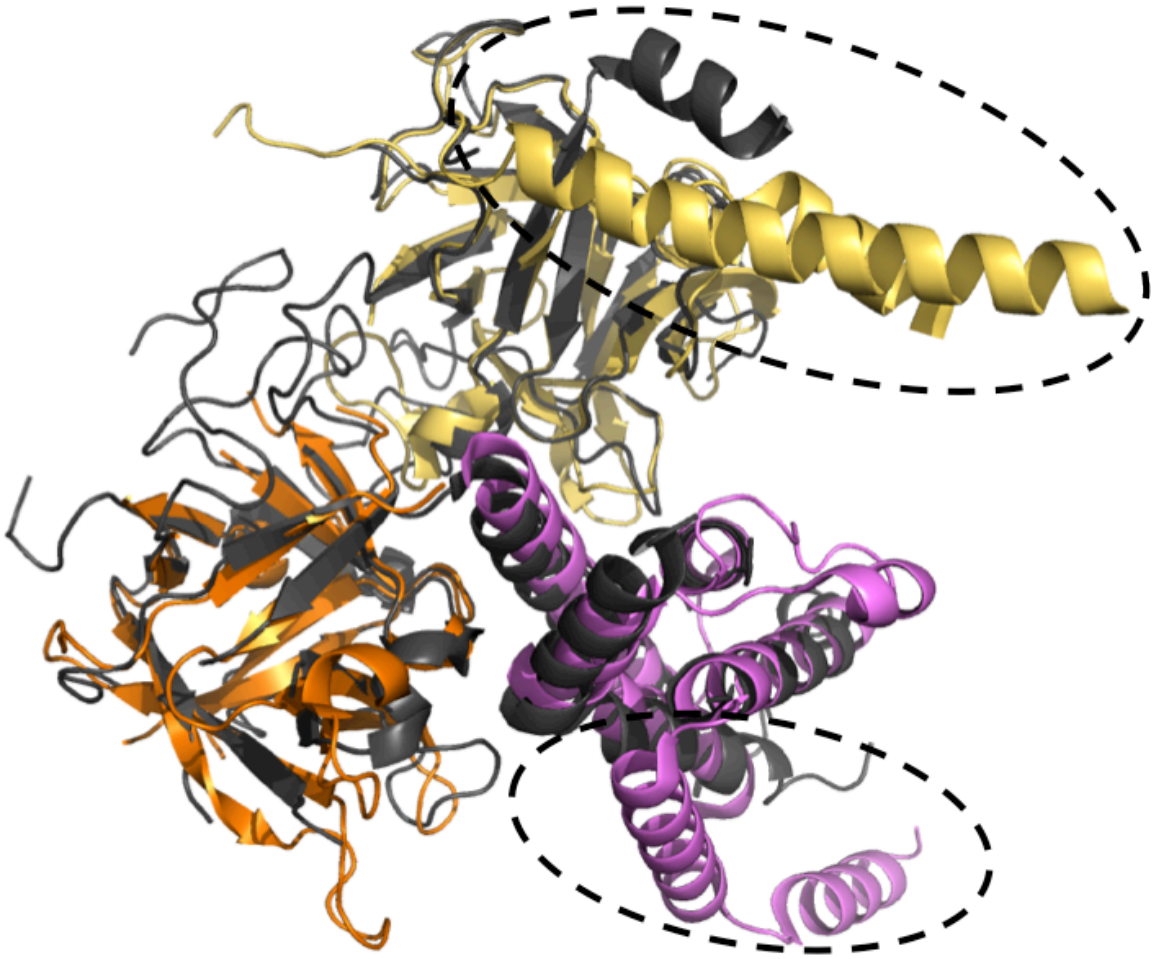

FIGURE 6. **IP3R1ABC vs RYR1ABC.** IP3R1 domain A (yellow), B (orange) and C (purple) are individually superposed onto RyR1ABC (black). Dashed circles highlight the major differences between the two: a large extra helix in IP3RA, and an extended domain C.

1.3 Disease Mutations

Ca^{2+} regulation in the cell is vital. With E-C coupling relying so heavily on Ca^{2+} as a second messenger, any disruption in this regulation causes severe muscular pathologies. Mutations in both RyR1 and RyR2 can cause acute genetic diseases. Kimlicka et al. (unpublished) have maintained a RyR mutation database that

currently shows over 290 mutations in RyR1 cause skeletal muscle disorders such as MH or Central Core Disease (CCD), and over 150 mutations cause diseases such as Catecholaminergic Polymorphic Ventricular Tachycardia (CPVT) or Arrhythmogenic Right Ventricular Dysplasia Type 2 (ARVD2) in RyR2. In both isoforms, disease mutations seem to be clustered into 'hotspots' in the channel that seem distant in primary structure, but may interact in 3D space according to the 'zipper hypothesis' (Ikemoto and Yamamoto, 2002, Oda et al. 2005, Liu et al. 2010). For this discussion, I will concentrate on MH and CCD.

MH is a life-threatening genetic disorder triggered by volatile anaesthetics. Some of the symptoms include metabolic acidosis, tachycardia, skeletal muscle rigidity, rhabdomyolysis and most notably, a dramatic rise in body core temperature (Pamukcoglu 1988, Denborough 1998). Its record as a human disorder began in 1960 with a twenty one year old man who required surgery after being run over by a car, and his accident-prone family. With 10 of the man's 24 relatives thought to have died in response to ether-based anaesthetics, there was more concern on how to proceed anaesthetically than there was about how to deal with the compound fractures in his leg. They decided to abandon ethers and proceed cautiously with the recently available halothane, but within twenty minutes this had to be stopped when both the man's body temperature and heart rate rose rapidly. In somewhat of a miracle, not only did they manage to save the man's life using ice packs to cool him down, but also successfully completed the required surgery. Still, Denborough and Lovell (1960) actually published the article 'Anaesthetic Deaths in a family' with the hope of finding others that had come across the clinical problem. Eventually, by 1966 enough cases and interest evolved that a symposium in Toronto was held that was dedicated solely to MH (Gordon, 1996).

Mutation in RyR1 became a candidate for blame when pigs with a single cysteine to arginine mutation at position 615 (C615R) in RyR1 exhibited the symptoms of MH (Fujii et al. 1991). Since then a large number of MH-causing mutations in human RyR1 have been found (McCarthy et al. 2000, Girard et al. 2006, Robinson et al. 2006, Groom et al. 2011). Thankfully, in the late 1970s, the muscle relaxant dantrolene was clinically approved to treat MH and successfully reduced the

mortality rate of MH from ~80% to less than 5% (Rosenberg et al. 2007). The mechanistic details of the treatment have not fully been understood although RyR1 is considered to be the major molecular target (Parness and Palnitkar 1995, Palnitkar et al. 1999, Krause et al. 2004). Jiang et al. (2008) popularized a theory involving the misregulated sensing of luminal Ca^{2+} concentration. RyRs were shown to recognize when the SR Ca^{2+} store is beyond its capacity and to trigger Store Overload-Induced Ca^{2+} release (SOICR). Physiological Ca^{2+} concentrations inside the SR rarely get high enough to cause SOICR, but mutations in RyR result in leaky channels that lower this threshold.

CCD is a rare congenital myopathy associated with reduced oxidative activity in muscle fibre. Muscle weakness causes an inability to independently walk, and with no curative treatment current therapeutic management is limited to physiotherapy (Jungbluth et al. 2002). With regards to RyR1, CCD can be explained in two separate ways. The first runs parallel with MH and involves a gain-of-function in RyR1. Here SR Ca^{2+} stores get depleted by constitutively active channels. As a result, there is an inability to sufficiently amplify Ca^{2+} signals required for muscle contraction (Zhang et al. 1993, Dirksen and Avila, 2002). The second involves a loss of function in the coupling between RyR1 and Ca_V. 'Uncoupled' receptors would then cause muscle weakness by decreasing RyR1-mediated SR Ca^{2+} release (Quane et al. 1993, Dirksen and Avila, 2002). Which of the two mechanisms best describes any particular case of CCD depends on the location of the mutation.

1.3.1 Phosphorylation and disease

The underlying cause of MH has been attributed to a gain-of-function in RyR1 channels, which become leaky and as a result cause irregular Ca^{2+} homeostasis (Tong et al. 1999). The symptoms of disease have been attributed to a variety of cellular processes that occur to restore proper Ca^{2+} levels. For example, in an attempt to re-establish normal Ca^{2+} concentrations, the ATP-consuming SERCA pump overworks,

thereby generating an increase in oxidative/nitrosative stress. As part of a brutal positive feedback loop, this stress causes S-Nitrosylation of RyR1 that makes it even more leaky (Durham et al. 2008). Others have shown a link between hyperphosphorylation of RyR2 in the heart and SR Ca^{2+} leak (Wehrens et al. 2003, Ai et al. 2005). It is thought that this is due to the phosphorylation causing detachment of the stabilizing FKBP proteins (Marx et al. 2000, Reiken 2003), but this mechanism is yet to be fully accepted. A similar link has been used to explain Ca^{2+} leak in RyR1 (Bellinger et al. 2009). The perpetrators of RyR phosphorylation are Protein kinase A (PKA), (Mayrleitner et al. 1995) and Ca^{2+}/CaM-dependent kinase II (CaMKII) (Wang and Best, 1992). There is some debate in the field though as to which sites in the channel are phosphorylated. Most of the conflict involves RyR2, and ultimately there has been a shift in focus away from the notion of one particular site being hyperphosphorylated in an RyR cluster. Instead the idea of multiple phosphorylation sites in a single receptor has been included (Huttlin et al. 2010, Yuchi et al. 2012). With regard to RyR1, so far serine-2843 (S2843) has been identified as a PKA and CaMKII phosphorylation site (Suko et al. 1993).

From a reverse perspective, phosphatases play their role in the RyR macromolecular complex as phosphate removers, thereby reducing the activity of the channels. In RyR2, heart failure associated with PKA hyperphosphorylation was shown to coincide with a drop in abundance of protein phosphatases 1 and 2A (PP1 and PP2A)(Marx et al. 2000). Interestingly PKA, as well as PP1 and PP2A are thought to use the same mode of attachment via leucine zippers in regulatory subunits to tether to RyR (Marx et al. 2001).

1.3.2 The Molecular Cause of Disease

The molecular details that actually cause RyR leakiness can be understood in analysis of the available crystal structures and their docking to cryo-EM maps. So far, the Van Petegem lab has been responsible for all published mutant crystal structures.

With regard to point mutations, the molecular effects of two disease mutations in RyR2A (Lobo and Van Petegem, 2009) and three disease mutations in the RyR1 phosphorylation domain (Yuchi et al. 2012) have been revealed. Looking at the primary structures alone, in each case, all that was involved was the replacement of a single amino acid. The little structural changes observed as a result though, are drastic enough to cause the aforementioned, severe genetic disorders. In a particularly interesting example though, the deletion of an entire exon in RyR2A is involved. The removal takes away some major wild-type structural elements, including a vital beta strand that is then replaced by a neighbouring stretch of residues. Remarkably, these residues are completely unstructured in a normal wild-type channel and seem to be able to mould into place. People with this disease mutation have a much worse version of CPVT (Lobo et al. 2011).

Most of the molecular insight into disease in RyR came from analysing the mutation sites in RyR1ABC, which are all clustered at interfaces between domains in the full-length channel (Tung et al. 2010). Evidently, RyRs must function as complex allosteric gear systems and mutations that blunt the teeth of these gears result in leaky channels. This breakdown of communication between subregions in RyR1 added some weight to the zipper hypothesis, which as mentioned, theorized that disease hotspots interact physically with each other (Ikemoto and Yamamoto, 2002, Oda et al. 2005, Liu et al. 2010). However, most disease mutations in the N-terminal disease hot spots are already involved in contacts with other domains within the same hot spot, so only a small subset of mutations remain available for interacting with the central disease hot spot. As such, the original zipper hypothesis can only apply to a small subset of mutations.

1.4 Small Molecule Drugs and Ligands

In addition to the numerous proteins that interact with RyR, various small molecules modulate the channel as well. Ca^{2+} and Mg^{2+} have already been discussed, but other physiological ligands include natural toxins that can either activate RyR,

such as imperatoxin A in scorpion venom (Tripathy et al. 1998, Gurrola et al. 1999), or cause inhibition, for example natrin in snake venom (Thomas et al. 2010). [^{3}H]-Ryanodine should be mentioned in addition to ryanodine as a ligand, as its production provided a new approach to studying RyR structure and function. Binding to ryanodine occurs only for open channels, and thus the amount of radiolabelled ligand bound represents a measure of the open probability of the RyRs. (Pessah et al. 1985). In an example, the immunosuppressants rapamycin (Kaftan et al. 1996) and FK-506 (Kraus-Friedmann and Feng, 1994) have been shown to reduce ryanodine binding. Single-channel experiments on RyR showed that the anticoagulant heparin increased the P_O of the channel (Bezprozvanny et al. 1993). 4-chloro-m-cresol (Hermann-Frank et al. 1996) and volatile anesthetics such as halothane (Connelly and Coronado, 1994, Bull and Marengo, 1994) are examples of non-physiological ligands that activated RyR in bilayer studies. In contrast, the polycationic dye ruthenium red inhibits the binding of ryanodine (Pessah et al. 1985). Relevant to this discussion are the drug dantrolene, and the purine derivatives: adenine nucleotides and caffeine.

1.4.1 Dantrolene

Dantrolene is a hydantoin derivative (Figure 7A) originally synthesized as a muscle relaxant (Snyder et al. 1967), used to treat skeletal muscle spasticity (Dykes, 1975). Its muscle relaxant properties were pinned on the depression of E-C coupling. With the number of fatal MH cases rising, this led to animal model testing using MH-susceptible pigs (Harrison, 1975). The remarkable results jumpstarted the drug into clinical trials just two years later that led to an approved treatment for MH shortly after (Kolb et al. 1982). Initially there were problems in administering the drug due to its inability to dissolve well in water, but doses today are added to mannitol, which significantly improves its solubility (Krause et al. 2004). A more water-soluble alternative is azumolene (Figure 7B) (Sudo et al. 2008).

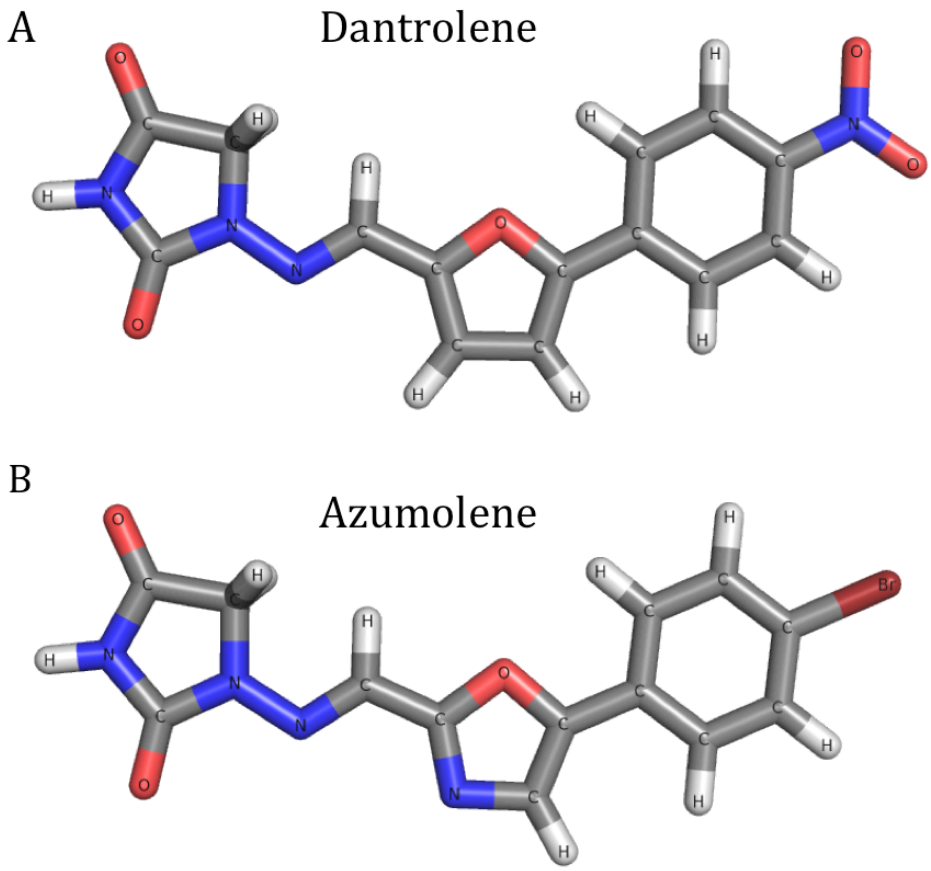

FIGURE 7. **The molecular structures of dantrolene and azumolene.** (**A**) Dantrolene is mostly planar and very poorly soluble in water. (**B**) Azumolene is a more water-soluble analog and differs by the presence of a bromide group in place of the nitro group in dantrolene.

The drug was shown to inhibit SR Ca^{2+} release at a concentration of ~10-50 μM (Van Winkle, 1976, Herbette et al. 1982, Loke and MacLennan, 1998), and as the therapeutic concentration is in the same range (Flewellen et al. 1983), the clinical effects are most likely due to this inhibition. But with regard to RyR, a clear mechanistic story is yet to be achieved. The most recent theories deal with SOICR in both RyR1 and RyR2 (Jiang et al. 2004, Jiang et al. 2005, Jiang et al. 2008, Maxwell et al. 2011). Dantrolene is suspected to remedy the inability of mutant RyRs to withstand a proper SR luminal Ca^{2+} concentration. Additionally, Kobayashi et al. (2005) used a fluorescent probe to track RyR1 domain movements upon mimicking

MH and noticed that dantrolene prevented them – apparently stabilizing the interdomain interactions. Whether or not these effects are due to a direct interaction with RyR though is debatable, with strong arguments both for and against.

As mentioned, [^{3}H]-Ryanodine binding has been a diagnostic tool to recognize an open RyR. Palnitkar et al. (1997) showed no effect of dantrolene on [^{3}H]-ryanodine binding, and that in linear centrifugation of SR membranes, distinct peaks for both [^{3}H]-ryanodine and [^{3}H]-dantrolene were attained. This initially led to the conclusion that dantrolene and ryanodine bind two different molecules. Later though, Zhao et al. (2001) described that [^{3}H]-ryanodine binding was indeed affected by 10 μM dantrolene. Together these conflicting results hint towards configuration-dependent ryanodine and dantrolene binding, and that perhaps open and closed RyRs fractionate differently in centrifugation due to changes in the RyR macrocomplex. One interesting difference between the two studies was the presence of an adenine nucleotide, required for dantrolene-inhibition of RyR (Zhao et al. 2001), suggesting that if there is a dantrolene binding site in RyR, that it is intimately linked to a purine binding site by some allosteric mechanism.

Single-channel experiments only provided more topics of discussion. In early lipid bilayer studies, Bull and Marengo (1994) stated that 100 μM dantrolene or less failed to affect halothane-induced activation of frog skeletal RyR, evidence that was corroborated more recently in recordings using 20 μM dantrolene on both RyR1 and RyR2 (Diaz-Sylvester et al. 2008). This went against reports that showed a biphasic pattern of regulation with activation at nanomolar and inhibition at micromolar dantrolene concentrations (Nelson et al. 1996). Both sets of experiments incorporated SR vesicles into lipid bilayers so again, differences in experimental conditions and preparations resulting in the purification of distinct RyR macrocomplexes could explain the discrepancies. Szentesi et al. (2001) purified RyRs alone by centrifugation through a sucrose gradient, and showed that in lipid bilayers, they were not affected by dantrolene. This convincing evidence though, still does not clarify if RyR is the direct molecular target or not. More accurately, it proves that RyR and dantrolene alone do not result in channel inhibition; the two could still bind and

exhibit a latent effect on Ca^{2+} release. This direct mechanism would then require subsequent change in RyR structure, due to the binding of modulators. Similarly, an indirect mechanism could just as easily be described in which one of the modulators is in fact the molecular target of dantrolene. Strengthening the latter theory are observations that dantrolene inhibits the binding of dihydropyridine analogs to $Ca_V1.1$ more effectively than the binding of [^{3}H]-ryanodine to RyR1 (el-Hayek et al. 1992). In general, it can be concluded that other proteins are definitely involved in the mechanism of inhibition by dantrolene; in an example, it was shown to be dependent on CaM (Zhao et al. 2001, Kobayashi et al. 2005).

The most compelling argument for a direct mode of action comes from photoaffinity label experiments (Paul-Pletzer et al. 2001, Paul-Pletzer et al. 2002) using [^{3}H]-azidodantrolene. This reactive analog of the drug was specifically synthesized to locate a dantrolene binding site in skeletal muscle SR in the hope of clearing some of the controversy in the field (Palnitkar et al. 1999). Upon activation, [^{3}H]-azidodantrolene covalently bound to porcine sarcoplasmic reticulum, and after purification and cleavage by n-calpain, the N-terminal 1400 RyR1 residues were credited as containing the drug binding site. This prompted later experiments showing that it selectively attached to a synthetic peptide of RyR1 residues 590-609. Similar to the experiments with RyR1 4064-4120 mentioned earlier though, results from experiments using isolated peptides have to be interpreted carefully.

1.4.2 Purine derivatives

These are heterocyclic, aromatic compounds consisting of two fused rings: one imidazole and one pyrimidine. Even in early RyR research, the adenine nucleotide purines in particular were shown to be important activators of the channel (Morii and Tonomura, 1983; Nagasaki and Kasai, 1983; Meissner, 1984) with a half maximal effective concentration (EC_{50}) in the millimolar range (Meissner et al. 1986). Earlier still, it was known that the methylxanthine caffeine also favours the release of Ca^{2+}

from the SR (Endo, 1977) and shows a similar effect on RyR as adenine nucleotides. Given their closeness in structure (Figure 8), this is initially not surprising, but other evidence suggests that their interaction sites may not be the same: Ogawa and Harafuji (1990) for example showed that the *in vitro* effect of combining caffeine and adenine nucleotides on Ca^{2+}-dependent RyR1 stimulation, was additive in reaction media of high osmolarity, whereas it was potentiating in lower, physiological salt concentrations.

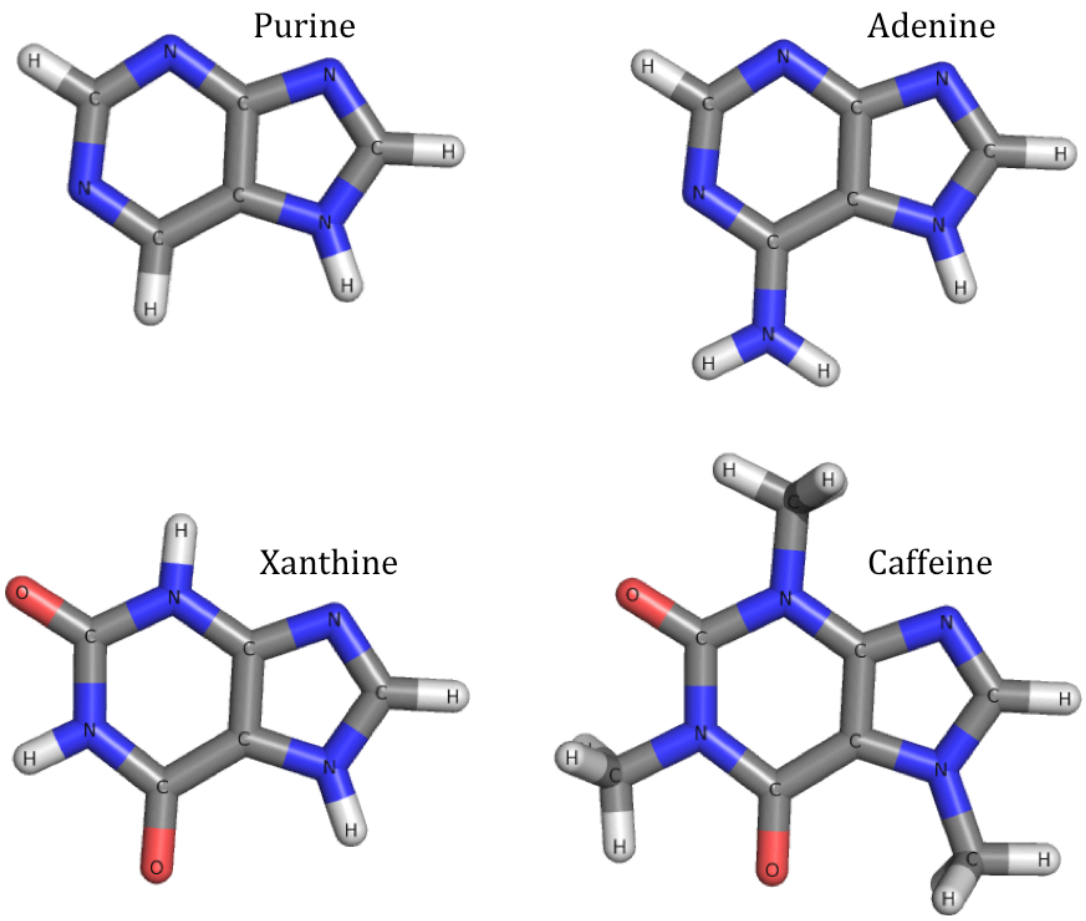

FIGURE 8. **Adenine nucleotides and xanthines.** The molecular structures of purine, adenine, xanthine, and the methylxanthine caffeine are shown. The purine ring exists in all three structures, highlighting their stuctural similarity.

Still, two cases in the PDB database exist, where both an adenine nucleotide and caffeine have been separately co-crystallized in the same receptor: 1) Adenosine (Lebon et al. 2011) and caffeine (Doré et al. 2011) bound to the adenosine A_{2A} receptor, and 2) Adenine (Lukacs et al. 2006) and caffeine (Oikonomakos et al. 2000) bound to a glycogen phosphorylase. In both cases, the two species are found in the same pocket (Figure 9A and 9B). Close analysis of the interactions show that all that may be required is a hydrophobic pocket, ideally containing an aromatic ring to stack against. A few charged and polar residues may supply some specificity. In fact, all published structures with caffeine bound seem to take advantage of an aromatic ring. Figures 9C, D and E highlight three examples (Ekstrom et al. 2002, Yang et al. 2010, Rao et al. 2005). Interestingly, the structure in figure 9C involves a glycogen phosphorylase as well and although it superposes well with the structure from 9B, contains an extra binding site for caffeine. Similarly, Figures 9D and E are both from easily superposable chitinase structures, but the latter contains an extra binding site. This kind of interaction seems very general and hints to the possibility of multiple binding sites in RyR.

The lack of specificity in binding is emphasized further when weighing the effects of other methylxanthines against each other. Rousseau et al. (1988) compared seven different methylxanthines, including caffeine, and although they established a hierarchy in effectiveness, the differences were not great. They did however show that the five-member imidazole ring, which is also present in adenine, was necessary, as 1,3-dimethyluracil was ineffective. It is likely then, that there are multiple binding sites for both adenine nucleotides and methylxanthines in RyR and that some of these pockets, maybe most, can accommodate either.

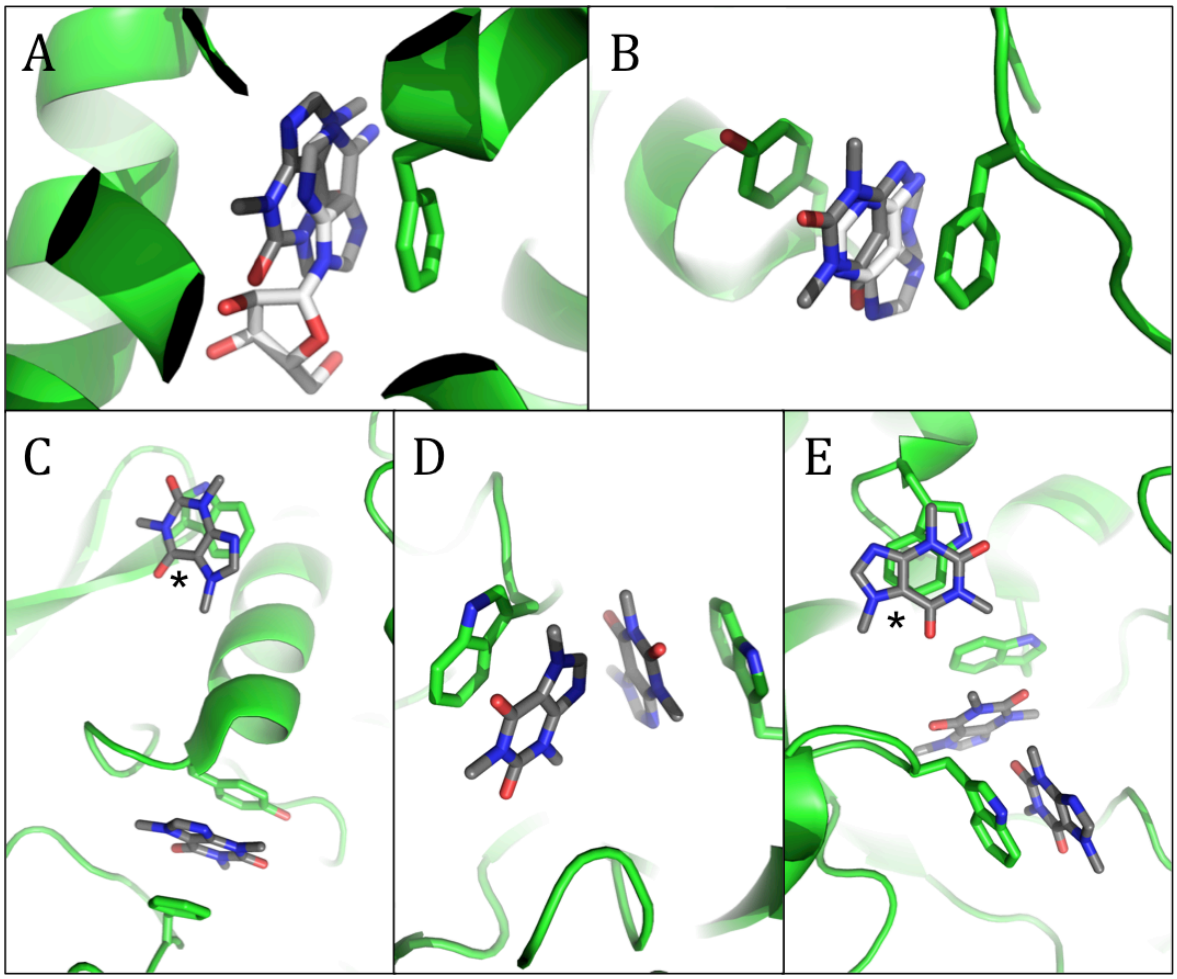

FIGURE 9. **Purine binding by aromatic stacking. A**) PDBs 2YDO (Lebon et al. 2011) and 3RFM (Doré et al. 2011) respectively show adenosine (*white*) and caffeine (*grey*) bound to the adenosine A_{2A} receptor **B**) PDBs 1Z8D (Lukacs er al. 2000) and 1GFZ (Oikonomakos et al. 2006)respectively show adenine (*white*) and caffeine (*grey*) bound to a glycogen phosphorylase. **C**) PDB 1L5Q (Ekstrom et al. 2002) shows another glycogen phosphorylase with an extra caffeine molecule (*) bound in the crystal structure. **D**) PDB 3G6M (Yang et al. 2010) shows caffeine bound to a chitinase. **E**) PDB 2A3B (Rao et al. 2005) shows another chitinase with an extra caffeine molecule (*) bound in the crystal structure. Together, the structures hint towards aromatic promiscuity in caffeine.

1.5 Hypotheses and Goals

This thesis aims to uncover some of the structural and functional characteristics of ligand binding in RyR1, findings that are transferable to other RyR isoforms. Given the size of the channel we hypothesize that distant allosteric mechanisms must be involved in most ligand-related processes including general regulation and drug action. To test this theory a range of known modulators, both physiological and pharmacological, have been chosen:

1. The drug dantrolene and the protein PP1, both of which negatively regulate RyR1, have been linked to the N-terminal ~600 residues of the channel.
2. Activators like caffeine (pharmacological) and adenine nucleotides (physiological), which may interact with RyR1 via similar mechanisms.
3. Ca^{2+} and Mg^{2+}, which are thought to interact with RyR EF-hands, domains that could regulate the RyR by competing with CaM for CaMBDs.

Specifically, to further our understanding of the effects of modulators on RyR1, the techniques of X-ray crystallography, ITC and *in silico* docking and modelling are implemented (Figure 10).

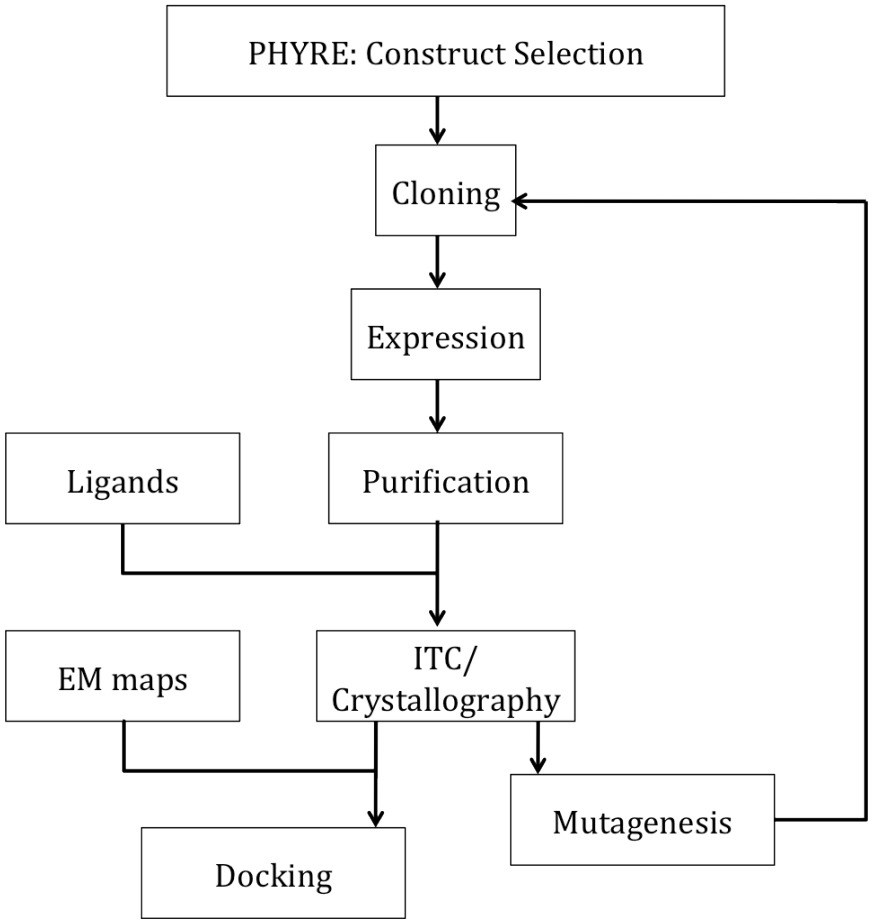

FIGURE 10. Method **flowchart.** A flow-chart describing the general procedures and aims of the projects in this thesis. The structural and thermodynamic properties of ligand binding in RyR1 are obtained from ITC and crystallographic studies. Information on large sub-region movements in RyR1 is obtained from the docking studies. Together, the results are used to attempt deciphering the details of allosteric interactions between domains in RyR1 that occur as a result of ligand binding. All experiments were carried out on the RyR1 *Oryctolagus cuniculus* clone, a sequence that is >96% identical to RyR1 *Homo sapiens* and in general is shifted in register by +1 residues.

2 Materials and Methods

2.1 Cloning and Expression

The program PHYRE^2 (Kelly and Stenberg, 2009) was used to aid in construct selection. A modified pET28 vector was used for all cloning (Van Petegem et al. 2004). A full-length RyR1 clone from *Oryctolagus cuniculus* (rabbit) provided the template for all construct selection using the Polymerase Chain Reaction (PCR). Constructs were inserted at the C-terminus of hexahistidine tagged Maltose Binding Protein (MBP). In resultant fusion proteins, a Tobacco Etch Virus (TEV) protease cleavage site (ENLYFQSNA) separates MBP and the construct of interest. As a result of cleavage, a serine-asparagine-alanine cloning artefact remained at the N-terminus of all constructs. Part of the vector design allows for Ligation Independent (LIC) cloning. Here, primers for PCR of constructs of interest were designed to include a complementary LIC sequence to the one in the vector (see Table 1). Constructs and the vector were treated with T4 deoxyribonucleic acid (DNA) Polymerase in the absence of all but one deoxyribonucleotide triphosphate (dNTP). Under these conditions the polymerase exhibits 3'→5' exonuclease activity until it reaches a point where the provided dNTP can be added. In this way, long complementary overhangs (between vector and constructs) can be created that hydrogen bond well enough that *in vitro* ligation is not required. Following annealing of constructs to the vector, transformation into a calcium chloride ($CaCl_2$) competent DH5α strain of *Escherichia coli* (*E. coli*) (Invitrogen) was performed and resultant colonies were grown in 2xYT media (16g/L Tryptone, 10 g/L yeast extract and 5 g/L sodium chloride) for DNA amplification.

The RyR1 217-536 W269A and 4071-4138 C4114A mutations were made using the QuikChange protocol (Stratagene). The process involves designing primers

that flank the desired mutation site and code for an alanine instead of tryptophan. Extension around the plasmid is done by Pfu Turbo Polymerase in a PCR reaction. The restriction enzyme DpnI was used to cut the methylated template DNA and leave a mutated plasmid (albeit with nicks in the DNA) for transformation yet again into DH5α for amplification.

For protein expression the *E. coli* Rosetta (DE3) pLacI cells (Novagen) were used. Cultures were grown at 37°C until the optical density at 600nm (OD_{600}) reached ~0.2-0.3 and then the temperature was lowered to 18°C. At an OD_{600} of ~0.6, cultures were induced with isopropyl-β-D-thiogalactoside (IPTG) and grown for a further ~24 hours. Cultures were then pelleted and stored at -20°C. In the case of EF-hand constructs, the temperature was kept at 37°C throughout expression and cells were pelleted after ~4 hours of induction.

RyR1 4295-4325, a CaMBD (Takeshima et al. 1989, Chen and MacLennan 1994), has been named CaMBD3 by the Van Petegem lab. A synthesized mutant peptide with a 4320-4322 LRR duplication (RyR1 CaMBD3dLRR) was available in the lab and purchased from Lifetein

Forward primers	
N1	TACTTCCAATCCAATGCAATGGGTGACGGAGGAGAGGG
N217	TACTTCCAATCCAATGCAGGCCACGTCCTCCGCCTC
N394	TACTTCCAATCCAATGCACAGCAGGAGGAGTCCCAGGC
N533	TACTTCCAATCCAATGCAAATCGTGCCAACTGTGCCCTC
N570	TACTTCCAATCCAATGCAGAGAGTCCCGAGGTGCTGAAC
N3487	TACTTCCAATCCAATGCATCGGGCGGCTCGGACCAGGAAC
N3497	TACTTCCAATCCAATGCAAAGAAGCGCCGGGGGGACAGG
N3507	TACTTCCAATCCAATGCACAGACGTCACTGATCGTGGCC
N3818	TACTTCCAATCCAATGCAGATTATCTGAAGGACAAGAAG
N3828	TACTTCCAATCCAATGCATTCTTCCAGAGCATCCAGGCG
N3838	TACTTCCAATCCAATGCAACATGCAGCGTCCTGGATCTC
N3997	TACTTCCAATCCAATGCAGCCCACATGATGATGAAGCTC
N4024	TACTTCCAATCCAATGCAGTGGTGATGCTGCTGTCCCTAC
N4031	TACTTCCAATCCAATGCACTGGAAGGGAACGTGGTGAAC
N4041	TACTTCCAATCCAATGCAGCCCGGCAGATGGTGGACATG
N4071	TACTTCCAATCCAATGCAATCGTGGGCTCCGAGGCCTTC
Reverse primers	
C536	TTATCCACTTCCAATGTTATTAGTTGGCACGATTGCCCCGGATC
C574	TTATCCACTTCCAATGTTATTACACCTCGGGACTCTCAATCAGG
C589	TTATCCACTTCCAATGTTATTAGAGGGAGATGATGGACTTG
C608	TTATCCACTTCCAATGTTATTACACACACAGGGAGCACAGC
C617	TTATCCACTTCCAATGTTATTAGTTGGAGCGCACAGCCACG
C627	TTATCCACTTCCAATGTTATTAAGGGAGCAGATTCTCGGTG
C635	TTATCCACTTCCAATGTTATTAGATGCTGGTGACGTAGTTG
C644	TTATCCACTTCCAATGTTATTAGATGCTGGTGACGTAGTTG
C654	TTATCCACTTCCAATGTTATTACTCGGCTCGGCCCACGAAG
C796	TTATCCACTTCCAATGTTATTAGCGGCCGCCAAGGAGAAACCG
C4070	TTATCCACTTCCAATGTTATTAGTCCTTGAGTTTCAGGAACATG
C4128	TTATCCACTTCCAATGTTATTAGAACTCCTCGAAGTTGATCATC
C4138	TTATCCACTTCCAATGTTATTAGTCCCGGGCTGGCTCCTGGAAG
C4148	TTATCCACTTCCAATGTTATTAGGTCAGCAGCACGGCCACGTTG
Quikchange primers	
W269A_F	GAACCCCTGAGAATCAGCGCGAGTGGAAGCCACCTGCGC
W269A_R	GCGCAGGTGGCTTCCACTCGCGCTGATTCTCAGGGGTTC
C4114A_F	GAAATCCAGTTTCTGCTCTCGGCCTCCGAAGCCGACGAGAATG
C4114A_R	CATTCTCGTCGGCTTCGGAGGCCGAGAGCAGAAACTGGATTTC

Table 1. **List of primers used to make constructs.** All sequences are shown 5'→3'. The LIC sequence for forward primers is: 5'-TACTTCCAATCCAATGCA-3', whereas for reverse primers it is: 5'-TTATCCACTTCCAATGTTATTA-3' which encodes two stop codons after the construct. Note that aside from Quikchange primers, in all cases an LIC sequence precedes a coding sequence. For Quikchange primers, highlighted in red are the codons that were changed and code for alanine.

2.2 Protein Purification

The following buffers are referred to in the purification protocol:

Buffer A: 250 mM KCl, 10 mM HEPES* at pH 7.4

Buffer B: 250 mM KCl, 500 mM Imidazole at pH 7.4

Buffer C: 250 mM KCl, 10 mM HEPES at pH 7.4, 10 mM Maltose

Buffer D(pH): 50 mM KCl, (10 mM HEPES pH 7.4 or Tris** at pH 8.0)

Buffer E(pH): 1 M KCl, (10 mM HEPES pH 7.4 or Tris at pH 8.0)

Buffer F: 150 mM KCl, 10 mM HEPES at pH 7.4

*HEPES: 4-(2-hydroxyethyl)-1-piperazineethanesulfonic acid

**Tris: tris(hydroxymethyl)aminomethane

Frozen pellets were thawed in a room temperature water bath but in all purification steps following, care was taken to keep samples at a maximum of 4°C. Cells were then lysed by sonication in ~60 mL of buffer A, containing in addition 25 μg/ml of deoxyribonuclease I, 25 μg/ml of lysozyme, 1 mM phenylmethylsulphonyl fluoride, 10% (vol/vol) glycerol and 14 mM β-mercaptoethanol (βME). In the case of RyR1 4071-4138 C4114A, the addition of βME was omitted, with no need for the reducing agent. The lysate was centrifuged at 30,000x g for 30 minutes to pellet any insoluble material.

Using protein liquid chromatography (AKTA purifier, GE Healthcare), the supernatant was injected onto a 25 ml Poros MC column (Tosoh Bioscience); a nickel column that binds hexahistidine tags. Samples were then washed with five column volumes (CV) of buffer A to remove unbound *E. coli* proteins, followed by 5 CV of 1% buffer B in buffer A (vol/vol) to remove non-specifically bound bacterial proteins. Fusion protein was eluted with 30% buffer B in buffer A (vol/vol). Samples were then dialyzed in the presence of recombinant TEV protease for at least 4 hours twice at 4°C in buffer A and 14 mM βME. The addition of the reducing agent here was done regardless of whether or not the sample contained cysteines; being a cysteine-protease, the TEV protease worked better in the presence of βME. For RyR1 217-536,

wild-type and W269A, cleavage was more difficult: more TEV protease and longer dialysis were required to completely cleave the constructs. Samples were then applied onto a 25 ml amylose column (New England Biolabs) followed by a second 25 ml Poros MC column. In both cases the flowthrough was collected and following the nickel column, samples were dialyzed in buffer D(8.0) for RyR1 1-536 and 217-536 wild-type or mutant constructs, or buffer D(7.4) for RyR1 4071-4138 and 1-617 constructs. Here and in further purification, 14mM βME was added to all buffers in which cysteine-containing constructs were purified. In some cases, the amylose column was instead run before TEV cleaving to increase purity.

Following dialysis, samples were transferred to a HiLoad Q Sepharose column (GE Healthcare) and subject to a 0% to 30% (vol/vol) buffer E in buffer D gradient (pHs for each were as mentioned for buffer D above). After the gradient, two CV of 100% buffer E were used to wash the column. Constructs would elute during the gradient and observed as peaks of UV absorbance at 280 nm on resulting chromatograms. In a final purification step, a HiLoad 16/60 Superdex 200 prep grade (GE Healthcare) gel filtration column was used to confirm a well-behaved, single species was purified. Ideally, a single symmetric peak, not in the void volume would be observed in the chromatogram.

Amicon concentrators (3K cut-off for RyR1 4071-4138 constructs and 10K cut-off for RyR1 1,217-536 and 1-617 constructs) were used to exchange the samples into 10 mM KCl, 10 mM HEPES 7.4 and 5 mM dithiothreitol, and then concentrate the protein to ~10-20 mg/ml (for crystallography). Mass spectrometry and sodium dodecyl sulphate polyacrylamide gel electrophoresis (SDS PAGE) were used to confirm the purity of final preparations.

2.3 X-ray Crystallography

864 random crystallization conditions (Qiagen) were set up using a Phoenix robot in 96-well Intelliplates (Hampton Research) and implementing sitting-drop vapour diffusion. Fine screens in 24-well VDX plates (Hampton Research) were performed around the conditions of any hits from the random screen. Crystals were obtained in these fine screens by hanging-drop vapour diffusion. RyR1 1-536 for soaking experiments was crystallized as before (Tung et al. 2010) at 4°C in solution of 20-40% (vol/vol) saturated ammonium sulphate ($(NH_4)_2SO_4$), 0.1 M Bicine pH 9 and 12% glycerol (vol/vol). Resulting crystals were soaked in 20-40% $(NH_4)_2SO_4$, 0.1 M Bicine pH 9, 25% glycerol and 90% (vol/vol) caffeine for at least 20 minutes before being flash-frozen in liquid nitrogen. RyR1 217-536 was co-crystallized by C-C. Tung in 0.1M Tris 8.0, 15-25% PEG 3350 and 30 mM caffeine and placed in a cryoprotectant of the same condition but with 25% glycerol before flash-freezing. RyR1 1-617 crystals were obtained at room temperature in a condition of 5-15% (w/vol) PEG 2000 MME, 0.1 M NaCl, 0.1 M Tris 6.5-8.0, with or without 90% (vol/vol) saturated dantrolene (in drop) and frozen in cryoprotectant of the same condition with 25% glycerol.

Datasets were collected at two Rigaku homesources and two synchrotron beamlines: the Canadian Light Source (CLS) beamline 08ID-1 and the Advanced Photon Source (APS) beamline 23-ID-D-GM/CA. RyR1 1-536 caffeine-soaked crystals produced datasets for final refinement at CLS 08ID-1. RyR1 217-536 and caffeine co-crystals produced datasets for final refinement at APS 23-ID-D-GM/CA. Two datasets were chosen for refinement on RyR1 1-617: A native crystal dataset from a homesource to 2.7 Å and a dataset from a crystal grown and frozen in the presence of dantrolene, which was taken at CLS 08ID-1 and exhibited diffraction to 2.2 Å.

Data processing from CLS was done using their autoprocess program, whereas data processing from APS was done using their online graphical user interface (GUI). In both cases, their automated programs used XDS (Kabsch, 2010). Processing from the homesource was done using HKL2000 (Minor et al. 2006).

In all cases, individual domains from PDB 2XOA (Tung et al. 2010) were used as models for molecular replacement using the program Phaser (Storoni et al. 2004). Successive rounds of manual building in COOT (Emsley and Cowtan, 2004) followed by refinement with REFMAC (Murshudov et al. 1997) led to the structures presented here.

2.4 ITC

Proteins were dialyzed against buffer F at 4°C with 14 mM βME if the construct contained cysteines. In the case of RyR1 4071-4138, samples were dialyzed once in the buffer F supplemented with 10 mM ethylenediaminetetraacetic acid (EDTA) pH 8.0, then dialyzed three to four times in buffer F to ensure neither Ca^{2+} nor EDTA were present. Small molecules and the RyR1 CaMBD 4295-4325 mutant were dissolved in buffer from the dialysis chamber on the day of the experiment. A 6M guanidine hydrochloride, 20 mM pH 6.5 phosphate solution was used to dilute protein samples for concentration measurement by absorbance at 280 nm (Edelhoch 1967).

In each experiment, 40 μl of titrant (small molecule or peptide) was added either as 20x2μl or 40x1μl injections to protein in the cell at a ~10 or ~20 fold lower concentration and stirred at 1000 rpm. Experiments on RyR1 4071-4138 and 1-617 were performed at 25°C while those on RyR1 1-536 and 217-536 were performed at 4°C, on an ITC200 instrument (GE Healthcare). Origin 7.0 was used to process all data and determine values for binding constants (K_a), Gibb's free energy (ΔG), enthalpy (ΔH), entropy (ΔS) and stoichiometry (n). The measured change in heat between injections (ΔQ(i)) due to the injection of dV_i μl of titrant into the active cell volume (V_o) is calculated by the equation:

$$\Delta Q(i) = Q(i) + \frac{dV_i}{V_o}\left[\frac{Q(i) + Q(i-1)}{2}\right] - Q(i-1)$$

From this K_a, ΔH, and n are determined by fitting to the equation:

$$Q = \frac{nM_t \Delta H V_o}{2}\left[1 + \frac{X_t}{nM_t} + \frac{1}{nK_a M_t} - \sqrt{\left(1 + \frac{X_t}{nM_t} + \frac{1}{nK_a M_t}\right)^2 - \frac{4X_t}{nM_t}}\right]$$

The macromolecular (M_t) and ligand (X_t) concentrations are additionally corrected to account for displaced volume effects which occur with each injection.

ΔG and ΔS are obtained from their relationship to the calculated values of ΔH and K_a ($1/K_d$, where K_d is the dissociation constant):

$\Delta G = -RT\ln K_d$ and $\Delta G = \Delta H - T\Delta S$

2.5 *in silico* Docking - RyR1 1-617 into Cryo-EM Maps

The program ADP_EM (Garzón et al. 2007) was used to dock the RyR1 1-617 crystal structure into three different cryo-EM maps: EMDB 1275 (Ludtke et al. 2005), EMDB 1606 (Samsó et al., 2009) and EMBD 1607 (Samsó et al., 2009). The following command was used for all docking:

adp_em <em_map.ccp4> <crystal_structure.pdb> <bw> <em_map_resolution> <cutoff>

In any run, the bandwidth (<bw>) and density threshold value of the map (<cutoff>) were set to 16 and 0.06 respectively. The program does not consider density levels below the density threshold value. Higher bandwidth values, used in a harmonic transformation step of the docking would increase the rotational accuracy.

Laplacian filters were used by default in all runs given their necessity in the docking of small crystal structures into large EM maps (Wriggers and Chacón, 2001, Chacón and Wriggers, 2002).

ADP_EM works by rotating and translating a simulated probe map, obtained by blurring the resolution of the atomic structure to be docked, to maximize a correlation function between it and a target experimental EM map (Garzón et al. 2007). Bar charts of docking contrast were made by taking these correlation values from the docking log file and plotting them in Microsoft Excel (2008).

2.6 *in silico* Docking - Caffeine into RyR1 1-536

Two separate programs were used to dock caffeine to the RyR1 1-536 (RyR1 ABC) crystal structure: AutoDock (Morris et al. 2009) and the DOCK 6 program suite from the University of California, San Francisco (Shoichet et al. 1992, Meng et al. 1992, Kuntz et al. 1982). In both programs, 10 standard docking runs were carried out and results were grouped into clusters that contained similar docking sites. Microsoft Excel (2008) was implemented to rank the hits according to binding energy (AutoDock) and grid score (DOCK). Initial files for DOCK were created using UCSF Chimera (Pettersen et al. 2004).

3 Results

3.1 A New Structural Domain

In the crystal structure of the first three domains of RyR1, there was intrepretable electron density up to residue 532 (Tung et al. 2010). The Protein Homology/analogY Recognition Engine version 2.0 (PHYRE^2) (Kelley and Sternberg 2009) helped in defining the rough boundaries for a fourth domain. To account for any errors in theoretical modelling, six different N-terminal constructs with different ending points were cloned: RyR1 1-608, 617, 627, 635, 644 and 654 (N1 to 6 respectively).

Expression was detectable for all six fusion proteins by SDS-PAGE but only the 1-617 construct had a significant amount of soluble material (Figure 11A and 11B). The calculated molecular weights of the smallest and largest fusion proteins were ~112 and ~117 kDa respectively. RyR1 1-617 was subjected to purification by column chromatography and yielded soluble, monomeric protein on a gel filtration superdex column (Figure 11C). Figure 11D shows an example SDS-PAGE gel from a purification. The gel filtration chromatogram shows that multiple oligomeric states of the protein exist in solution, but the monomeric fraction re-runs as a monomer on a subsequent superdex column.

RyR1 1-617 crystals diffracted to 2.7 Å at the in-house X-ray source (Figure 12). After solving the phase problem by using PDB 2XOA (Tung et al. 2010) as a molecular replacement model, its structure was deciphered. Crystals grown in the presence of dantrolene diffracted to 2.2 Å at the CLS synchrotron. Table 2 shows the statistics from both datasets.

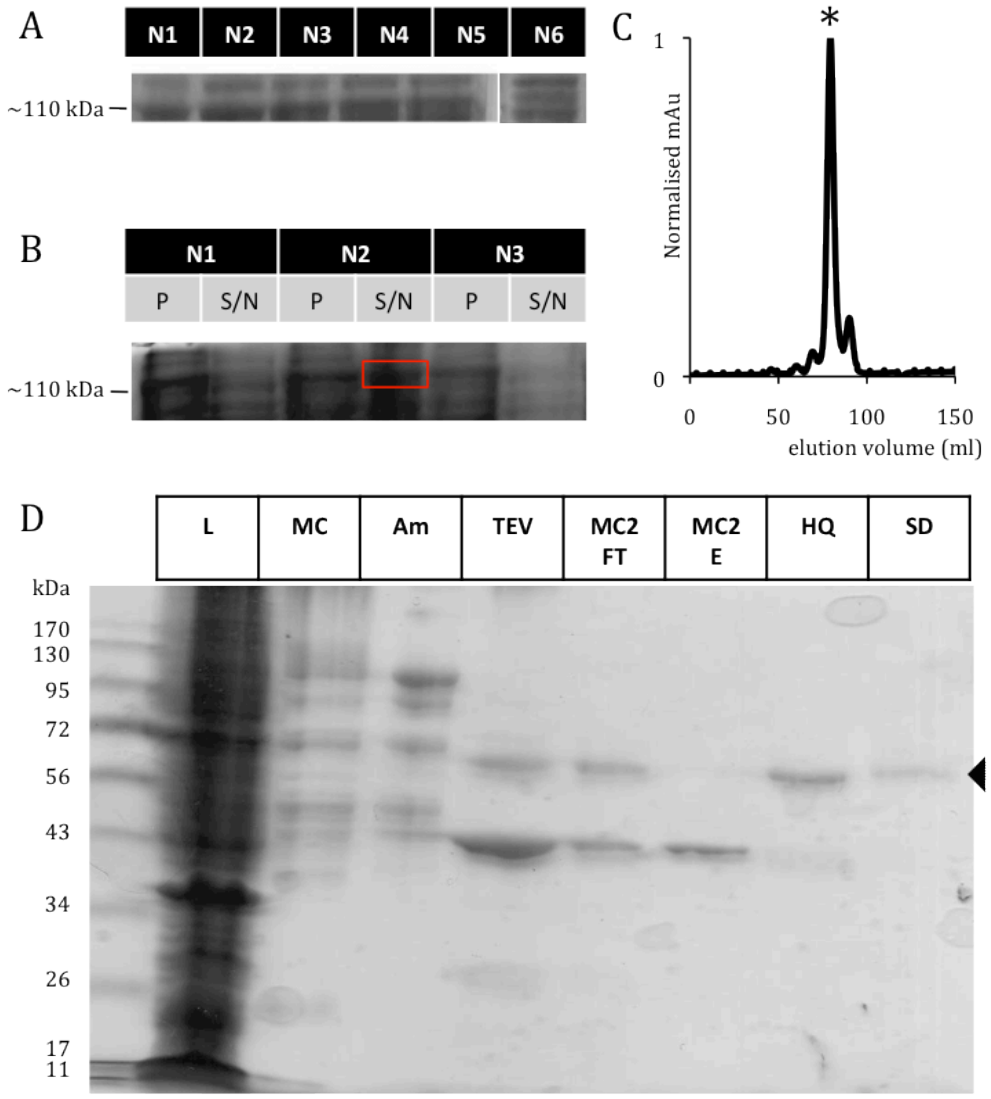

FIGURE 11. **Expression, solubility and purification of N-terminal constructs.** **A)** Expression of N1 through N6. The negative control is not shown but comparison of the six constructs shows a clear trend in expression of an increasing MW band from N1 to N6. **B)** Solubility tests on N1, N2 and N3 clearly show that only N2 contains soluble material (*red box*) in the supernatant following lysis and centrifugation. Note: the N6 expression is from a different SDS-PAGE gel and is shown here for illustrative purposes only. **C)** A gel filtration column superdex column elution profile shows that a monomer (*) does exist and can be separated. **D)** A purification gel of RyR1 1-617 (*triangle*) showing the lysis supernatant (*L*), first nickel column elution (*MC*), amylose elution (*Am*), TEV-cleaved sample (*TEV*), post-TEV nickel flowthrough (*MC2FT*) and elution (*MC2E*), anion exchange column (*HQ*) and gel filtration elution (*SD*) from a single prep.

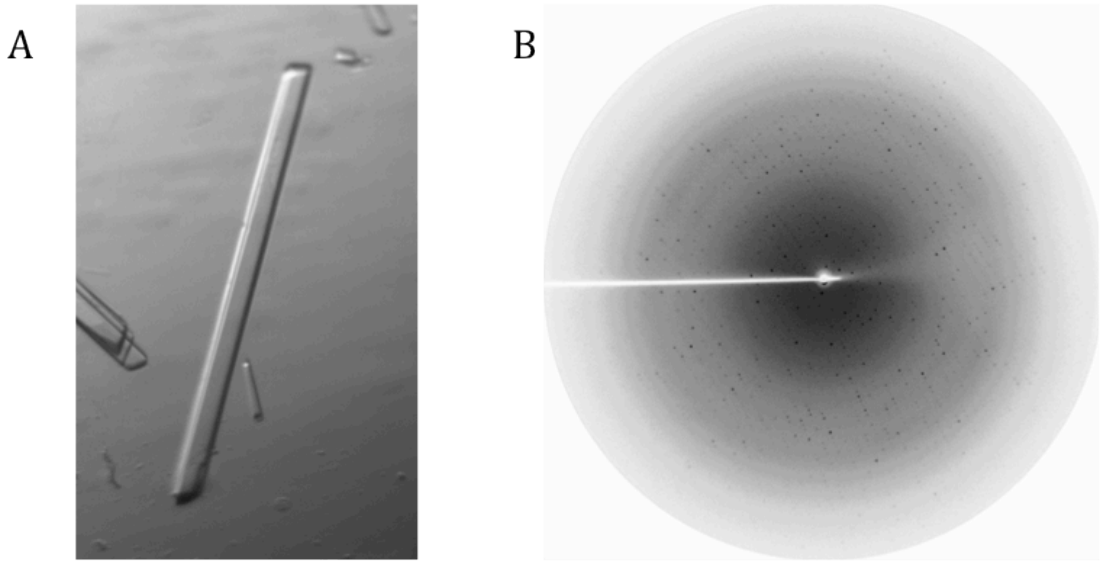

FIGURE 12. **RyR1 1-617 crystals.** Crystals of RyR1 1-617 (**A**) diffracted to 2.7 Å (**B**) at a homesource.

With the previously identified dantrolene binding site in RyR1 presumably located in residues 590-609 (Paul-Pletzer et al. 2002), there was a lot of interest in the RyR1 1-617 structure. There were two molecules in the asymmetric unit, but unfortunately, electron density was only visible to residue ~577 in both (Figure 13A). This meant that the C-terminal residues were too flexible to be trapped in a crystal lattice. Often, constructs are degraded to a stable core that can be crystallized, but mass spectrometry suggested that with a molecular weight of 68.6 kDa, the construct was still intact. The co-crystals with dantrolene, which diffracted to ~2.2 Å in the same space group again showed interpretable electron density to residue ~577, suggesting that dantrolene did not induce structure in the flexible part. The concentration of dantrolene in the soaking solution though was very limited due to the drug's inherent lack of solubility.

As expected, the first three domains look very similar to the ones already described by RyR1ABC: two beta trefoil domains followed by an α-helical bundle (Figure 13B).

	RyR1 1-617	RyR1 1-617 & Dantrolene
Data collection	Homesource	CLS
Space group	$P2_1$	$P2_1$
Cell dimensions		
a, *b*, *c* (Å)	69.3, 103.2, 128.7	69.2, 103.3, 127.9
α,β,γ (°)	90.0, 96.7, 90.0	90.0, 95.9, 90.0
Resolution (Å)	50.00-2.70 (2.80-2.70)	50.00-2.16 (2.22-2.16)
R_{sym} or $R_{meas.}$	11.7 (35.3) (R_{sym})	16.8 (152.2) (R_{meas})*
I / σ(I)	4.47 (1.83)	7.93 (1.16)
Completeness (%)	82.6 (45.3)	99.5 (98.9)
Refinement		
Resolution (Å)	127.86-2.70	47.86-2.35
No. reflections	38924	70630
R_{work} / R_{free}	27.98/31.23	29.12/31.49
No. atoms	8377	8339
Protein	8309	8272
Water	68	67
B-factors	39.57	35.34
Protein	39.33	35.13
Water	68.54	61.46
R.m.s. deviations		
Bond lengths (Å)	0.005	0.004
Bond angles (°)	0.861	0.776
Ramachandran (core/allowed %)	96.41/3.59	92.25/4.75

Table 2. **Data collection and refinement statistics for RyR1 1-617.** Values in parentheses are for the highest-resolution shell. The R-factor R_{sym} (Arndt al. 1968), obtained by HKL2000 (Minor et al. 2006) measures the qualtity of data collection. R_{meas}, obtained from XDS (Kabsch, 2010), is version of R_{sym}, modified to be redundancy independent (Diederichs and Karplus, 1997).

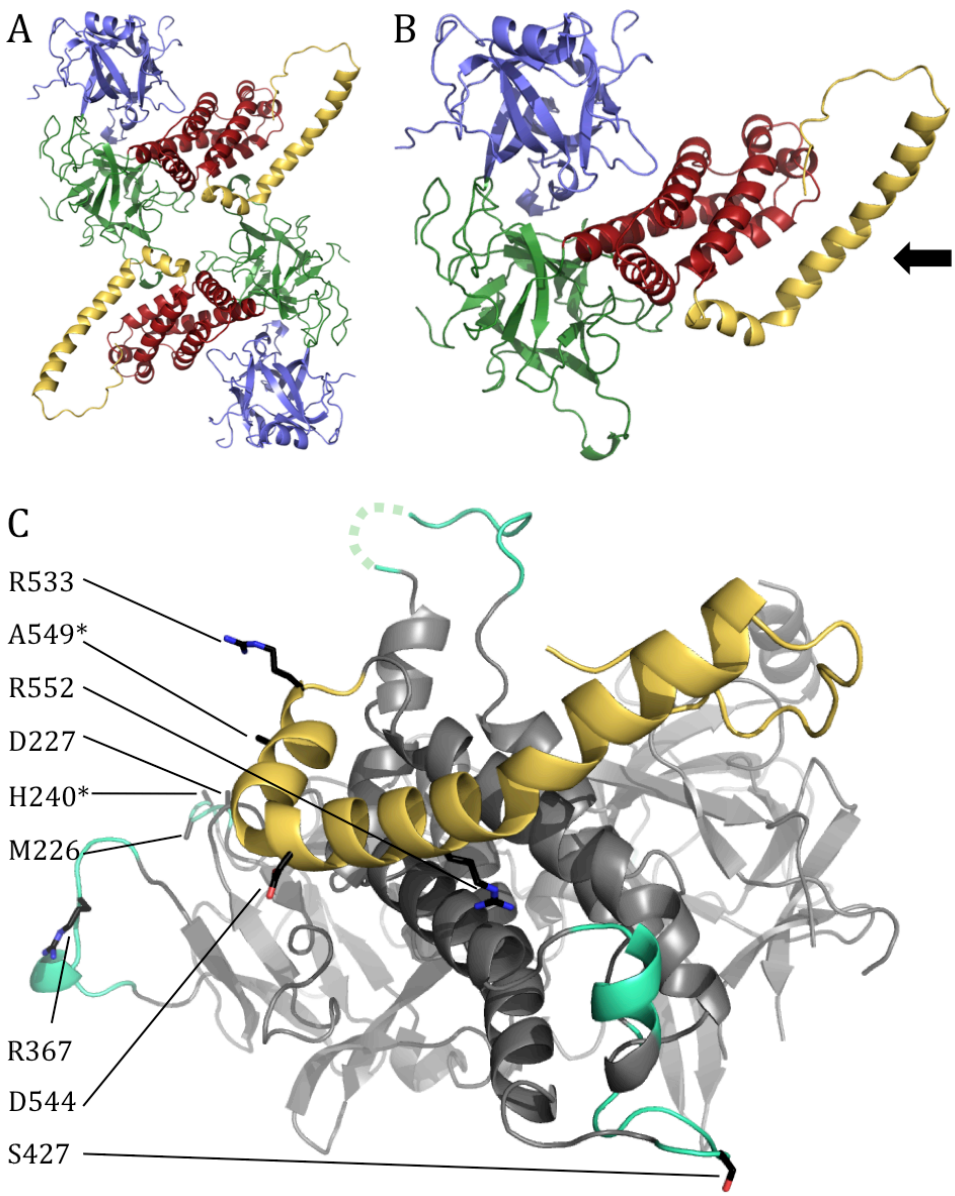

FIGURE 13. **RyR1 1-617 structure.** The protein crystallized with two molecules in the asymmetric unit (**A**), both of which show a similar structure to domains A (*blue*), B (*green*) and C (*red*) of PDB 2XOA (Tung et al. 2010). A 34-residue α-helix (*yellow*) describes the main structural addition (**B**). (**C**) RyR1 1-617 is shown from the direction of the arrow in (**B**), with everything gray except for the new helix (*yellow*) and some buildable loops (*teal*). Black side-chains highlight the sites of newly built disease mutation; due to inherent flexibility in the crystal structure, some side-chains have been truncated. Construct numbering: RyR1 *Oryctolagus cuniculus,* mutation numbering: RyR1 or RyR2 (*) *Homo sapiens.*

3.1.1 New Loops and Disease Mutations

The new structure extends ~45 residues at the C-terminus, compared to the previously published RyR1ABC structure (Tung et al. 2010). In addition, several loop regions, previously displaying poor density, could now be modelled. A detailed look at the sites of disease-causing mutations has already been performed on RyR1ABC (Tung et al. 2010), but due to flexibility in the crystal structure, some of the molecular insight was limited for a number of mutation sites. In this extended structure, we now observe seven additional mutation sites in RyR1, and two that correspond to mutations in RyR2 (Figure 13C). In addition, the structure provided some molecular insight into some mutation sites whose structures were already known, but whose interaction networks were not (Table 3 and Chapter 4.1.3).

New Information	**RyR1 Human Mutation**	**Disease**	**Reference**
Structure	M226K	MH	Levano et al. 2009
Structure	D227V	MH	Monnier et al. 2005
Structure	R367Q	MH	Galli et al. 2006
Structure	R367L	MH	Levano et al. 2009
Structure	S427L	CCD	Wu et al. 2006
Interaction	Q474H	MH, CCD	Ibarra et al. 2006
Interaction	Y522C	MH	Yeh et al. 2006
Interaction	Y522S	MH, CCD	Quane et al. 1994
Structure Interface	R533H	MH	Brandt et al. 1999
Structure Interface	R533C	MH	Tammaro et al. 2003
Structure Interface	D544Y	MH	Levano et al. 2009
Structure Interaction	R552W	MH	Keating et al. 1997
	RyR2 Human Mutation	**Disease**	**Reference**
Structure	H240R	CPVT	Tester et al. 2006
Structure Interaction	V507I	CPVT	Medeiros-Domingo et al. 2009
Structure Interface	A549V	CPVT	Medeiros-Domingo et al. 2009

TABLE 3. **Additional mutations or their interactions in the RyR1 1-617 structure.** The first column indicates whether the new information on a mutation site was solely in its structure, in its interaction network or its interface predictions.

3.1.2 Docking into Cryo-EM Maps

The RyR1 1-617 structures (2.2 Å and 2.7 Å) were docked into three available cryo-EM maps: EMDB 1275 (Ludtke et al. 2005), EMDB 1606 and EMDB 1607 (Samsó et al. 2009) using Laplacian filters. In all cases, the top four solutions corroborated the tetrameric vestibule found in the docking of RyR1ABC (Tung et al. 2010). To validate the docking, correlation coefficients were grouped into sets of four, to accommodate the inherent symmetry of the channel, and averaged for comparison. The top sets exhibited correlation coefficients that were 27, 92, and 98 times the standard deviation from the mean of the next ten sets for EMDB 1275, 1606 and 1607 respectively (Figure 14). These values for docking contrast are very high and add a great deal of confidence to the placement of the structure.

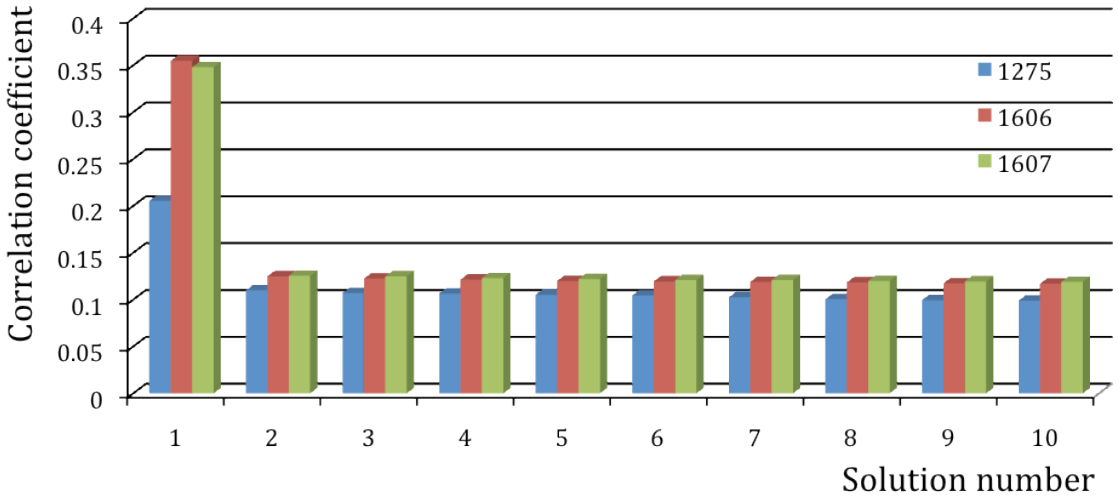

FIGURE 14. **Docking contrast.** The correlation coefficients of solutions from docking are shown for different maps. Each bar represents an average of four solutions that group due to the symmetry of the tetrameric channel.

Visualizing the interactions between subunits in RyR1 1-617 is best observed in structures docked into an EM map of a channel in the closed conformation (EMDB 1606). When examined we see that four B domains form the bulk of the central rim and combined with domain A, form the aforementioned vestibule. With the additional structural information from the extended helix from domain C, it seems that this third, helical moiety acts as a bridge between the central rim and the clamp region (Figure 15A, B and C). Looking at the new, visible disease mutation sites, there is a general agreement with previous findings. Disease-causing mutations occur at sites that would affect interactions between domains in RyR1. One interesting exception is the S427L (human RyR1) CCD-causing mutation that seems to be completely solvent accessible and not involved in interface interaction. Upon analysis though, Wu et al. (2006) showed that the mutation was sequenced as heterozygous and accompanied by another mutation that had previously been linked to CCD (Monnier et al. 2001, Romero et al. 2003). This suggests that the S427L mutation may not be a causative mutation for CCD.

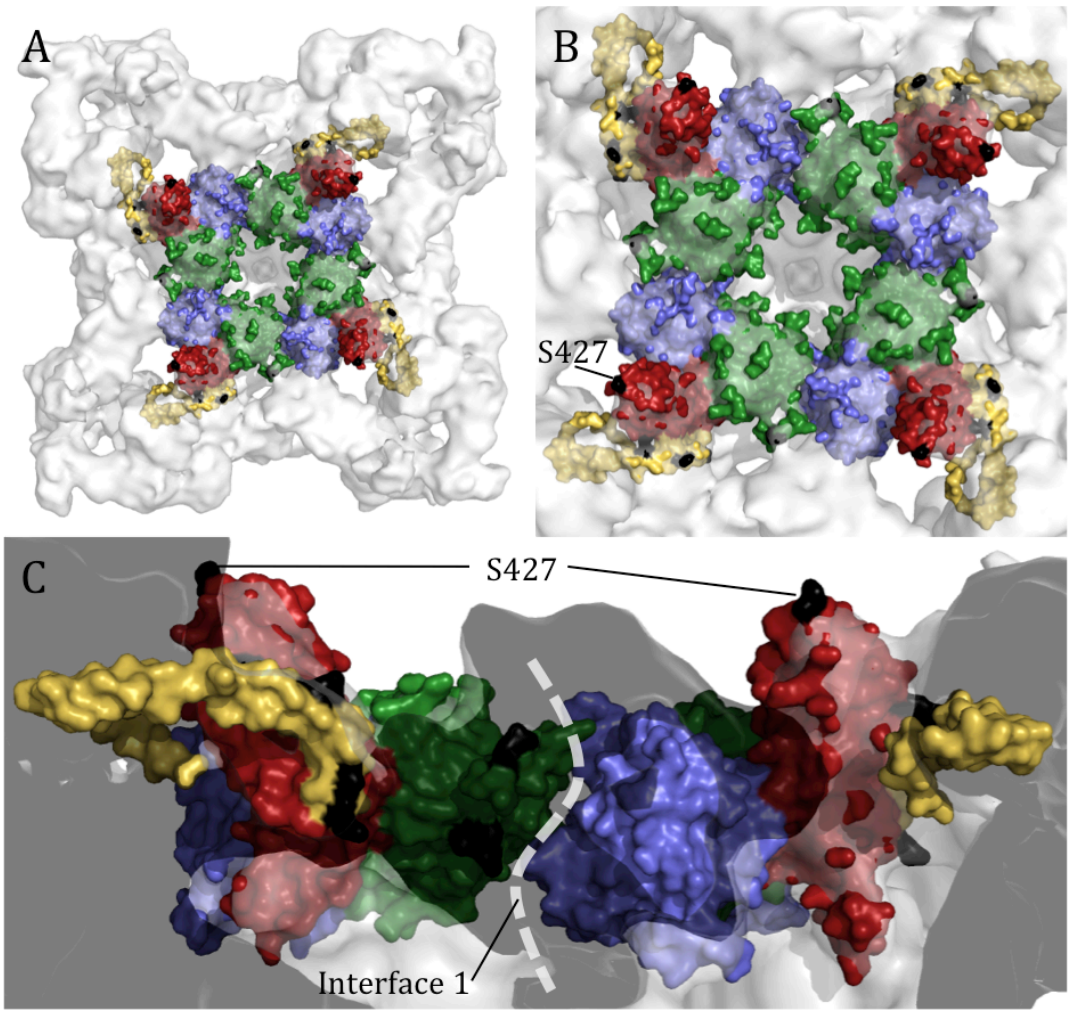

FIGURE 15. **Docking of the RyR1 1-617 crystal structure into EMDB 1606.** Docking into the closed conformation of RyR1 (Samsó et al. 2009) visually enhances the interactions between subunits. RyR1A (*blue*) and B (*green*) form a ring around the cytoplasmic pore as seen from the top view (**A**). Domain C (*red*) and its extended helix (*yellow*) attach between the two and seem to link the vestibule to domains in the clamp region. Zoomed in views from the top (**B**) and side (**C**) show that the new structural information on mutation sites from the structure generally agrees with previous results. Human mutations (*black*) except S427 (labelled) occur at interfaces between domains in the full-length channel and probably affect allosteric communication. Interface 1 (Tung et al. 2010) is labelled as a dashed white line. Note: blackened here are only newly structured mutation sites. A detailed analysis including mutation sites that *interact* with freshly built structural motifs is covered in Chapter 4.1.3. Constuct numbering: RyR1 *Oryctolagus cuniculus,* mutation numbering: RyR1 *Homo sapiens*.

3.1.3 Dantrolene Binding

Despite the lack of success in determining the structure of dantrolene bound to RyR1 1-617, as mentioned the measured molecular weight of the protein resembled that of full-length construct. Although crystals were grown in the presence of dantrolene, they were grown in a condition optimized for unbound RyR1 1-617. In the dynamic equilibrium of binding, large structural rearrangements may be required. Experiments such as this can bias structures to the assembly most beneficial for crystal lattice formation, and not one suited for binding. This effectively pulls unbound RyR1 1-617 out of solution and into crystal formation. It is then possible that in solution, binding to dantrolene could still be occurring and we could not eliminate the possibility based purely on the lack of crystallographic evidence.

ITC experiments performed by K. Lau were carried out in an attempt to clarify whether RyR1 1-617 does in fact contain the dantrolene binding site. Both dantrolene, and its more water-soluble homolog azumolene showed no measurable affinity between the two (data not shown). This is in direct conflict to earlier work in the field (Paul-Pletzer et al. 2002). However, ITC measurements rely on changes in enthalpy. If a reaction is driven by entropy and is enthalpically silent, it cannot be detected. In addition, we aim to retry the experiment with a new batch of purified RyR1ABCD to make sure our observations are reproducible.

3.1.4 N-terminal Construct Summary

Several different constructs were tried before and after the crystallographic success of RyR1 1-617. Figure 16 shows a schematic of the constructs tried and Table 4 summarizes the problems and potentials in the attempted N-terminal clones.

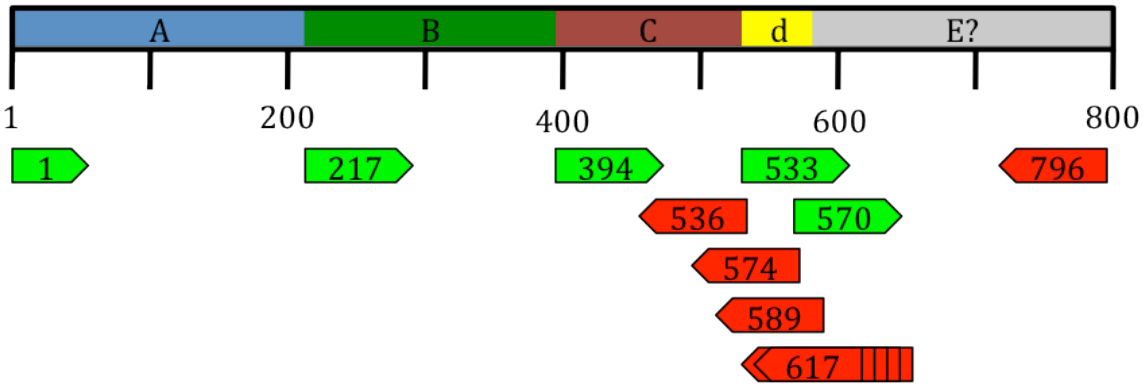

FIGURE 16. **N-terminal construct schematic.** An illustration describing the constructs attempted in the search for the next N-terminal RyR1 domain. Domains A, B and C from PDB 2XOA are coloured blue, green and red respectively, and the new structure from RyR1 1-617 is labelled 'd' and coloured yellow. Forward (*bright red*) and reverse (*bright green*) primers for construct PCR are numbered according to the first (forward) or last (reverse) amino acid they code for. Of the reverse primers ending at residues 607, 617, 627, 635, 644 and 654, only 617 is numbered. Numbering: RyR1 *Oryctolagus cuniculus*.

Construct	Expression	Solubility	Purification
1-536	18°C, ~24 hours	very soluble	Large yield, crystallized.
1-574	18°C, ~24 hours	slightly	Aggregate on SD
1-589	18°C, ~24 hours		Low yield, ~50% aggregate on SD
1-608	18°C, ~24 hours	slightly	N/A
1-617	18°C, ~24 hours	slightly	Purified successfully, crystallized
1-627	18°C, ~24 hours	slightly	Very low yield, stopped after first MC
1-635	18°C, ~24 hours	slightly	N/A
1-644	18°C, ~24 hours	slightly	N/A
1-654	18°C, ~24 hours	slightly	Low yield, ~50% aggregate on SD
1-796	18°C, ~24 hours	slightly	Digested into smaller domains by proteases, aggregate on SD
217-536	18°C, ~24 hours	very soluble	Large yield, sometimes crashes out upon addition of TEV. Lots of TEV and time required to cleave. Crystallized.
217-574	18°C, ~24 hours	slightly	50% aggregate on SD as fusion protein, low yield.
217-589	18°C, ~24 hours	slightly	Crashes out with TEV, associates with MBP
217-654	18°C, ~24 hours	slightly	Associates with MBP
394-574	18°C, ~24 hours	slightly	Lost on HQ
394-654	18°C, ~24 hours	slightly	Associates with MBP
533-796	18°C, ~24 hours	slightly	Some monomer attainable as fusion protein (~60% aggregate on SD)
570-796	18°C, ~24 hours	slightly	Mostly monomer on SD as fusion protein, low yield

TABLE 4. **N-terminal constructs.** A list of the different constructs attempted in the search for a crystallisable fourth domain from the N-terminus. The RyR1ABC and BC (1-536 and 217-536) constructs were made based on the PDB 2XOA – purification was optimized for these clones by C-C. Tung.

3.2 Caffeine Binding

RyR1 1-617 is responsible for a large portion of the full-length channels solvent exposed surface area with many large valleys and nooks available. With the large number of small molecules and ligands that have been shown to modulate RyR, it made sense to systematically test some of them, quantitatively for binding. Being relatively inexpensive and readily accessible, caffeine provided a great starting point.

The EC_{50} of caffeine on full-length RyR1 is ~2.8 mM (Groom et al. 2011). In order to detect binding with low affinities, high concentrations of protein and ligand are required for a better signal. Previously, C-C. Tung optimized the purification procedure for two, well-expressed constructs in RyR1 1-536 (RyR1ABC) and RyR1 217-536 (RyR1BC). Their levels of expression resulted in large yields that made high-concentration ITC feasible.

ITC experiments showed that caffeine bound RyR1BC and ABC with affinities of ~150 μM and ~520 μM respectively, (Figures 17A and 17B). With similar ΔH (~ -6000 cal/mol) and ΔS (~ -6 cal/mol/K) values this suggested that the caffeine-binding site was located in RyR1BC. The stoichiometry of the interaction remains somewhat of a mystery. An N value of ~0.5 could be explained either by errors in concentration measurement and preparation purity, or claim that a dimer of RyR1BC or RyR1ABC binds a single caffeine molecule. Interestingly, both dynamic light scattering and a calibrated gel filtration column output a molecular weight of ~110 kDa for RyR1ABC (MW: 59 kDa). However, these techniques provide a more accurate estimation of hydrodynamic radius than they do molecular weight.

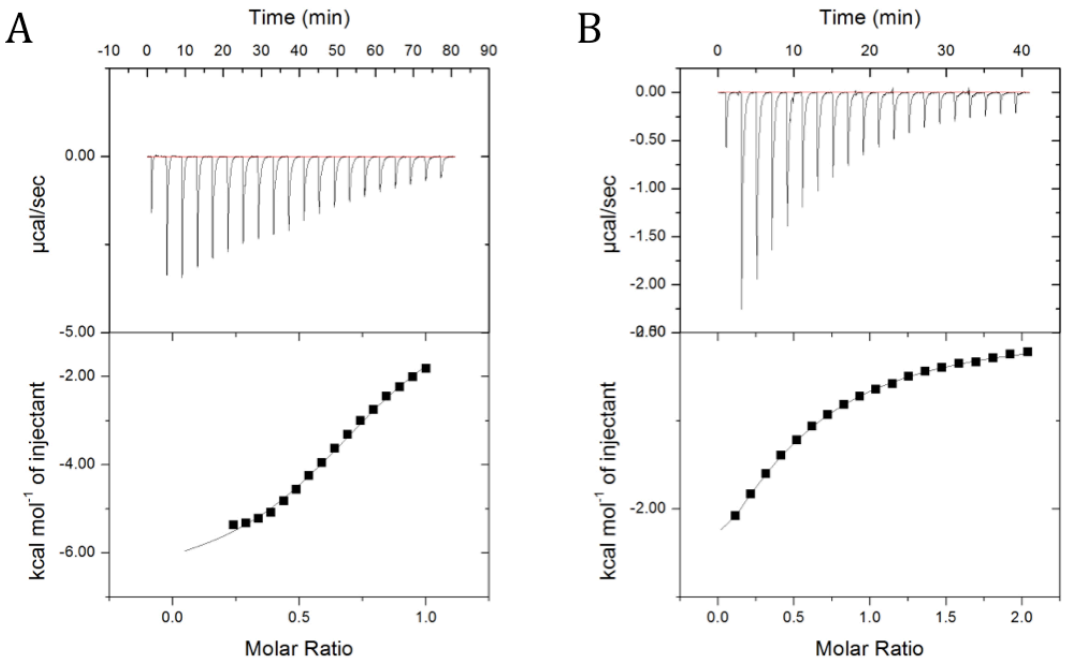

N	0.780	±0.00794 Sites	N	0.437	±0.0149 Sites
K_A	6.72E3	±602 M^{-1}	K_A	1.86E3	±57.5 M^{-1}
ΔH	-6759	±153.1 cal/mol	ΔH	-5426	±223.3 cal/mol
ΔS	-6.86 cal/mol/deg		ΔS	-4.62 cal/mol/deg	

FIGURE 17. **Caffeine binds RyR1BC.** ITC experiments in which (**A**) 15 mM caffeine was titrated into 1.5 mM RyR1BC and (**B**) 8.97 mM caffeine was added to 0.88 mM RyR1ABC. The integrations (*lower panels*) of the raw heats (*upper panels*) were fit to a one site binding model and outputted similar thermodynamic details of interaction suggesting RyR1BC accommodates the caffeine binding site.

3.2.1 Structural Insight?

In order to visualize the molecular details involved in caffeine binding, RyR1BC crystals were grown in the presence of 60 mM caffeine and RyR1ABC crystals were soaked in a 90% saturated caffeine cryoprotectant solution before flash-freezing. Data collection and refinement statistics for both RyR1BC and caffeine co-crystals, and RyR1ABC crystals soaked in caffeine, are shown in Table 5.

Analysis of the resultant structures showed that in both cases caffeine is indeed bound. To prove this, the F_O-F_C maps were calculated using models without the ligand. Positive difference density was visible to 9.56σ and 18.92σ in the RyR1BC and ABC structures respectively. In combination with the compelling density exhibited in the $2F_O$-F_C maps created from refinement on a model with caffeine, we could unquestionably confirm its presence (Figure 18).

However, in both cases, caffeine takes advantage of hydrophobic pockets and aromatic faces to stack somewhat promiscuously. Furthermore, the binding sites differ considerably between the two structures. Looking closely at the interactions involved in binding, we see that in the RyR1BC structure, caffeine recruits two tryptophan-269 (W269) residues from different RyR1B domains and two tyrosine-523 (Y523) residues from different RyR1C domains. It stacks between the tryptophans and sits on a hydrophobic bed provided by the two tyrosines ~ 4 Å away (Figures 18A and 18B). With RyR1ABC the interaction is a little more complex. Five RyR1A residues in total are involved, three from one protein chain, and two from a symmetry-related molecule. The main hold on the ligand can be attributed to an aromatic stacking sandwich between histidine-151 (H151) in the 'master' structure and phenylalanine-195 (F195) in a neighbouring molecule. Some specificity is created by proline-151's main-chain oxygen (P151) and a polar tyrosine-179 (Y179) in the master molecule, and a symmetry-related methionine-196 (M196), which completes a hydrophobic pocket (Figures 18C and 18D).

	RyR1BC & Caffeine	RyR1ABC & Caffeine
Data collection	APS	CLS
Space group	$P3_121$	R32
Cell dimensions		
a, *b*, *c* (Å)	68.6, 68.6, 133.0	170.6, 170.6, 300.9
α,β,γ (°)	90.0, 120.0, 90.0	90.0, 90.0, 120.0
Resolution (Å)	50.00-2.13 (2.19-2.13)	50.00-2.05 (2.10-2.05)
$R_{meas.}$	8.0 (163.1)	22.0 (763.7)
I / σ(I)	19.75 (1.56)	7.93 (1.16)
Completeness (%)	99.8 (98.0)	99.5 (98.9)
Refinement		
Resolution (Å)	59.38-2.30	132.62-2.40
No. reflections	15842	62534
R_{work} / R_{free}	23.92/30.63	20.23/23.14
No. atoms	2308	3931
Protein	2257	3802
Water	37	95
Caffeine	14	14
Other		20
B-factors	45.89	49.53
Protein	45.71	49.13
Water	50.44	57.81
Caffeine	62.41	52.02
Other	N/A	90.06
R.m.s. deviations		
Bond lengths (Å)	0.018	0.035
Bond angles (°)	1.756	2.638
Ramachandran (core/allowed %)	93.80/6.20	91.10/8.90

TABLE 5. **Data collection and refinement statistics for RyR1BC and RyR1ABC with caffeine.** Values in parentheses are for the highest-resolution shell. R_{meas}, obtained from XDS (Kabsch, 2010) is a redundancy independent R-factor (Diederichs and Karplus, 1997).

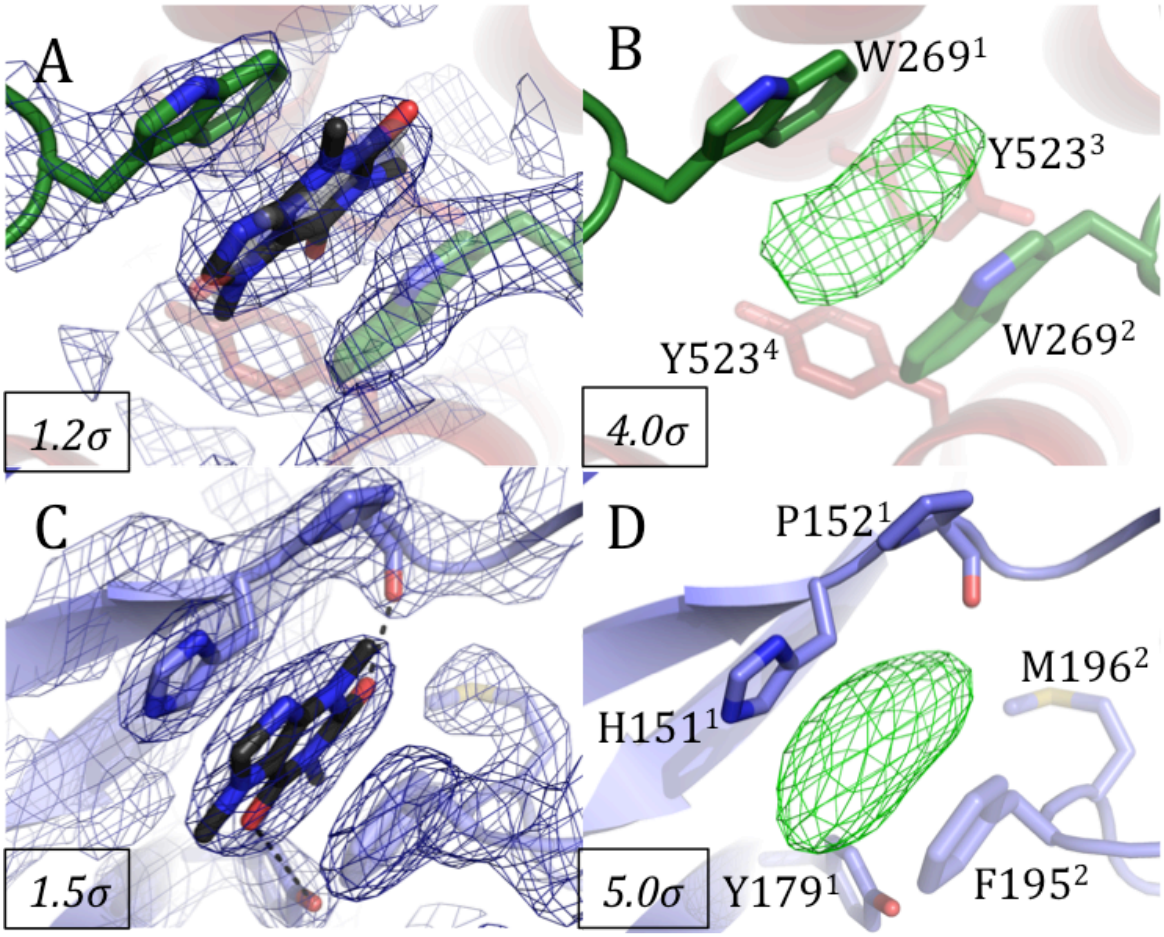

FIGURE 18. **Crystallographic caffeine binding interactions.** A detailed look at the binding of caffeine to RyR1BC (**A**, **B**) and RyR1ABC (**C**, **D**). The $2F_o$-F_c maps calculated from a model with caffeine built in are shown as blue meshes (**A**, **C**) and the F_o-F_c maps calculated from a model without caffeine built in are shown as green meshes (**B**, **D**). The sigma cut-offs for each map are labelled. Caffeine is shown as black sticks. Side-chains of interacting residues are shown as sticks and coloured according to the domain they belong (*blue* – RyR1A, *green* – RyR1B, *red* – RyR1C). Some non-carbon atoms are highlighted red (oxygen), blue (nitrogen) or yellow (sulphur). Residues are marked with a superscript number denoting which symmetry-related molecule they belong to (1 - master, 2,3,4 - symmetry-related). Numbering: RyR1 *Oryctolagus cuniculus.*

In RyR1BC, four different symmetry-related structures including the master molecule are involved in holding caffeine and both domains B and C are engaged (Figure 19A). Conversely, only RyR1A plays part in binding caffeine to RyR1ABC between two symmetry-related molecules (Figure 19B). The requirement of symmetry-related molecules strongly suggested that the binding sites observed might not occur in solution and prompted ITC experiments to confirm them.

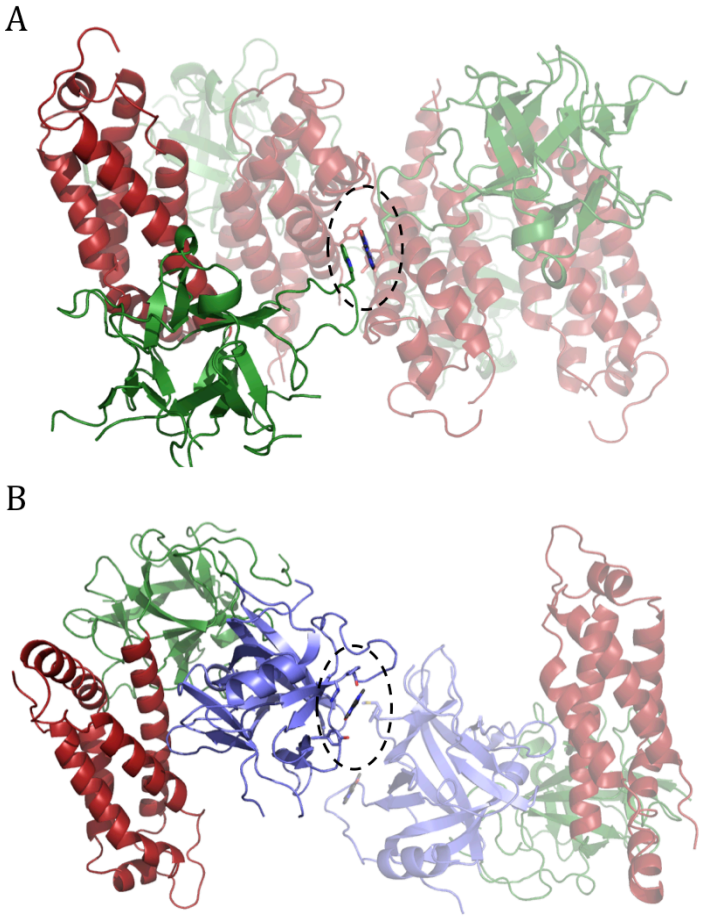

FIGURE 19. **Structural insight into caffeine binding to RyR?** Crystal structures of both RyR1BC (**A**) and RyR1ABC (**B**) are shown bound to caffeine. In both cases, interactions involve aromatic rings from symmetry-related molecules. Caffeine is shown in the dashed ring interacting with four RyR1BC molecules (**A**) or two RyR1ABC molecules (**B**). The side-chains of interacting residues inside the dashed ring are shown, and highlighted in figure 18. For RyR1ABC, only the residues (from both molecules) interacting with the caffeine from the 'master' molecule are shown. Domains A, B and C are coloured blue, green and red respectively.

3.2.2 W269A Mutant Binding

With conflicting results between crystal structures, the search instead for the binding site in solution began. With the knowledge that both RyR1 BC and ABC bind caffeine with the same general thermodynamic parameters, we focused first on the information from the RyR1BC co-crystal structure, as the soaking experiments with RyR1ABC yielded a binding pocket in domain A alone. More specifically, we began investigation into W269, and its potential as a caffeine binder.

To test this, W269 was mutated to an alanine in RyR1BC (Figure 20A). The mutant construct expressed and purified as normal, indicating the mutation was not destructive to the overall folding of the protein. An ITC experiment showed binding with an affinity ~300 μM, and similar values of ΔH, ΔS and N to those of the wild-type protein (Figure 20B). Evidently, W269 is not the binding site of caffeine in solution. The RyR1BC-caffeine structure represents a crystallographically trapped conformation. The high concentrations of caffeine used in crystallography seemed to promote caffeine's non-specific attachment to aromatic residues. This conclusion can be extended to the RyR1ABC-caffeine structure, which disagrees with our ITC results.

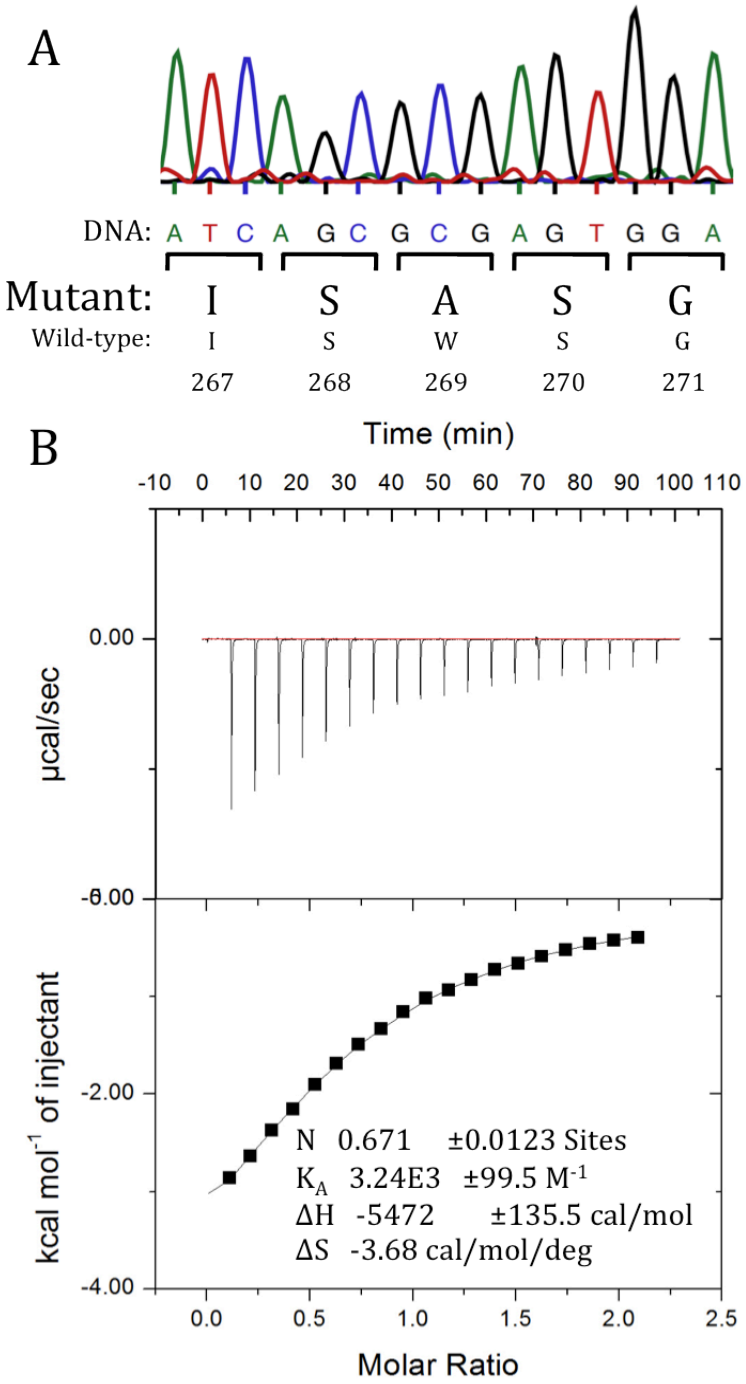

FIGURE 20. **W269A mutation. (A)** A section of the chromatogram from a sequencing reaction (Eurofins) showing the successful mutation of W269 to an alanine. Two bases were changed simultaneously by Quikchange in the mutation from a TGG triplet codon to GCG. **(B)** 6mM caffeine was titrated into 0.575 mM RyR1BC W269A. The calculated thermodynamic values were similar to those obtained from the same experiment with wild-type RyR1BC (Figure 17). Numbering: RyR1 *Oryctolagus cuniculus*.

3.2.3 An *in silico* Search for a Caffeine Binding Site

The programs DOCK (Shoichet et al. 1992, Meng et al. 1992, Kuntz et al. 1982) and AutoDock (Morris et al. 2009) were implemented to search for potential sites for caffeine binding in RyR1ABC. Each program outputs different scoring numbers that were used in choosing hits for analysis. AutoDock scores based on intermolecular energy, internal energy and torsional energy. A 'docking energy' is computed by combining the first two, and a 'binding energy' from the first and third. DOCK uses a grid score that is based on the electrostatic energy and Van der Waals forces. In addition, given their importance in small-molecule docking (Mackey and Melville, 2009), the cluster numbers of each hit were taken into account. It is worth noting that in both cases, the number of docking runs is very low (10 runs) and a more exhaustive dock will be done in the future to add validity to the results.

From DOCK, seven solutions from ten runs were ranked according to their grid score (the second ranked run had three species in its cluster, and the third had two). Analysis of the hits though showed that the top five clusters contained caffeine in the same site but rotated or flipped. This is unsurprising given the pseudo-symmetry of the molecule. As a result, these runs were combined manually, increasing the number of species in the top cluster (D1) to eight. AutoDock offered five solutions from ten runs; the first ranked solution (AD1) had the best binding energy and a cluster number of 6. With both programs, there seemed to be a clear docking contrast between the top solutions (D1 and AD1) and the rest (Figures 21A and 21B), but the physical locations of these solutions did not match each other. Besides the top ranked solutions, one more from DOCK (D2) and three from AutoDock (AD2, AD3 and AD4) were analysed based on their docking positions.

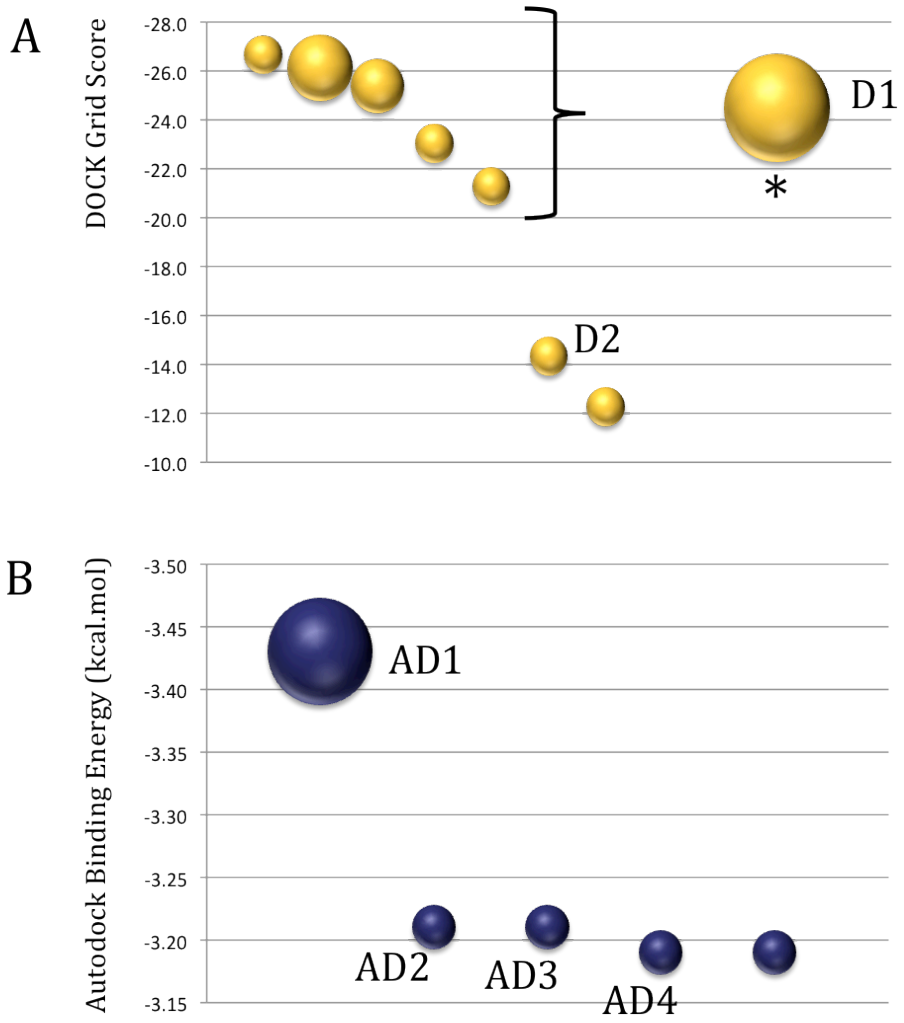

FIGURE 21. **DOCK and AutoDock scoring bubble charts.** (**A**) DOCK (Shoichet et al. 1992, Meng et al. 1992, Kuntz et al. 1982) grid scores for the docking of caffeine into RyR1ABC. The cluster number is reflected in the size of each bubble. The top five hits based on grid score were all located in the same pocket but with caffeine rotated, consequently for examination, they were averaged and their cluster numbers added to produce the last bubble (*) labelled D1 (cluster number = 8). In addition, D2 (cluster number = 1) was chosen for analysis. (**B**) The binding energies from AutoDock (Morris et al. 2009) are shown with cluster numbers represented by bubble size. Solutions AD1-4 were chosen for analysis.

In summary, four different sites were identified as having potential for caffeine binding (Figure 22A). Site 1 contains D1 and AD2, further increasing the cluster number (Figure 22B). Binding involves four residues, all in domain B and therefore agreeing with ITC results that suggested caffeine bound in RyR1BC. Site 2 also houses a solution from each computational program in D2 and AD3. It locates at the interface between domains A and B, engaging residues from both, and is in close proximity to W269, the culprit for binding in the RyR1BC structure (Figure 22C). Site 3 represents the top hit from AutoDock (AD1) and suggests only residues in domain A are required for binding (Figure 22D). Lastly, site 4 places caffeine close to the location determined by the RyR1ABC caffeine-soaked crystal structure (Figure 22E).

With our preliminary, rigid docking, one of the sites determined does stand out in site 1. As mentioned, it is the only site that does not involve RyR1A, and therefore agrees with our ITC results. Adding to its validity is the presence of an MH causing disease mutation R328W (R329 in *Oryctolagus cuniculus*)(Loke et al. 2003), which is located in very close proximity to this caffeine binding site (Figure 22B). Caffeine sensitivity could be explained in this disease mutant by an increase in affinity for the drug due to stacking interactions with the tryptophan. Future ITC experiments on RyR1 ABC mutants in site 1, including R329W, will hopefully shed light on the physiological and functional binding site of caffeine in RyR1ABC.

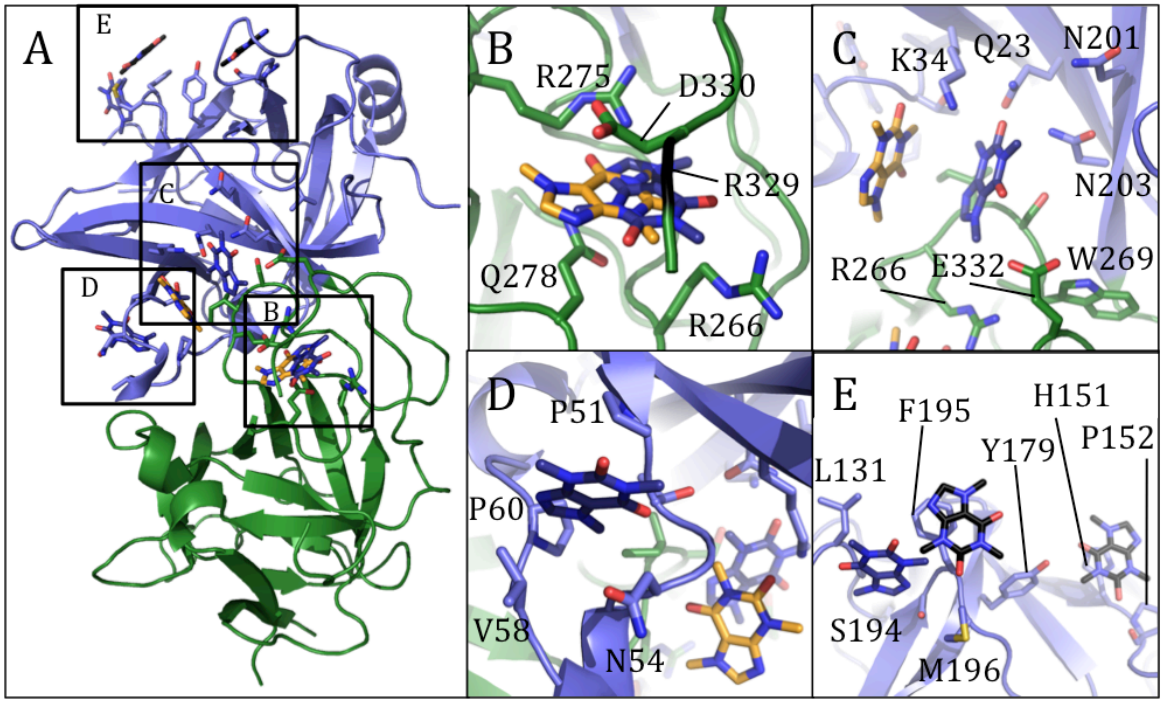

FIGURE 22. **Docking caffeine *in silico*.** (**A**) A look at some docking solutions from both AutoDock (Morris et al. 2009) and DOCK (Shoichet et al. 1992, Meng et al. 1992, Kuntz et al. 1982) programs. Caffeine is coloured according to which method positioned it, AutoDock (*dark blue*), DOCK (yellow) or crystal structure (black). The results could be summarized into four locations: (**B**) Site 1, which contained D1 and AD2. The position of an R329 disease mutation site is marked by a black main-chain. (**C**) Site 2, which contained D2 with AD3 nearby in the same binding pocket. Not labelled are residues I267 and S268 directly behind the blue caffeine molecule. W269, the residue involved in binding caffeine in the RyR1BC structure is in close proximity to site 2. (**D**) AD1, the top solution from AutoDock. (**E**) AD4, near one of the sites seen in the RyR1ABC crystal structure. Interacting residues are labelled and domains are coloured blue (domain A) and green (domain B). Note: although the docking studies were performed using RyR1ABC, domain C is not shown for clarity. Boxes on (**A**) are drawn to indicate the rough positions of the sites highlighted in the following panels. Numbering: RyR1 *Oryctolagus cuniculus*.

3.2.4 ATP Binding Experiments

Given the similarities in structure between different purine derivatives, it made sense to test binding to ATP as well. Some problems though halted progress in determining whether or not the coenzyme bound RyR1ABC. Presumably due to its reactive nature, titrating high concentrations of ATP into buffer alone resulted in very large heat signals (data not shown). As a result more dilute solutions had to be used in ITC measurements; a serious problem given the compound's millimolar EC_{50} on RyR (Meissner et al. 1986).

ITC did indicate some heat that is significantly different from background dilution experiments, but the curve was too shallow to fit reliably (Figure 23). It will be interesting to try the experiment with higher concentrations of adenine instead of ATP, which may lead to smaller dilution heats.

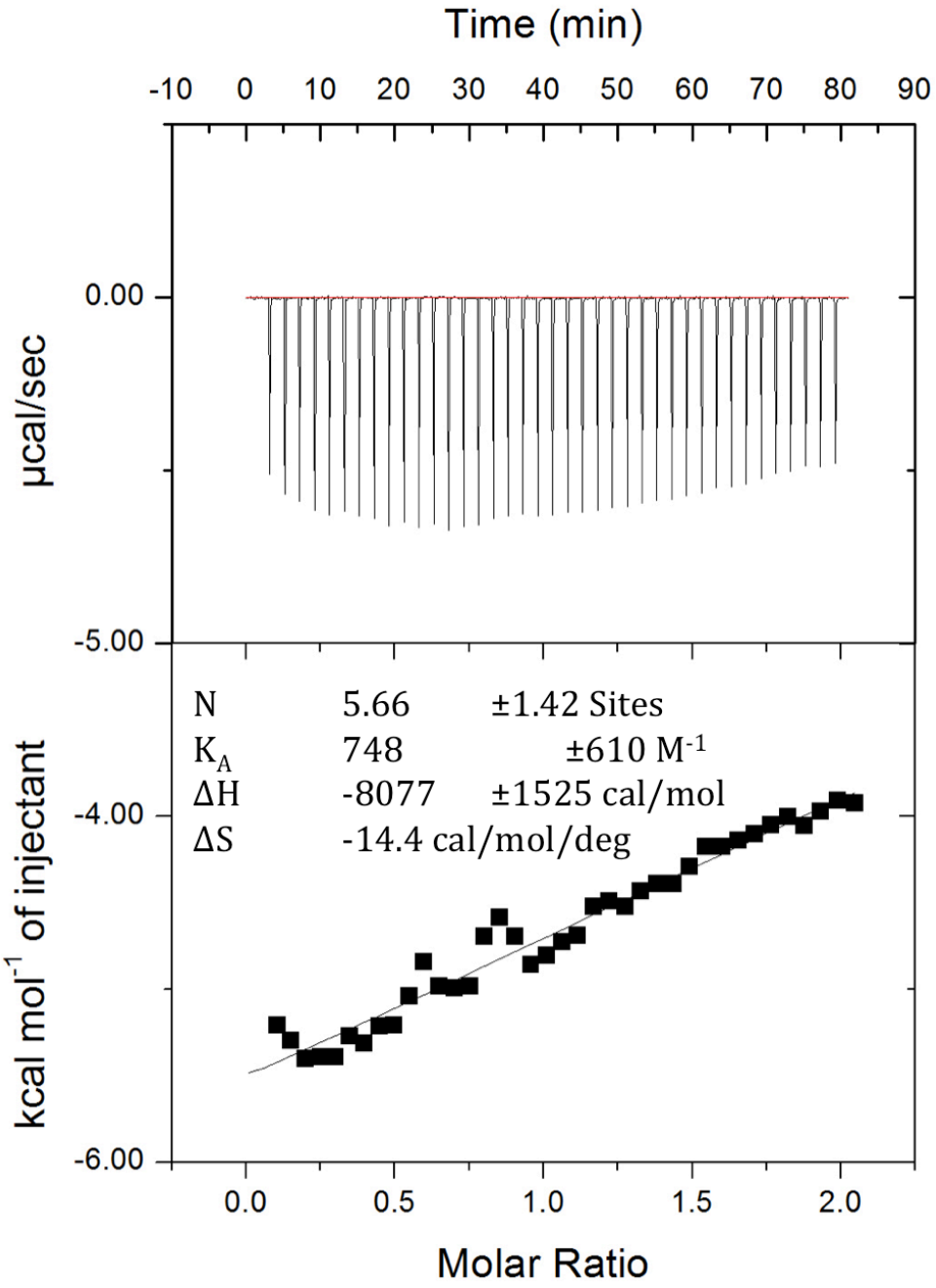

FIGURE 23. **ATP binding to RyR1ABC.** *5* mM ATP was titrated into *500* µM RyR1ABC and an affinity of ~1.3 mM was attained by ITC measurements. With the errors associated though, the thermodynamic values shown cannot be fully trusted.

3.3 RyR1 4071-4138

Xiong et al. (2006) have previously described a construct in RyR1, encompassing residues 4064-4210, which after refolding, binds Ca^{2+}, $Ca_V1.1$ and RyR1 CaMBDs. A few main areas of improvement remain from their work. Firstly, a well-behaved, soluble construct that does not require refolding would strengthen their claims of specific binding. Secondly, quantifying the thermodynamic details of the interactions, using ITC for example, would allow us to test whether the binding affinity is in a physiological range. Ideally, co-crystallization with proposed binding partners would provide the most insight. Both goals rely heavily on the ability to obtain a soluble domain that does not aggregate. PHYRE^2 (Kelley and Sternberg 2009) was implemented again to aid in the location of a soluble EF-hand-containing domain. Several possible constructs were tried from these results, based on alignment with actinin (RyR1 ~3500-4140), Ca^{2+}-binding protein 40 – CaBP40 (RyR1 ~3830-4140), parvalbumin (RyR1 ~4030-4140) and CaM (RyR1 ~3980-4140). A summary of the successes and failures in purification are described in Table 6 and a schematic that sums up the PHYRE^2 results is shown in Figure 24A. Constructs were tested for expression (Figure 24B) and solubility by small-scale purification of ~30 ml cultures on cobalt gravity columns. Successful constructs were scaled up and purified by fast protein liquid chromatography.

Construct	Expression	Solubility	Purification
3487/3497/3507 - 4128/4138/4148	Slightly 30°C, ~5-6 hrs induction.	All nine constructs not soluble	Not soluble
3818/3828/3838 - 4128/4138/4148	Slightly 30°C, ~5-6 hrs induction	All nine constructs not soluble	Not Soluble
3997-4070	Success 30°C, ~5-6 hrs induction	Soluble	Difficult to purify- does not absorb at 280 nm Crashes out in concentrator
3997-4138	Success 30°C, ~5-6 hrs induction	Soluble	Multiple species in gel filtration Variable success on HQ
4024/4031/4041 - 4128/4138/4148	Success 30°C, ~5-6 hrs induction	All nine constructs **are** soluble	RyR1 4041-4138 was the most soluble (see below)
4041-4138	Success 30°C, ~5-6 hrs induction	Soluble	Successfully purified, but low yield
4071-4138	Success 30°C, ~5-6 hrs induction	Soluble	A lot of pure, soluble protein attainable

TABLE 6. **EF-hand constructs.** A list of the different constructs attempted in the search for an EF-hand-containing domain.

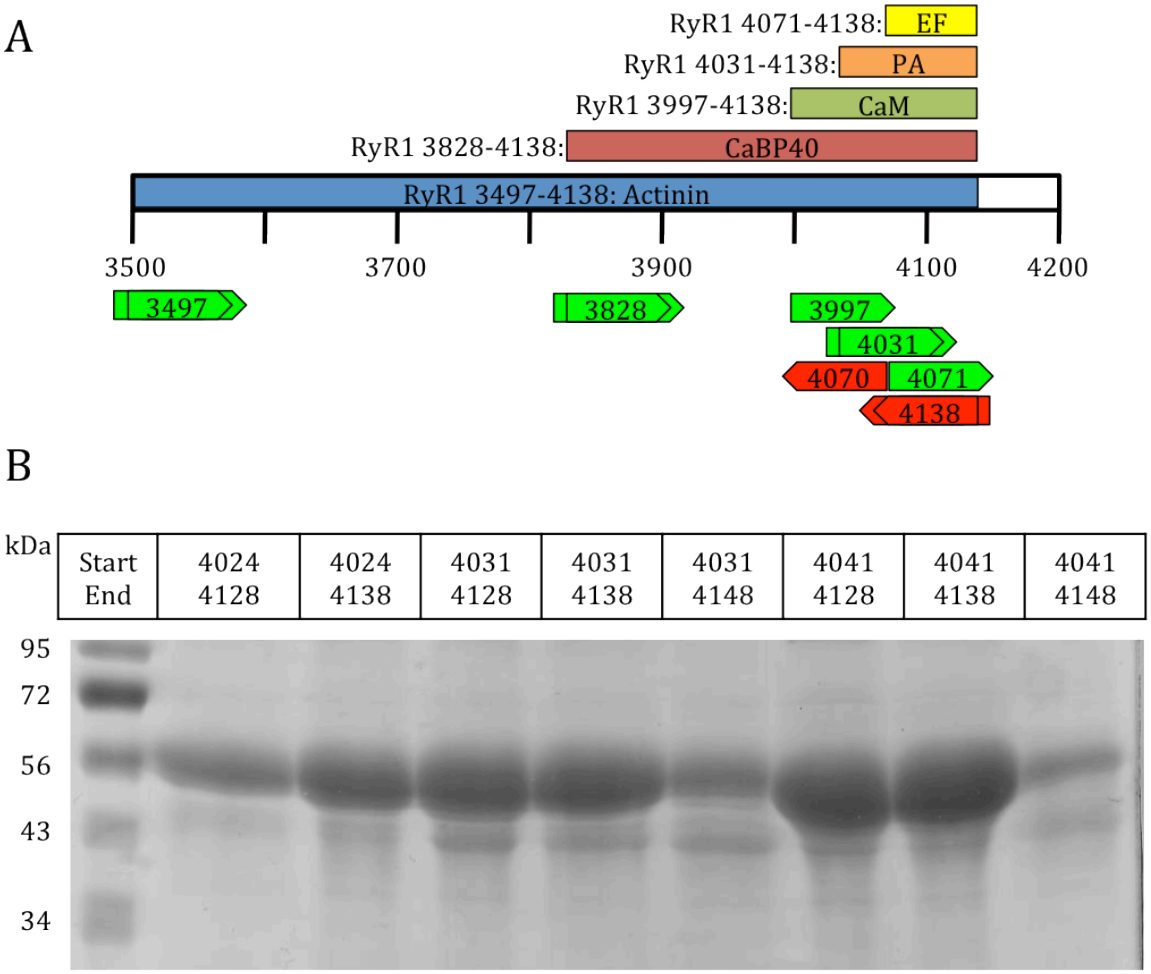

FIGURE 24. **Expression of PHYRE² guided domains.** (**A**) A schematic describing the constructs attempted using homology information from PHYRE² (Kelley and Sternberg 2009). Forward (*bright red*) and reverse (*bright green*) primers for construct PCR are numbered according to the first (forward) or last (reverse) amino acid they code for. For systematic primers (± ~10 residues), only the middle one is labelled by number (see Table 1 for a list of primers). (**B**) An example gel showing the expression of some of the constructs tried in the search for RyR1 EF-hands. The molecular weights (MW) of the fusion proteins range from ~54 kDa (RyR1 4041-4128 + MBP) to ~58 kDa (RyR1 4031-4148). Numbering: RyR1 *Oryctolagus cuniculus.*

The most promising constructs showed homology to CaM: Individual CaM lobes (PDB 1CLL, Chattopadhyaya et al. 1992) could be superposed onto a RyR1 EF-hand model generated from PHYRE^2 (Kelley and Sternberg 2009) (Figure 25A). From the structural alignment we could analyze the potential for Ca^{2+}-binding in the predicted EF-hands. Of the four modelled, only the most C-terminal one (EF-hand 4) portrays a probable binding site. In the others, hydrophobic or basic residues position themselves in locations that would need to co-ordinate Ca^{2+} (Figure 25B). Looking closer at the different lobes, we were able to predict the hurdles that would have to be overcome to bind Ca^{2+} in the first three EF-hands. In addition to the mentioned hydrophobic and basic clashes, this included for example, the presence of positively charged residues in the vicinity of EF-hand 3, which could obstruct Ca^{2+} ions from access (Figures 25C and 25D). Analysing the superposition, we saw that the C-lobe of CaM lined up with RyR1 4071-4134, a finding that eventually resulted in the RyR1 4071-4138 construct.

RyR1 4017-4138 expressed and purified very well yielding pure, soluble protein and confirmed by mass spectrometry to be the correct molecular weight (8111 kDa). The construct did however readily dimerize in the absence of a reducing agent as shown on a gel filtration column as well as by SDS-PAGE (Figures 26A and 26B). A mutant C4114A form removed the only cysteine residue and resulted in a purifiable monomer even in the absence of a reducing agent. RyR1 4071-4138 was used for ITC experiments and kept permanently in a reducing condition. Random crystallographic screens were applied to both the wild-type and C4114A constructs. So far, there are no promising crystallographic hits to report.

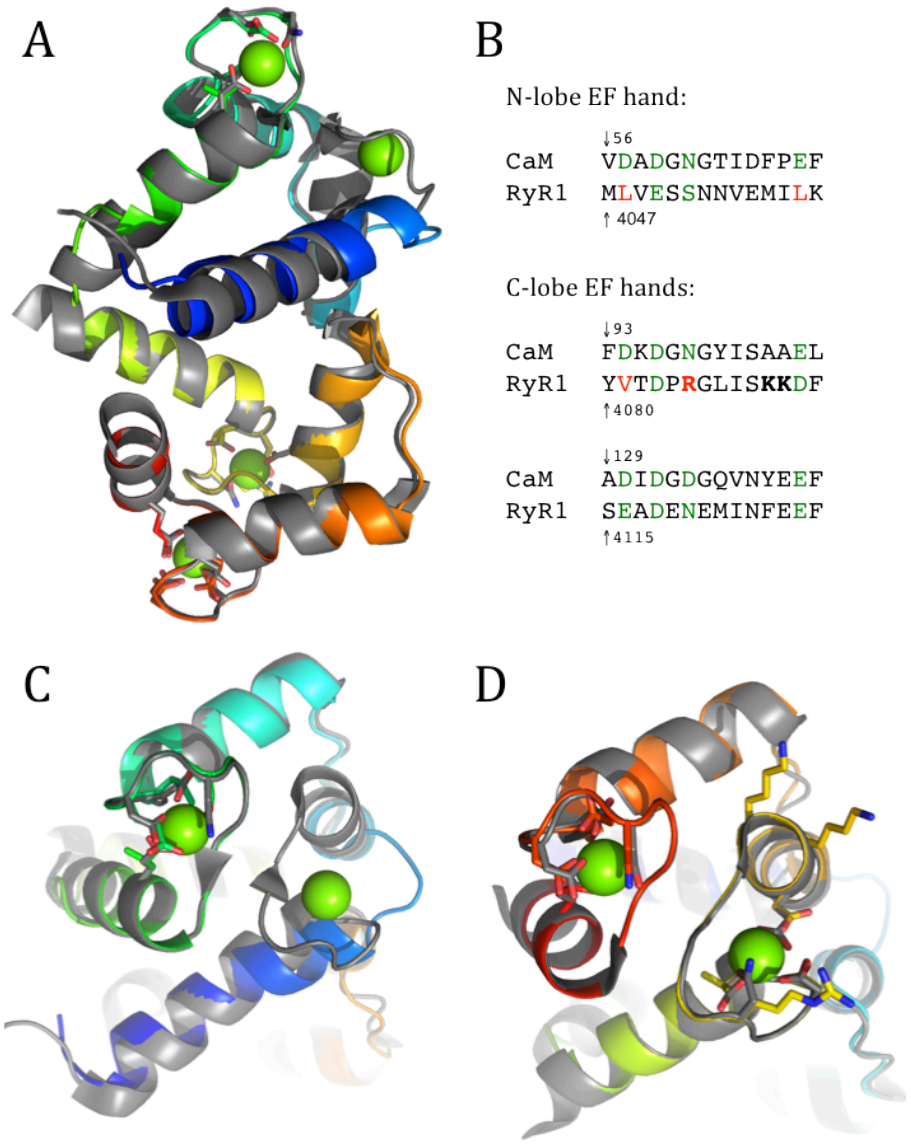

FIGURE 25. **Potential EF-hands in RyR.** (**A**) A model of RyR ~4000-4140 from PHYRE[2] (Kelley and Sternberg 2009) is coloured in a spectrum from its N-teminus (*blue*) to C-terminus (*red*) and superposed to CaM (PDB 1CLL, Chattopadhyaya et al. 1992), coloured grey. (**B**) Structural alignments of the EF-hands. Ca^{2+} binding residues in the CaM sequences are highlighted green, as are compatible residues in RyR1. Positively charged (*bold*) and hydrophobic residues in Ca^{2+} binding positions are coloured red, and in addition, two lysines (K4090 and K4091), which may hinder access to Ca^{2+} are bolded. The highlighted residues are shown as sticks in zoomed in views of the N-lobe (**C**) and C-lobe (**D**) superpositions. Ca^{2+} ions are shown as green spheres. Numbering: RyR1 *Oryctolagus cuniculus*.

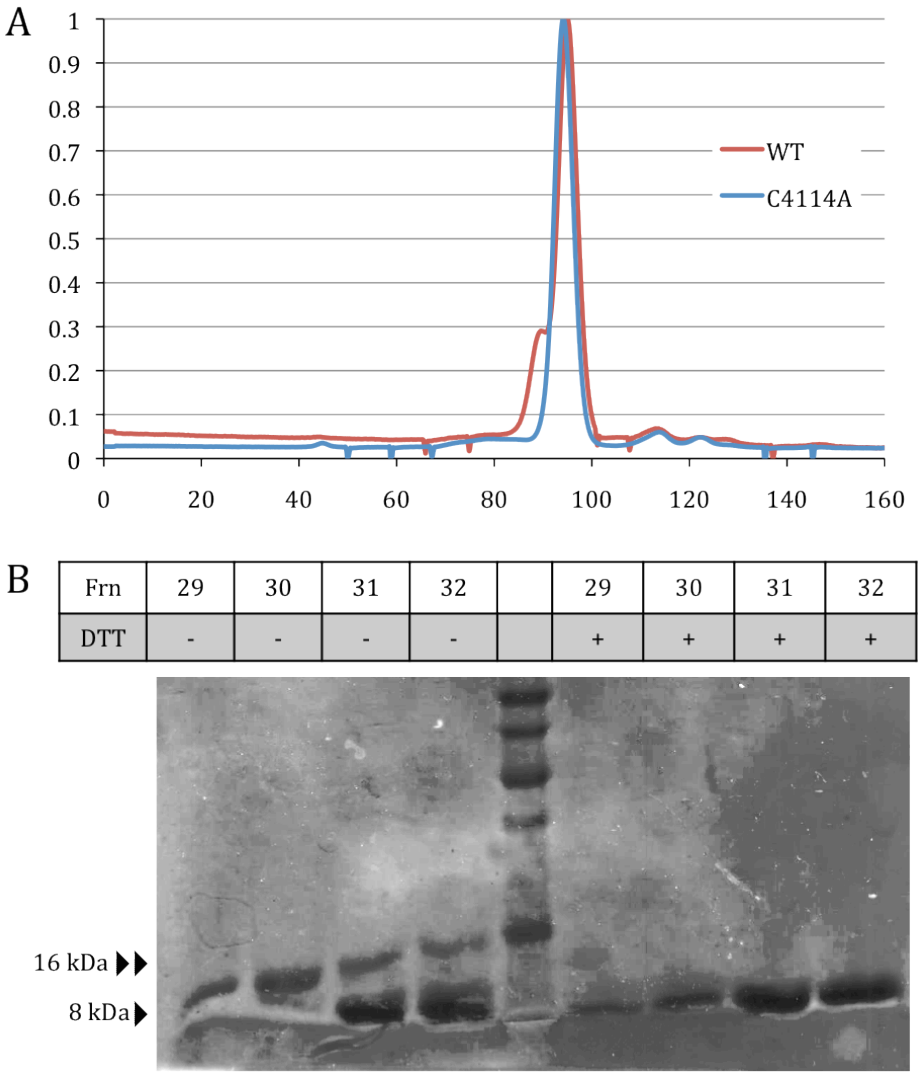

FIGURE 26. **Cysteine dimerisation in RyR1 4071-4138.** (**A**) Wild-type (WT) RyR1 4071-4138 was run on a gel filtration column without βME and showed a showed a shoulder peak. The cysteine-4114 alanine mutant ran as a monomer in the absence of a reducing agent. (**B**) In the presence of a strong reducing agent (DTT), fractions (Frn) from the superdex column in (**A**) ran as a ~8 kDa monomer on an SDS PAGE gel. Numbering: RyR1 *Oryctolagus cuniculus.*

3.3.1 Ca^{2+} and Mg^{2+} Binding to RyR1 EF-hands

ITC detected very weak binding between RyR1 4071-4138 and the Ca^{2+} (Figure 27A) as well as Mg^{2+} (Figure 27B). The ~10 mM K_d values indicate an affinity much lower than something physiologically relevant but an explanation may be suggested in construct selection. Neighbouring domains could stablilize the EF-hand and enhance its binding to both Ca^{2+} and Mg^{2+}. From our experiments, although absolute thermodynamic values cannot be quoted with certainty, we can say that the ions definitely bind RyR1 4071-4138. The raw endothermic heats of binding observed were in sharp contrast to the exothermic background titrations of Ca^{2+}/Mg^{2+} into buffer.

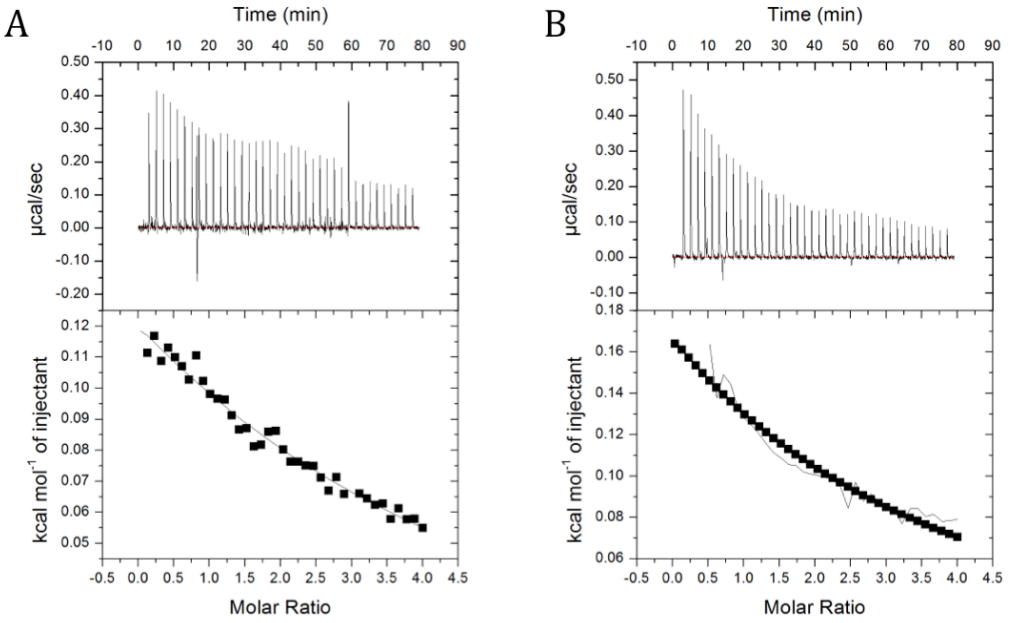

N	0.0113	±11.8 Sites	N	3.33	±1.11 Sites
K_A	53.4	±105 M^{-1}	K	97.8	±52.6 M^{-1}
ΔH	1.818E5	±1.892E8 cal/mol	DH	362.5	±215.1 cal/mol
ΔS	618 cal/mol/deg		DS	10.3 cal/mol/deg	

FIGURE 27. **RyR1 4071-4138 binds Ca^{2+} and Mg^{2+}.** Weak binding was detectable by ITC for RyR1 4071 with both Ca^{2+} (**A**) and Mg^{2+} (**B**). In both cases, 30 mM of Ca^{2+}/Mg^{2+} was titrated into 1.5 mM RyR1 4071-4138. Given the weak affinity, the absolute thermodynamic values, although shown here, cannot be taken to be accurate.

Binding to Ca^{2+} was further tested using nuclear magnetic resonance experiments. U. Brath compared Heteronuclear Single Quantum Coherence spectra from ^{15}N-labelled RyR1 4071-4138 with and without Ca^{2+}. The dramatic change observed confirmed that Ca^{2+} does indeed bind the protein (data not shown).

3.3.2 Interaction with RyR1 CaMBDs

RyR1 4071-4138 was identified as homologous to CaM. In addition, RyR1 4064-4210 has been shown to bind to the second CaMBD (in sequence) in RyR1 3614-3643 (Xiong et al. 2006). We therefore wished to perform binding experiments to additional CaMBDs that we have previously characterized in the lab.

A synthesized RyR1 CaMBD3dLRR peptide was available in the lab for ITC experiments with RyR1 4071-4138. Preliminary ITC experiments have showed an affinity of ~7μM in conditions without Ca^{2+} (Figure 28). The success in binding has opened a multitude of opportunities for the construct.

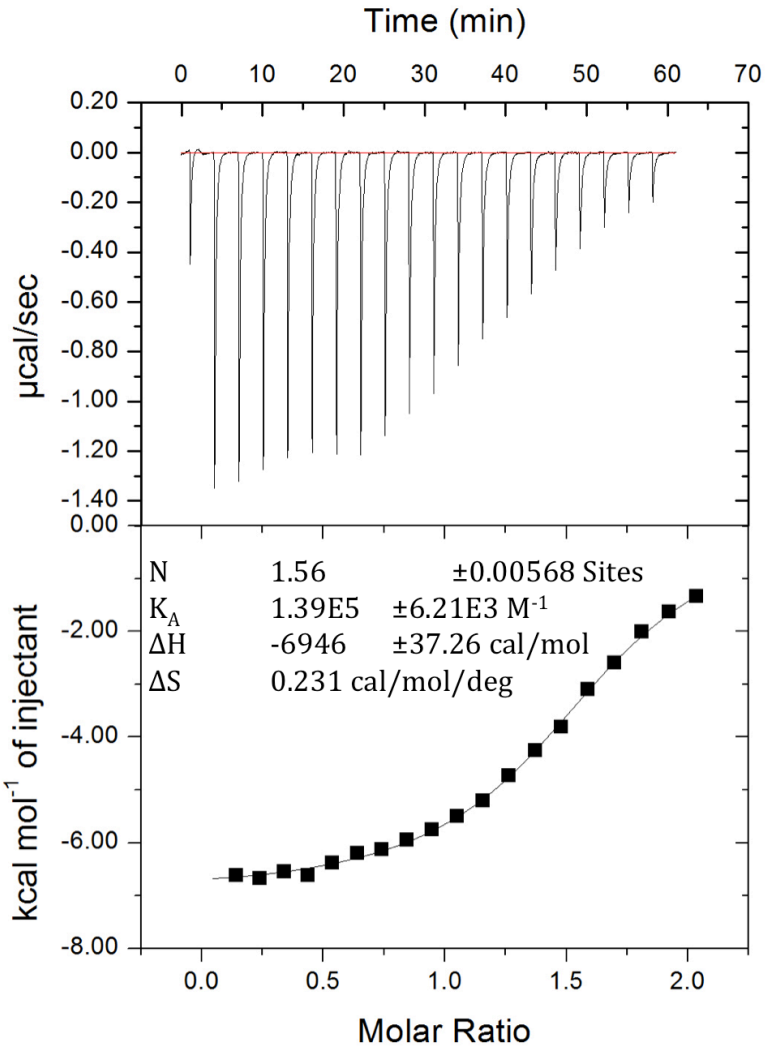

FIGURE 28. **RyR1 4071-4138 binds a CaMBD3 mutant.** 1.2 mM RyR1 4071-4138 was titrated into 0.12 mM of a RyR1 CaMBD3 mutant peptide. The concentration of the peptide was not accurately measured, perhaps explaining the N value of ~1.5. The thermodynamic values obtained from ITC are displayed on the graph.

4 Discussion

4.1 RyR1 ABCd

The addition of a small helix, and the structuring of previously flexible loops are more than just requirements for crystal lattice formation. The relative orientations of these new loops may just be crystallographic artefacts, but it is worth noting that they can adopt structure when in proximity to hydrophilic domains. Given the observed polar and electrostatic interactions between domains in RyR1ABC, it can be concluded that this sort of dynamic structuring must take place in full-length RyR1 allosteric communication.

Still, looking at the big picture, does the structure presented here expand the understanding of RyR1? Majority of the structure is already known in RyR1ABC, the theory of disease mutations affecting interface interactions is repeated here, and in comparing the structure docked in the open and closed EM maps, the observed domain movements are very similar to those seen with the first three domains alone. Described here however, are the exciting, new conclusions that can be drawn from this structure.

4.1.1 A Larger Surface Area for Binding

For a channel to be well regulated, there needs to be a relative ease of access for small-molecule modulators to bind. Although the extended helix only represents ~9% of the structure, docking studies suggest that a large majority of it is exposed to the cytoplasm. This enhances the potential for finding regulatory binding sites using ITC as a high-throughput screen. In the search for RyR ligands, it makes sense to consult a related channel in IP_3R.

IP_3R and RyR have travelled down similar evolutionary roads and still today share similar functions as tightly-regulated Ca^{2+} channels. Proving this, Seo et al. (2012) completely replaced the N-terminal domain of an IP_3R with RyR1A and reproduced a functional channel. Similarly Yuchi and Van Petegem (2010) have done some preliminary structural analysis on the two N-termini and concluded that that they operate with parallel allosteric mechanisms. Consequently, anything we can structurally determine from one channel can be translated to extend the knowledge in the field of the other. Compared to the structure of $IP_3$1ABC, we learn that the structured residues presented here (~10-577) define a better ending point for domain C than we previously described (Tung et al. 2010) (Figure 29A). The solved structure will therefore be referred to as RyR1ABCd. The binding sites of regulators to IP_3R1 can help in locating similar sites in RyR. PDB 1N4K (Bosanac et al. 2002) represents a high-resolution structure of IP_3RBC in which its most important triggering ligand, IP_3 itself, is bound. Given the potency of IP_3 on IP_3R, a ligand that could bind in the same pocket in RyR, could be of serious importance.

However, RyR1 is not modulated by IP_3, and analysis of the superposed structures helps to explain why. In the binding pocket, only two residues are conserved between the receptors (Figure 29B): in IP_3R, arginine-504 and arginine-568, both of which are involved in binding the 1-phosphate of IP_3, with the latter being essential for it (Yoshikawa et al. 2006). In human RyR1 these represent R471 and R533. Fascinatingly, R533 has twice been documented to cause malignant hyperthermia as a result of a mutation to a histidine (Brandt et al. 1999) or a cysteine (Tammaro et al. 2003). Here the molecular mechanism of disease can be explained by directly affecting the binding of a crucial modulator. Finding the modulator in RyR though, is yet to be done; something far from trivial. In RyR1, the positively charged IP_3 pocket has been altered dramatically, both in sterics and electrostatics.

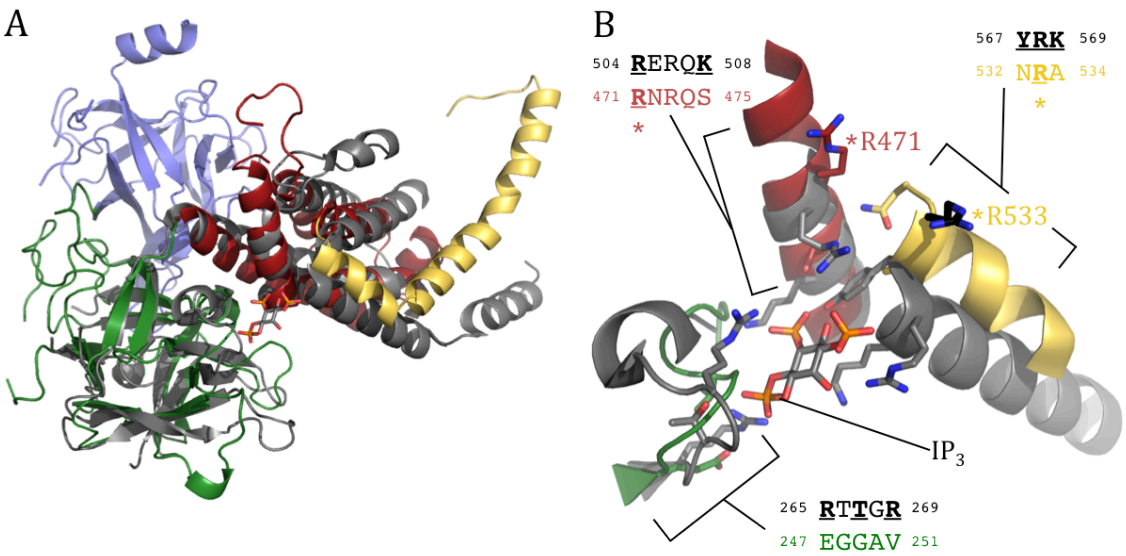

FIGURE 29. **A comparison between IP$_3$R and RyR1 1-617.** (**A**) Superposition of the 2.2 Å IP$_3$R1BC (PDB 1N4K, Bosanac et al. 2002) onto RyR1 1-617 shows that in the search for a fourth domain, we have actually redefined domain C. The extra structural information from 'RyR1ABCd' provides more of a surface for potential binders. RyR1 A, B, C and d domains are coloured blue, green, red and yellow respectively and the IP$_3$R is shown as grey. (**B**) A detailed view of the residues involved in binding IP$_3$. In the structural alignments, residues that directly interact with IP$_3$ in IP$_3$R are bolded and underlined. Shown in bold, underlined and marked by an asterisk (*), are RyR1 R471 and R533: the only conserved residues involved in binding. R533 is also a disease mutation (*black sticks*). Numbering: RyR1 *Homo sapiens*.

4.1.2 PP1 Recruitment by a Leucine Zipper

Leucine zippers (LZ) are coiled coils that force the adhesion of two or more parallel (common) or antiparallel (rare) α-helices (Lupas, 1996, Kohn et al. 1997). Originally found in DNA-binding proteins, they described a mechanism for dimerisation between two LZ-containing proteins. Orthodox descriptions define a heptad repeat (abcdefg) as having hydrophobic residues at positions 'a' and 'd' with

leucine residues occupying the latter (Crick, 1953, Landschulz et al. 1988). Isoleucine and valine have also been accepted as residues that can contribute to this 'zipping'.

Marx et al. (2001) manually identified three LZ motifs in RyR2. LZ1, in residues 555-604 was shown to bind Protein Phosphatase 1 (PP1) via its regulatory subunit spinophilin. LZ2, defined by RyR2 1603-1631 pulled down Protein Phosphatase 2A (PP2A), and LZ3 (RyR2 3003-3039) interacted with PKA. They went on to show that LZ1 and LZ3 are conserved between the cardiac and skeletal RyR and as expected, RyR1 fusion peptides containing these zippers pull down PP1 and PKA as well. A LZ-motif in spinophilin (residues 485-510) was classified as the binding site for RyR2, and mutating out 'd' leucines in either RyR2 or spinophilin abolished the interaction.

LZ1 in RyR1 corresponds to residues 534-592, almost exactly describing the gain in structure due to RyR1ABCd. The structure agrees well with their prediction, lining hydrophobic residues for dimer interactions down one face of the new helix and scattering charged and polar amino acids on the other side (Figure 30).

The hydrophilic face contains several RyR1 and RyR2 disease mutations that cause MH or CPVT respectively. This side of the coil could therefore play an important role in anchoring the helix in position, primed for PP1 attachment. Phosphatases are essential players in the inhibition of RyR channels (Marx et al. 2000). Hyperphosphorylation of RyR is thought to cause FKBP dissociation and result in leaky channels (Bellinger et al. 2009). From our results, we can propose yet another mechanism for disease in RyR1. Mutations in RyR1d could directly affect the binding of the phosphatase PP1, required in recovery from hyperphosphorylation (Marx et al. 2000). In wild-type channels then, RyR1d may serve as the recruitment domain for PP1, transiently increasing the phosphatase's local concentration near sites of requirement.

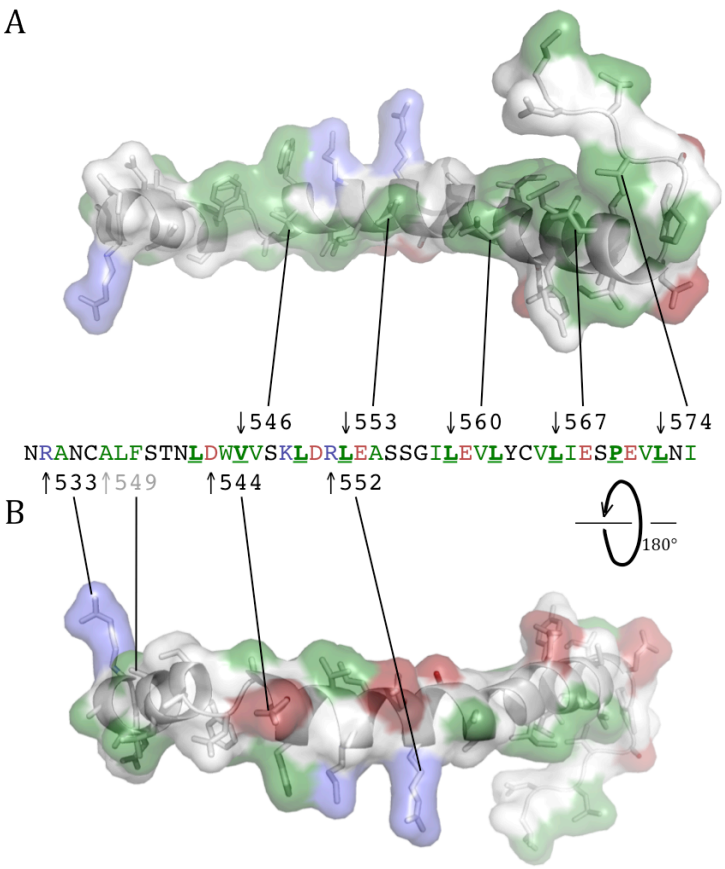

FIGURE 30. **A LZ motif in RyR1d.** Below the sequence and marked by up-arrows (↑) are human disease mutation sites. Above the sequence and marked by down-arrows (↓) are the valine or leucine residues that are arranged in the correct canonical spacing for the formation of a leucine zipper. In addition, other hydrophobic residues that could contribute to a zipper are bolded and underlined in the sequence. Hydrophobic, basic and acidic residues have their transparent surfaces coloured green, blue and red respectively. Disease mutations locate on the opposite helical side to potential zipper 'action', requiring a 180° rotation of the structure in (**A**) to view them (**B**). Numbering: RyR1 (*black*) or RyR2 (*grey*) *Homo sapiens*.

Interestingly, upon analysis of the crystal lattice, we observed that the additional helix in our structure contacts a symmetry-related molecule through a coiled-coil interaction (Figure 31). The observed LZ differs slightly from the strict definition of interacting heptads, hinting that some degree of plasticity may be involved in RyR1 modulator recruitment.

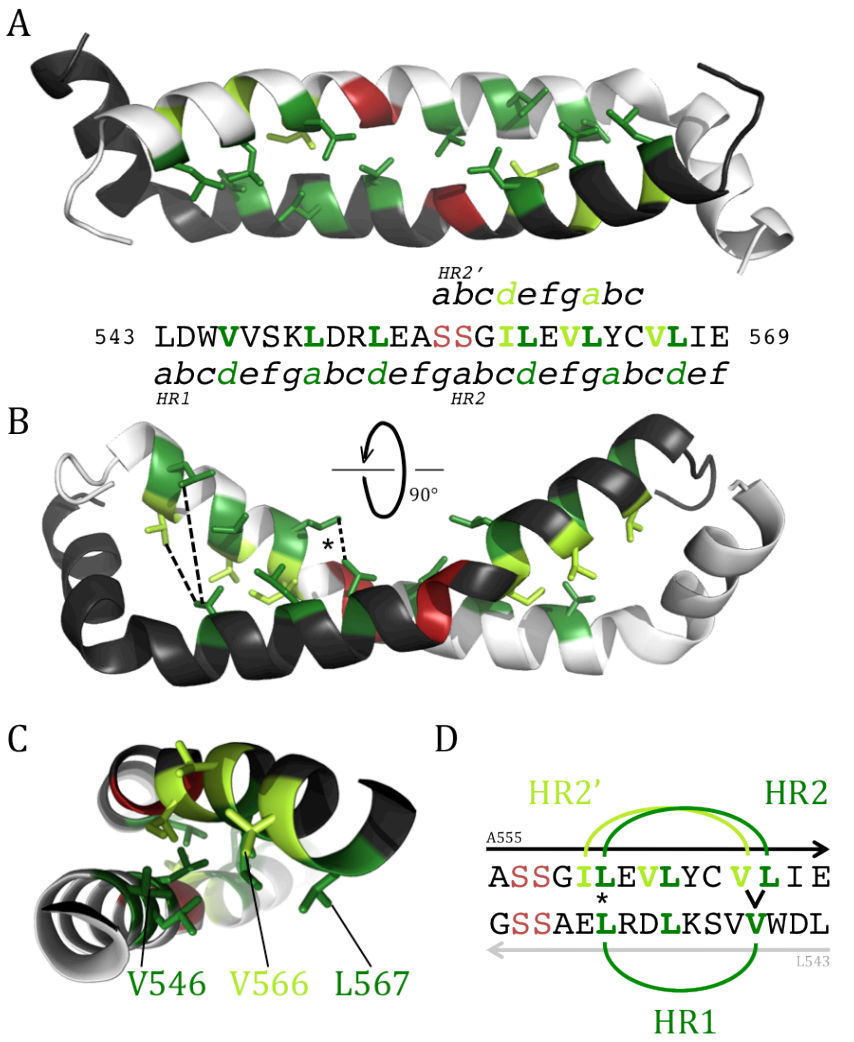

FIGURE 31. **An antiparallel LZ in the RyR1ABCd crystal structure.** (**A**) and (**B**) show two perpendiuclar views of a coiled coil formed between RyR1d domains from different asymmetric units in the crystal lattice. Leucine, Isoleucine and valine residues involved in 'zipping' are green or lime green and are aligned in the sequence between (**A**) and (**B**) to the black helices. An unusual bend occurs at a polar S556-S557 gap (red) between canonical LZ heptads (HR1 and HR2). (**C**) The bend is allowed due to a possible register shift employing the HR2' LZ residues in lime green. (**D**) A schematic explaining the atypical interactions in the zipper. L553 initiates a zipper with L560 in the other helix (asterisk). Seven positions from there on both helices, V546 in HR1 would be expected to interact with L567 in HR2, but it instead is closer to V566 in HR2'. Numbering: RyR1 *Homo sapiens*.

4.1.3 Molecular Insight from Docking

There are two related hurdles to the theory of LZ-mediated dephosphorylation of RyR1 by PP1/spinophilin. Firstly, PP1 (37 kDa) and spinophilin (90 kDa), together form a large, bulky complex and secondly, considerable structural rearrangements would be required to allow for dimerisation by coiled-coils. As such, a special right of entry may be necessary for recruitment. In analysis of RyR1ABCd docked into an EM map (EMDB 1606, Samso et al, 2009) from the cytoplasmic surface (Figure 32A) we see such a portal, or Phosphatase Access Channel (PAC) (Figure 32B).

From further docking investigation, new interaction surfaces within RyR1 have been characterized. Previously, we have described six interfaces in the full-length RyR structure that gear against facial planes in RyR1ABC: Interface 1 marks the junction between RyR1A of one monomer and RyR1B of the next in the tetrameric assembly. Interfaces 2 and 3 describe respectively as the lateral junctions of RyR1A and RyR1C to adjacent domains in the full channel. And interfaces 4, 5 and 6 link RyR1A, RyR1B and RyR1C 'downwards' in the direction of the channel pore (Tung et al. 2010). Docking RyR1ABCd has redefined interface 3 and brought to light some details about a novel interaction surface in interface 7.

The RyR1 MH/CCD causing mutations Q474H, Y522C/S and R530H, as well as the CPVT mutation in RyR2 V507I, were all previously predicted to affect interface 3 (Tung et al. 2010). In addition, three further MH mutations in RyR1 (R533C/H, D544Y and R552W) and one in RyR2 that causes CPVT (A549V) can be mapped onto the RyR1ABCd structure for analysis (Figure 32C). An intricate web of polar and electrostatic interactions decorates the junction between RyR1C and RyR1d. Two props from below, in RyR1C stabilize the LZ raised arm: Q474 and Y522. The former interacts with N532, the very first residue in RyR1d, and the latter pokes up from domain C below, into the RyR1C-d hydrophilic interaction network. On the inner side of this arm, RyR1d contributes its own variety of hydrophilic binders. These include R552 and surprisingly a rogue tryptophan that has abandoned its hydrophobic nature to hydrogen bond via its N1 atom (Figure 32C).

RyR1 D544 and RyR2 A549 lie at interface 3, at the shoulder of the RyR1d arm. Mutations at these sites that cause disease introduce more bulky and hydrophobic side-chains in tyrosine and valine respectively. This corroborates well with our earlier studies that blamed disease on a breakdown of hydrophilic communication between domains in RyR (Tung et al. 2010).

The mapped RyR2 V507 is shown as a black surface for clarity in figure 32B and grey sticks in figure 32C. Mutation to an isoleucine causes CPVT, emphasizing that even very small perturbations in an interface are large enough to cause serious problems. This demonstrates the fragility of the interactions in the area. Evidently a stable LZ-motif in RyR2d as well, is an absolute requirement. For RyR in general then, our mutational analysis suggests that a well-positioned LZ arm is required for the proper function and regulation of RyR.

Finally, our docking studies have allowed the definition of a new interaction plane in interface 7 (Figures 32B and 32E). This can be seen as the elbow of the LZ arm and pokes out in a radial direction towards the clamp region. It must be noted though, that the absolute location seen in the crystal structure of this elbow may be a result of LZ dimerisation and not truly reflect a physiological positioning. In support of this, the forearm, past the elbow, extrudes out of the EM map into the PAC (figures 32B and 15B). The general location of interface 7 though, is undeniable and supplies the first piece of structural evidence for communication between the clamp and central rim. With this we can begin to understand how modulators that bind in the periphery or the RyR cytoplasmic face can affect the channel close to the pore. RyR1d can therefore be designated two hypothetical roles. The first involves a LZ arm-grip with spinophilin, an interaction that would mediate the dephosphorylation of the channel, and the second is as a vestibule-clamp translator that sets up the potential for allosteric communication.

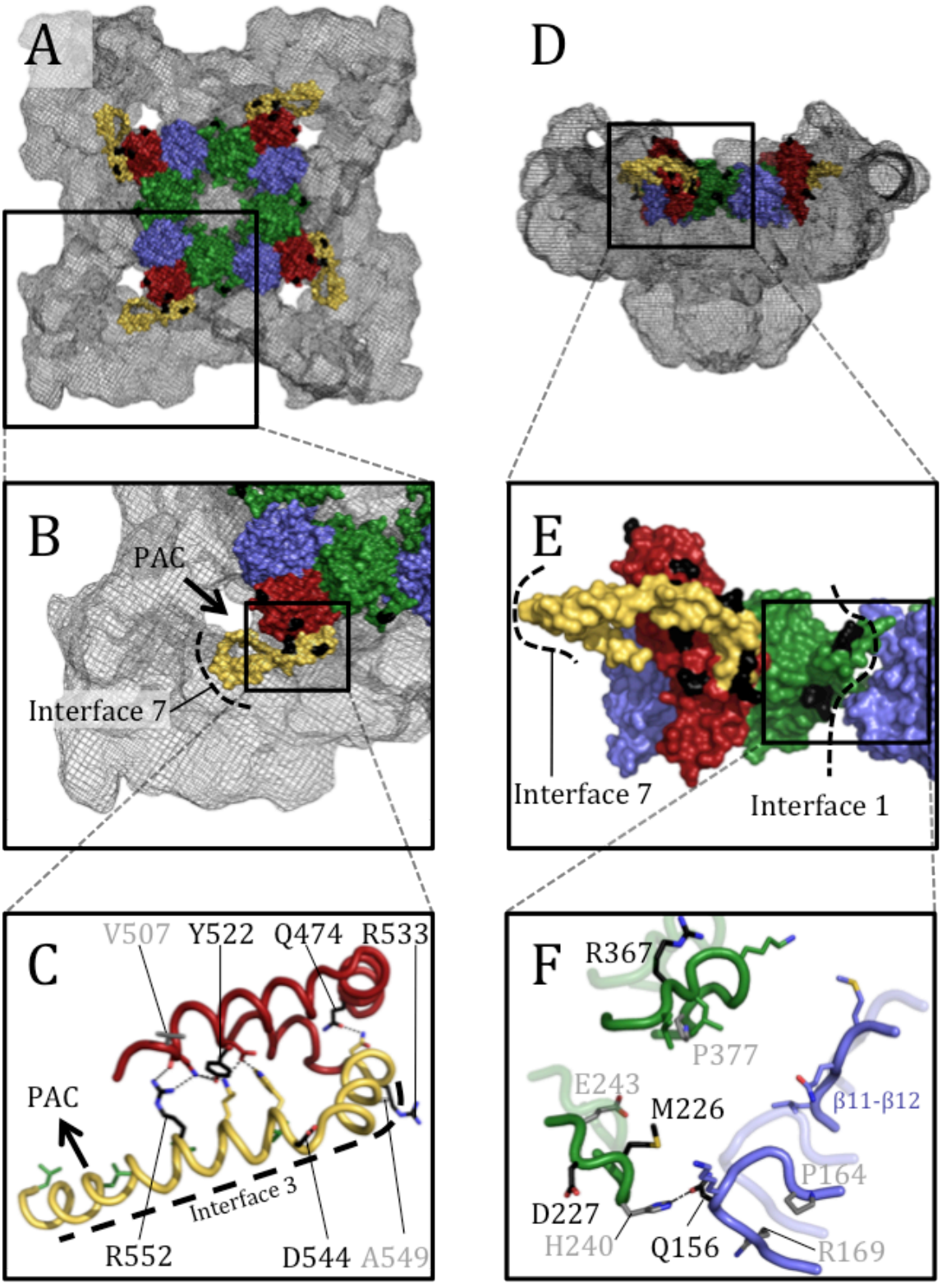

FIGURE 32. **RyR1ABCd docking analysis.** *Legend on next page.*

FIGURE 32. **RyR1ABCd docking analysis.** (**A**), (**B**) and (**C**) represent progressively zoomed in 'top' views of RyR1ABCd docked into a closed EMDB 1606 (Samsó et al. 2009). Similarly (**D**), (**E**) and (**F**) do the same but from a 'side' view. In surface representation, RyR1/2 mutations are coloured black but in stick representation RyR2 mutations are grey. A new interaction plane in interface 7 is defined and marks the join between the central rim of RyR1 and its clamps. Interface 3, or the lateral face to domain C (Tung et al. 2010) can now be modified to include areas adjacent to domain d. A Phosphatase Access Channel (PAC) is arrowed in (**B**) and has access to LZ-motif residues coloured green in (**C**). For illustration, in (**F**), the side-chains of RyR1 M226 and D227, as well as RyR2 H240 have been modelled in despite their flexibility in the crystal, and are seen to protrude into interface 1. A transparent cartoon shows interface 1 from RyR1ABCd docked into the open EMDB 1607. Numbering: RyR1 (*black*) or RyR2 (*grey*) *Homo sapiens.*

4.1.4 Interface 1

Interactions at interface 1 (labelled in Figure 32D and 32E) are of special interest as they sew the vestibule together forming seams between monomers. Previously we hypothesized that gain of function mutations in the region could easily be explained by causing these subunit seams to loosen (Tung et al. 2010). The RyR1 MH mutations M226K, D227V and R367L/Q as well as the RyR2 CPVT mutation H240R can now be positioned and agree with this previous model. Although these residues are flexible in the crystal structure, they can presumably interact transiently in the full-length channel. As an example, in Figure 32E, the residues labelled H240 and Q156 could form a potential hydrogen bond. If Ca^{2+}-release involves movement around the cytoplasmic opening, interactions such as these necessarily have to be weak and transient to allow for channel opening.

During opening and closing of the channel to accommodate Ca^{2+}, an increase in the transmembrane pore size is expected. But in addition, analysis of open and closed EM maps has indeed shown that large allosteric movements in the central rim accompany pore opening (Kimlicka and Van Petegem, 2011). Molecular details can be

attained by docking RyR1ABCd into cryo-EM reconstructions of the same resolution in both the open (EMDB 1607) and closed (EMDB 1606) RyR1 conformations (Samsó et al. 2009). Comparing these docked structures, it is clear that interface 1 must 'break' during channel opening, allowing the movement of subunits ~4 Å further apart (Figure 32E). A look at the overall structure motion portrays four RyR1ABCds as a cap, tightening to close the channel (Figures 33A and 33B). This screw-like constriction may continue towards the pore, providing an allosteric explanation for channel closing upon ligand binding.

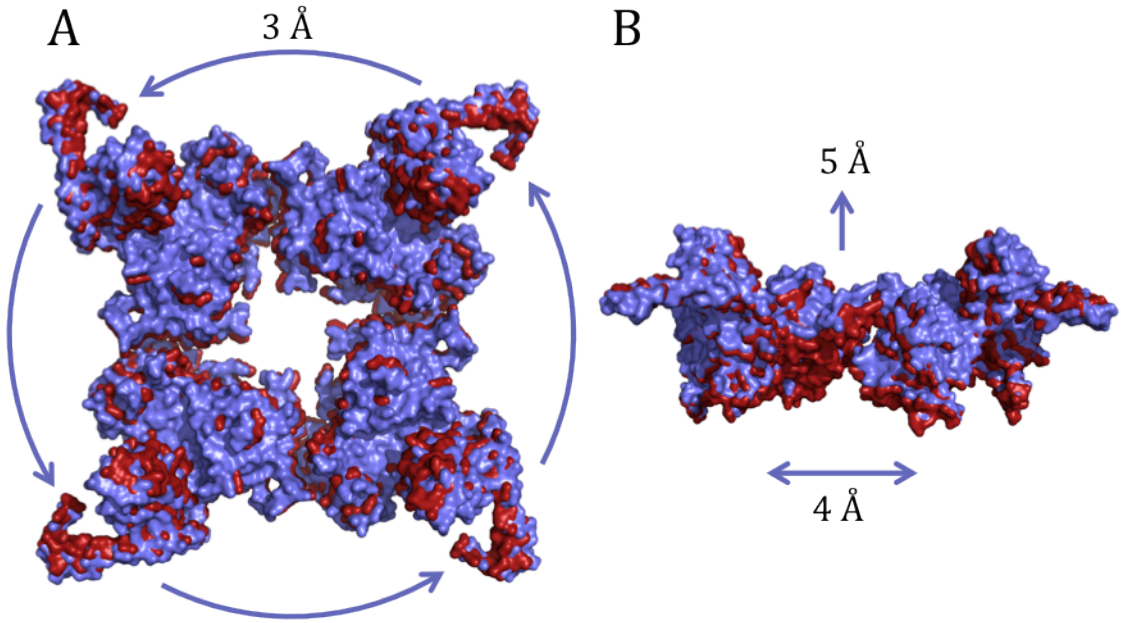

FIGURE 33. **RyR1ABCd in channel opening.** (**A**) Top and (**B**) side views of RyR1ABCd docked into the open (EMDB 1607) and closed (EMDB 1606) reconstructions of full-length channel (Samsó et al. 2009). The surface representations of the structure in the open and closed state are shown in blue and red respectively. In opening, RyR1ABCd motion can be described as a ~3 Å twist, lifting the domains ~5 Å towards the cytoplasm and widening interface 1 by ~4 Å.

4.1.5 Continuing the Debate on Dantrolene

The possibility of RyR1 as the molecular target of dantrolene has been a topic of serious discussion. Evidence in the field, on both sides of the argument have been described, but work by the Parness lab (Paul-Pletzer et al. 2001, Paul-Pletzer et al. 2002) has strongly suggested that the ligand does directly interact with RyR1, and specifically residues 590-609.

Characterizing an accurate, thermodynamically well-defined interaction between RyR1 590-609 would finally put to rest further discussion on the topic and confirm RyR as a molecular target of dantrolene. Our results though, could not provide this valuable information. ITC experiments failed to detect binding between RyR1 1-617 and dantrolene or azumolene. Initial attempts at explaining the results involved low protein concentrations. Weak binders would require higher concentrations to detect their interactions. But mentioned already, therapeutically both drugs work at ~10 μM (Flewellen et al. 1983), well below the concentration tested here (final cell concentrations of drug and protein were ~125 μM and ~30 μM respectively). If binding does take place then, there is little enthalpic contribution to it. If this were the case ligands that bind at the same site could be used in competition experiments to obtain an apparent affinity. As a separate explanation for the lack of detectable binding, it is possible that a prerequisite binder such as ATP is necessary to put RyR in a dantrolene-accessible state.

4.2 Purines and RyR1

Increased sensitivity to caffeine is a diagnostic tool for MH mutations in RyR1. Zhao et al. (2001) have shown that dantrolene tames this sensitivity and lowers the affinity for caffeine. In the same study they illustrate a necessity for the presence of an ATP analog in dantrolene inhibition. This could be explained by the existence of a

purine binding site in intimate, allosteric communication with a dantrolene binding site in RyR. Our results indicate that indeed, the two could be closely related. Already discussed, Paul-Pletzer et al. (2002) have identified a dantrolene binding site in RyR1 590-609. Here we have presented data confirming that RyR1ABC and RyR1BC both interacted with caffeine, narrowing the caffeine binding site to RyR1 217-536 and in addition we show potential for an ATP binding site in the same domains. Whether or not these interaction sites are the same, remains to be seen.

In the aim of structurally characterizing these positions, both RyR1BC and RyR1ABC were crystallized with caffeine, but provided different binding solutions. These results although outwardly contradictory may not be completely irrelevant *in vivo*. Given the relatively non-specific modes of attachment to aromatic residues discussed in Chapter 1.4.3 (Figure 9), there could be multiple sites of attachment, whether these are all functional sites is a different story. Further experiments would need to be carried out to distinguish between sites of casual interaction, and sites of biological relevance. Still, the crystallographic binding we observed, in both cases heavily involved symmetry related molecules arranged in a physiologically incompatible manner. A couple of options are available to bypass this hurdle. 1) Crystallization in lower concentrations of caffeine, although given the low measured affinity, this may not be an effective solution. 2) Random screens in the presence of caffeine, here the hope would be to attain a different crystal form. In a different space group, the non-physiologically binding aromatic residues would be in different orientations and be unable to 'sandwich' caffeine.

In addition, we plan to use ITC to probe the interaction in solution. Through *in silico* docking experiments, we have identified a few possible locations for caffeine binding. We aim to prepare mutants in these locations, and will test via ITC whether they alter the binding affinity. Sequential ITC experiments with purines followed by dantrolene might provide an added benefit in finding the drug's illusive binding site.

4.3 Regulation by EF-hands

RyR1 4064-4210 was suggested to interact with Ca^{2+}, CaMBD and $Ca_V1.1$ (Xiong et al. 2006). The major drawback from these experiments was inherent behavioural problems of the isolated peptide – refolding following denaturation by urea was required to solubilize this fragment. To convince the field though, CD was used to confirm that the protein was rich in α-helices, as would be expected from their initial sequence alignment with CaM. But a helical, CaM-like structure should not be exclusively expressed in inclusion bodies. It is likely that even after refolding, there could be flexible N- and/or C-terminal ends that are misfolded and bias results. In our construct selection, there was a stringent requirement for proteins to behave as well-folded, soluble monomers as portrayed by a single Gaussian peak on a gel filtration column. This was achieved in RyR1 4071-4138 (Figure 27A).

ITC investigation into Ca^{2+} and Mg^{2+} binding provided affinities in the millimolar range, much lower than the ~60 μM K_d reported for RyR1 4064-4120 (Xiong et al. 2006). The construct length though, matches a full length CaM and equilibrium dialysis showed two Ca^{2+} bound per molecule of RyR1 4064-4210 with a Hill co-efficient of ~1.6. The added affinity observed could be explained by this positive co-operativity. Additionally, with respect to Ca^{2+} binding, the protein must have contained only two out of four functional EF-hands, agreeing with our modelling of 'dead' EF-hands (Figure 26). Interestingly, the CaM alignment we present in RyR1 ~4000-4138 is partially upstream of 4064-4210, and both show a sequence identity of ~20%. This hints at the possibility of three repeats of EF-hand domains. It will be interesting to test constructs that are inclusive of all putative EF-hands.

4.3.1 The Involvement of CaMBDs

Introducing CaMBDs adds to the complexity of Ca^{2+} regulation. Here we show binding to a RyR1 CaMBD3 mutant, and Xiong et al. (2006) in addition have shown Ca^{2+}-dependent binding to RyR1 CaMBD2. There is evidence for multiple CaMBDs (Zorzatto et al. 1990, Menegazzi et al. 1994, Chen and MacLennan, 1995), and now as well, multiple EF-hands. Slowly, a complex picture is beginning to form that involves all of the above and includes in addition, CaM, Ca^{2+} and Mg^{2+}; CaM and RyR1 EF-hands exhibit Ca^{2+}/Mg^{2+}-dependent regulation of RyR1 via CaMBDs each of which have different affinities. In summary, some kind of Ca^{2+}-regulated competition between CaM and RyR1 EF-hands must take place.

The obvious next experiments would involve the other CaMBDs and determining their affinities; an outstanding binder might give us clues as to where RyR1 4071-4138 is located in 3D space relative to the CaMBDs. Competition experiments can now be used to further analyze the roles of Ca^{2+} or Mg^{2+}. The change in structure of RyR1 4071-4138 as a result of Ca^{2+} binding or unbinding, as suggested by the NMR experiments, may affect the interactions with CaMBDs. Conversely, CaMBD binding may stabilize the structure and allow for a quantifiable Ca^{2+}/Mg^{2+} affinity by ITC.

4.3.2 Disease and RyR1 EF-hands

The importance of the RyR EF-hands can be seen in the number of disease mutations found in the region. Within the three predicted lobes (RyR1 4000-4210, RyR2 3954-4164), 11 and 23 mutations have been shown to cause disease in RyR1 and RyR2 (summarized in Table 7). In effect, this defines a 'hotspot' of mutations and emphasizes the regions importance in Ca^{2+} regulation.

RyR1 Human Mutation	Disease	Reference
M4022V	MH	Lee et al. 2010
R4041W	MH	Galli et al. 2006
S4050Y	MH	Robinson et al. 2006
T4081M	MH	Ibarra et al. 2006
G4104R	MH	Kraeva et al. 2011
S4112L	CNM	Jungbluth et al. 2005
N4119Y	MH	Sambuughin et al. 2005
R4136S	MH	Galli et al. 2002
R4179H	UCM	Berilacqua et al. 2011
E4181K	UCM	Berilacqua et al. 2011
A4185T (& V4842M)	MH	Kraeva et al. 2011
RyR1 Human Mutation	**Disease**	**Reference**
S3959L	CPVT	Tester et al. 2006
M3972I	CPVT	Medeiros-Domingo et al. 2009
D3973H	CPVT	Medeiros-Domingo et al. 2009
L3974Q	CPVT	Medeiros-Domingo et al. 2009
K3997E	CPVT	Medeiros-Domingo et al. 2009
F4020L	CPVT	Postma et al. 2005
E4076K	CPVT	Postma et al. 2005
N4097S	E-IVF	Tester et al. 2004
N4104I	CPVT	Postma et al. 2005
N4104K	CPVT	Priori et al. 2001
L4105F	CPVT	Hasdemir et al. 2008
H4108N	CPVT	Postma et al. 2005
H4108Q	CPVT	Postma et al. 2005
M4109R	CPVT/SCD	Nof et al. 2011
S4124G	CPVT	Medeiros-Domingo et al. 2009
S4124T	UCP	Tester et al. 2005
R4144G	CPVT	Berge et al. 2008
E4146K	E-IVF	Tester et al. 2004
Y4149S	CPVT	Medeiros-Domingo et al. 2009
S4153R	CPVT	Kazemian et al. 2011
R4157Q	CPVT	Medeiros-Domingo et al. 2009
T4158P	SUD	Tester et al. 2004
Q4159P	CPVT	Medeiros-Domingo et al. 2009

Table 7. **Disease mutations in RyR1/2 EF-hands.** A list of all currently documented disease mutations within RyR1 4000-4210 and the corresponding residues in RyR2 (3954-4164). CNM: Centronuclear myopathy, Idiopathic Ventricular Fibrillation induced by emotion or exercise, SCD: Sudden Cardiac Death, SUO: Sudden Unexplained Death, UCP: Undefined Clinical Phenotype.

Concerning MH, RyR1 EF-hands may provide a means of furthering our understanding of its mechanistic details. Volatile anaesthetics trigger MH episodes, and RyR1 could potentially be their target as shown by activation in lipid bilayers (Connelly and Coronado, 1994, Bull and Marengo, 1994). Testing the binding of anaesthetics to RyR1 EF-hands may give clues as to whether or not this is the case.

4.4 Allostery in RyR1

Samsó and Wagenknecht (2002) have provided a cryo-EM structure depicting the locations of Ca^{2+}- and apocalmodulin in RyR1 (Figure 34A). Ca^{2+}-CaM appears to localize to the PAC, within reach of an extended LZ arm. Taken with the data presented here, this portrays the PAC and regions around it as a complex hub for allosteric communication in RyR regulation (Figure 34B) in which:

1) Purine activators bind to RyR1ABC
2) PP1 targets RyR1d, due to a LZ coiled coil with spinophilin
3) Dantrolene may interact with the flexible residues past RyR1d
4) The inhibitory Ca^{2+}-CaM attaches, presumably to a CaMBD
5) RyR1 EF-hands may be involved in Ca^{2+}-dependent competition with CaM

In all, these findings just scratch the surface of the molecular and mechanistic details involved in RyR regulation by ligands and modulators. Many more details about the structure and function of the channel remain to be discovered.

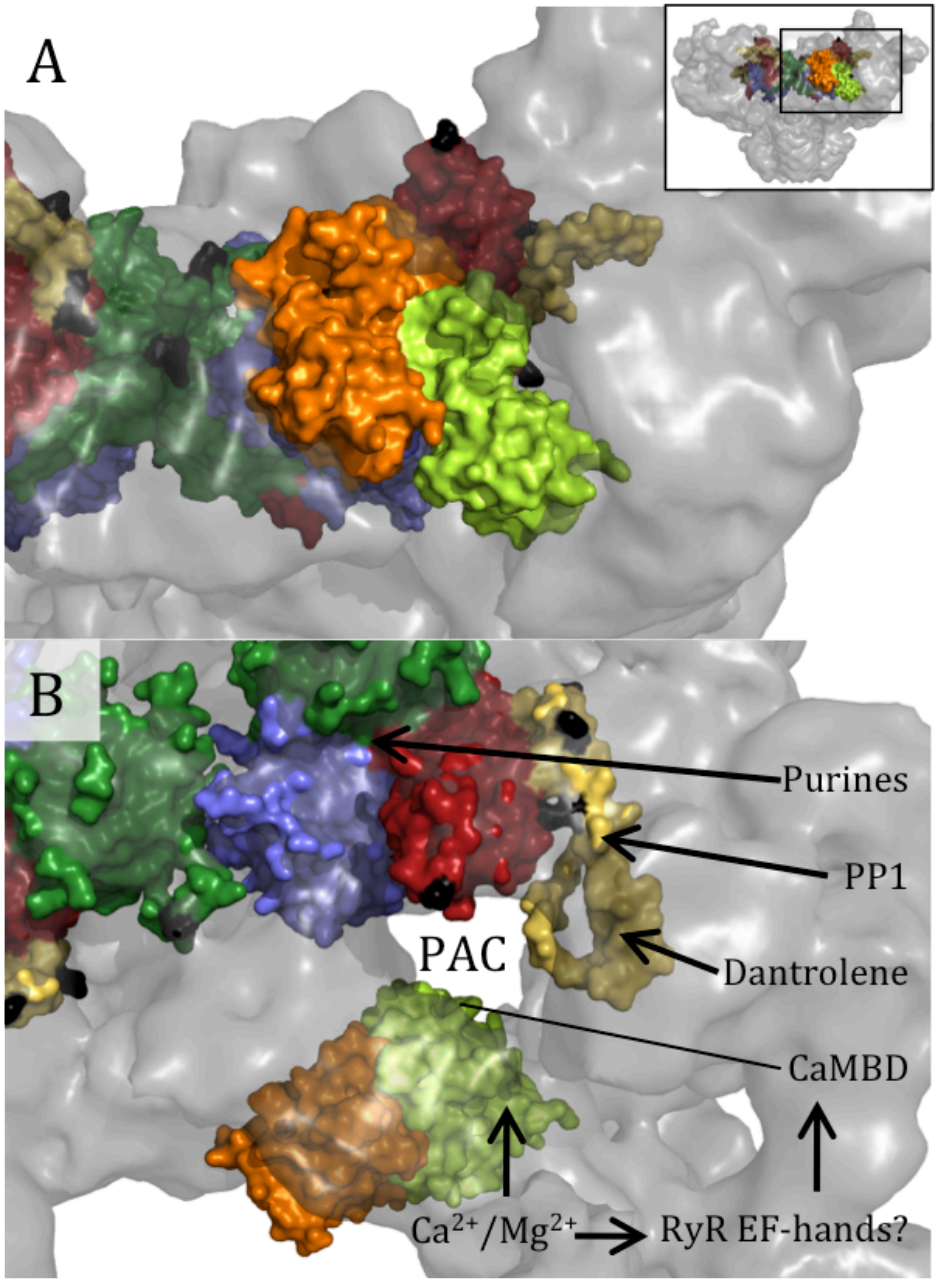

FIGURE 34. **Allosteric communication in RyR.** Side (**A**) and top (**B**) views of apo- (*orange*) and Ca^{2+}- (*lime green*) CaM in their approximate locations in RyR1. Manual placement of CaM was done in PyMOL based on cryo-EM maps identifying its positions (Samsó and Wagenknecht, 2002). CaM comes in contact with the PAC upon binding of Ca^{2+}. RyR1 A, B, C and d are coloured blue, green, red and yellow and shown docked into EMDB 1606 (Samsó et al. 2009). Labelled are some of the modulators mentioned in this thesis. Their interactions are arrowed to emphasize the complexity of the allosteric reactions that must be involved in RyR ligand regulation.

References

Ai, X., Curran, J.W., Shannon, T.R., Bers, D.M. and Pogwizd, S.M. Ca^{2+}/calmodulin-dependent protein kinase modulates cardiac ryanodine receptor phosphorylation and sarcoplasmic reticulum Ca^{2+} leak in heart failure. *Circ Res.* 2005. **97** :1314–22

Amador, F.J., Liu, S., Ishiyama, N., Plevin, M.J., Wilson, A., MacLennan, D.H. and Ikura, M. Crystal structure of type I ryanodine receptor amino-terminal β-trefoil domain reveals a disease-associated mutation "hot spot" loop. *Proc. Natl. Acad. Sci*. U.S.A. 2009 **106**: 11040–11044

Armstrong, C.M., Bezanilla, F.M. and Horowicz, P. Twitches in the presence of ethylene glycol bis(beta-aminoethyl ether)-N,N'-tetracetic acid. *Biochimica et biophyica acta*. 1972. **267**: 605-608

Arndt, U.W., Crowther, R.A. and Mallett, J.F. A computer-linked cathode-ray tube microdensitometer for x-ray crystallography. *J Sci Instrum.* 1968. **1**: 510-6.

Babu, YS, Bugg, CE and Cook W.J. Structure of calmodulin refined at 2.2 A resolution*. J Mol Biol.* 1988. **204**: 191-204

Baker, M.L., Serysheva, I.I., Sencer, S., Wu, Y., Ludtke, S.J., Jiang, W., Hamilton, S.L. and Chiu, W. The skeletal muscle Ca^{2+} release channel has an oxidoreductase-like domain. *Proc. Natl Acad. Sci.* 2002 USA **99**: 12155–12160

Balshaw, D.M., Xu, L., Yamaguchi, N., Pasek, D.A. and Meissner, G. Calmodulin binding and inhibition of cardiac muscle calcium release channel (ryanodine receptor). *J Biol Chem.* 2001. **276**: 20144–20153

Beard, N.A., Laver, D.R. and Dulhunty, A.F. Calsequestrin and the calcium release channel of skeletal and cardiac muscle. *Prog Biophys Mol Biol.* 2004. **85**: 33-69

Beard, N.A., Wei, L. and Dulhunty A.F. Ca2+ signaling in striated muscle: the elusive roles of triadin, junctin, and calsequestrin. *Eur. Biophys. J*. 2009. **39**: 27–36

Bellinger, A.M., Reiken, S., Carlson, C., Mongillo, M., Liu, X., Rothman, L., Matecki, S., Lacampagne, A. and Marks, A.R. Hypernitrosylated ryanodine receptor calcium release channels are leaky in dystrophic muscle. *Nat Med.* 2009. **15** :325–30

Berge, K.E., Haugaa, K.H., Früh, A., Anfinsen, O.G., Gjesdal, K., Siem, G., Oyen, N., Greve, G., Carlsson, A., Rognum, T.O., Hallerud, M., Kongsgård, E., Amlie J.P. and Leren, T.P. Molecular genetic analysis of long QT syndrome in Norway indicating a high prevalence of heterozygous mutation carriers. *Scand J Clin Lab Invest.* 2008. **68**: 362-8.

Betzenhauser, M.J. and Marks, A.R. Ryanodine receptor channelopathies. *Pflugers Arch.* 2010. **460**: 467–80

Bevilacqua, J.A., Monnier, N., Bitoun, M., Eymard, B., Ferreiro, A., Monges, S., Lubieniecki, F., Taratuto, A.L., Laquerrière, A., Claeys, K.G. Marty, I., Fardeau, M., Guicheney, P., Lunardi, J. and Romero, N.B. Recessive RYR1 mutations cause unusual congenital myopathy with prominent nuclear internalization and large areas of myofibrillar disorganization. *Neuropathol Appl Neurobiol*. 2011. **37**: 271-84

Bezprozvanny, I.B., Ondrias, K., Kaftan, E., Stoyanovsky, D.A. and Ehrlich, B.E. Activation of the calcium release channel (ryanodine receptor) by heparin and other polyanions is calcium dependent. *Mol. Biol. Cell*. 1993. **4**: 347–52

Block, B.A., Imagawa, T., Campbell, K.P. and Franzini-Armstrong, C. Structural evidence for direct interaction between the molecular components of the transverse tubule/sarcoplasmic reticulum junction in skeletal muscle. *J. Cell Biol.* 1988. **107**: 2587–2600

Bosanac, I., Alattia, J.R., Mal, T.K,. Chan, J., Talarico, S., Tong, F.K., Tong, K.I., Yoshikawa, F., Furuichi, T., Iwai, M., Michikawa, T., Mikoshiba, K. and Ikura M. Structure of the

inositol 1,4,5-trisphosphate receptor binding core in complex with its ligand. *Nature* 2002; **420**: 696-700

Bosanac, I., Yamazaki, H., Matsu-Ura, T., Michikawa, T., Mikoshiba, K. and Ikura, M. Crystal structure of the ligand binding suppressor domain of type 1 inositol 1,4,5-trisphosphate receptor. *Mol Cell.* 2005; **17**: 193-203

Brandt, A., Schleithoff, L., Jurkat-Rott, K., Klingler, W., Baur, C. and Lehmann-Horn, F. Screening of the ryanodine receptor gene in 105 malignant hyperthermia families: novel mutations and concordance with the in vitro contracture test. *Hum Mol Genet*. 1999. **8**: 2055-62

Brillantes, A.B., Ondrias, K., Scott, A., Kobrinsky, E., Ondriasova, E., Moschella, M.C., Jayaraman, T., Landers, M., Ehrlich, B.E. and Marks, A.R. Stabilization of calcium release channel (ryanodine receptor) function by FK506-binding protein. *Cell*. 1994. **77**: 513–523

Bull, R. and Marengo, J.J. Calcium-dependent halothane activation of sarcoplasmic reticulum calcium channels from frog skeletal muscle. *Am. J. Physiol*. 1994. **266**: C391–6

Buratti, R., Prestipino, G., Menegazzi, P., Treves, S. and Zorzato, F. Calcium dependent activation of skeletal muscle Ca^{2+} release channel (ryanodine receptor) by calmodulin. *Biochem Biophys Res Commun*, 1995, **213**: 1082–1090

Carafoli, E. Intracellular calcium homeostasis. *Annu Rev Biochem.* 1987. **56**: 395–433

Chacón, P. and Wriggers, W. Multi-resolution contour-based fitting of macromolecular structures. *J. Mol. Biol.* 2002, **317**: 375–384

Chattopadhyaya, R., Meador, W.E., Means, A.R. and Quiocho, F.A. Calmodulin structure refined at 1.7 A resolution. *J Mol Biol.* 1992. **228**: 1177-92

Chen, S.R. and MacLennan, D.H. Identification of calmodulin-, Ca^{2+}-, and ruthenium red-binding domains in the Ca^{2+} release channel (ryanodine receptor) of rabbit skeletal muscle sarcoplasmic reticulum. *J Biol Chem.* 1994. **269**: 22698–22704

Connelly, T.J. and Coronado, R. Activation of the Ca2+ release channel of cardiac sarcoplasmic reticulum by volatile anesthetics. *Anesthesiology.* 1994. **81**: 459–69

Crick, F.H.C. The packing of α-helices: simple coiled-coils. *Acta Crystallgr.* 1953. **1**: 689–97

De Smedt, H., Missiaen, L., Parys, J.B., Bootman, M.D., Mertens, L., Van Den Bosch, L. and Casteels, R. Determination of relative amounts of inositol trisphosphate receptor mRNA isoforms by ratio polymerase chain reaction. *J Biol Chem.* 1994. **269**: 21691–8

Denborough, M. and Lovell, R. Anaesthetic deaths in a family. *Lancet*. 1960 2: 45

Denborough, M. Malignant hyperthermia. *Lancet.* 1998. **352**: 1131–1136

Diaz-Sylvester, P.L., Porta, M. and Copello, J.A. Halothane modulation of skeletal muscle ryanodine receptors: dependence on Ca^{2+}, Mg^{2+}, and ATP. *Am J Physiol Cell Physiol.* 2008. **294**: C1103–12

Diederichs, K. and Karplus, P.A. Improved R-factors for diffraction data analysis in macromolecular crystallography. *Nat Struct Biol*. 1997. **4**: 269-75

Dirksen R.T. and Avila G. Altered ryanodine receptor function in central core disease: leaky or uncoupled Ca^{2+} release channels? *Trends Cardiovasc Med.* 2002. **12**: 189–97

Doré, A.S., Robertson, N., Errey, J.C., Ng, I., Hollenstein, K., Tehan, B., Hurrell, E., Bennett, K., Congreve, M., Magnani, F., Tate, C.G., Weir, M. and Marshall, F.H. Structure of the adenosine A(2A) receptor in complex with ZM241385 and the xanthines XAC and caffeine. *Structure*. 2011. **19**: 1283-93

Dulhunty, A.F. The voltage-activation of contraction in skeletal muscle. *Prog Biophys Mol Biol*. 1992. **57**: 181–223

Durham, W.J., Aracena-Parks, P., Long, C., Rossi, A.E., Goonasekera, S.A., Boncompagni, S., Galvan, D.L., Gilman, C.P., Baker, M.R., Shirokova, N., Protasi, F., Dirksen, R. and Hamilton, S.L. RyR1 S-nitrosylation underlies environmental heat stroke and sudden death in Y522S RyR1 knock-in mice. *Cell*. 2008. **133**: 53–65

Dykes, M.H. Evaluation of a muscle relaxant: dantrolene sodium (Dantrium). *J Am Med Ass*. 1975. **231**: 862–4

Edelhoch, H. Spectroscopic determination of tryptophan and tyrosine in proteins. *Biochemistry*. 1967. **6**: 1948–54

Ekstrom, J.L., Pauly, T.A., Carty, M.D., Soeller, W.C., Culp, J., Danley, D.E., Hoover, D.J., Treadway, J.L., Gibbs, E.M., Fletterick, R.J., Day, Y.S., Myszka, D.G. and Rath, V.L. Structure-activity analysis of the purine binding site of human liver glycogen phosphorylase. *Chem Biol.* 2002. **9**: 915-24

el-Hayek, R., Parness, J., Valdivia, H.H., Coronado, R. and Hogan, K. Dantrolene and azumolene inhibit [^{3}H]-PN200-110 binding to porcine skeletal muscle dihydropyridine receptor. *Biochem Biophys Res Commun.* 1992. **187**: 894–900

Emsley, P., Cowtan, K. Coot: model-building tools for molecular graphics. *Acta Crystallogr. D Biol. Crystallogr.* 2004. **60**: 2126–2132

Endo, M. Calcium release from the sarcoplasmic reticulum. *Physiol. Rev.* 1977 **57**: 71–106

Endo, M., Tanaka, M. and Ogawa, Y. Calcium-induced release of calcium from the sarcoplasmic reticulum of skinned skeletal muscle fibers. *Nature*. 1970. **228**: 34–36

Fabiato, A. Calcium-induced release of calcium from the cardiac sarcoplasmic reticulum. *Am. J. Physiol*. 1983. **245**: C1–C14

Ferguson, D.G., Schwartz, H.W. and Franzini-Armstrong, C. Subunit structure of junctional feet in triads of skeletal muscle: A freezedrying, rotary-shadowing study. *J Cell Biol*, 1984, **99**: 1735–1742

Flewellen, E.H., Nelson, T.E., Jones, W.P., Arens, J.F. and Wagner, D.L. Dantrolene dose response in awake man: implications for management of malignant hyperthermia. *Anesthesiology*. 1983. **59**: 275–280

Fujii, J., Otsu, K., Zorzato, F., de Leon, S., Khanna, V.K., Weiler, J.E., O'Brien, P.J. and Maclennan, D.H. Identification of a mutation in porcine ryanodine receptor associated with malignant hyperthermia. *Science*. 1991 **253:** 488–551

Galli, L., Orrico, A., Cozzolino, S., Pietrini, V., Tegazzin, V. and Sorrentino, V. Mutations in the RYR1 gene in Italian patients at risk for malignant hyperthermia: evidence for a cluster of novel mutations in the C-terminal region. Cell Calcium. 2002. **32**: 143-51

Galli, L., Orrico, A., Lorenzini, S., Censini, S., Falciani, M., Covacci, A., Tegazzin, V. and Sorrentino, V. Frequency and localization of mutations in the 106 exons of the RYR1 gene in 50 individuals with malignant hyperthermia. *Hum Mutat.* 2006. **27**: 830

Garzón, J.I., Kovacs, J., Abagyan, R. and Chacón, P. ADP_EM: fast exhaustive multi-resolution docking for high-throughput coverage. *Bioinformatics*. 2007. **23**: 427–33

Girard, T., Johr, M., Schaefer, C. and Urwyler, A. Perinatal diagnosis of malignant hyperthermia susceptibility. *Anesthesiology*. 2006. **104**: 1353–4

Gordon, R.A. Malignant hyperpyrexia during general anaesthesia. *Can Anaesth Soc J.* 1996. **13**: 415–416

Groom, L., Muldoon, S.M., Tang, Z.Z., Brandom, B.W., Bayarsaikhan, M., Bina, S., Lee, H.S., Qiu, X., Sambuughin, N. and Dirksen, R.T. Identical de novo mutation in the type 1 ryanodine receptor gene associated with fatal, stress-induced malignant hyperthermia in two unrelated families. *Anesthesiology*. 2011. **115**: 938–45

Gurrola, G.B., Arevalo, C., Sreekumar, R., Lokuta, A.J., Walker, J.W. and Valdivia, H.H. Activation of ryanodine receptors by imperatoxin A and a peptide segment of the II-III loop of the dihydropyridine receptor. *J Biol Chem.* 1999. **274**: 7879–86

Hakamata, Y., Nakai, J., Takeshima, H. and Imoto, K. Primary structure and distribution of a novel ryanodine receptor/calcium release channel from rabbit brain. *FEBS Lett*, 1992, **312**: 229–235

Hamilton, S. L. and Serysheva, I. I. Ryanodine receptor structure: progress and challenges. *J. Biol. Chem.* 2009. **284**: 4047–51

Harrison, G.G. Control of malignant hyperpyrexia syndrome in MHS swine by dantrolene sodium. *Br J Anaesth*. 1975 **47**: 62–65

Hasdemir, C., Aydin, H.H., Sahin, S. and Wollnik, B. Catecholaminergic polymorphic ventricular tachycardia caused by a novel mutation in the cardiac ryanodine receptor. *Anadolu Kardiyol Derg.* 2008. **8**: E35-6.

Herbette, L., Messineo, F.C. and Katz, A.M. The interaction of drugs with the sarcoplasmic reticulum. *Annu. Rev. Pharmacol. Toxicol.* 1982. **22**: 413–434

Herrmann-Frank, A., Richter, M., Sarközi,, S., Mohr U. and Lehmann-Horn, F. 4-chloro-m-cresol, a potent and specific activator of the skeletal muscle ryanodine receptor. *Biochim. Biophys. Acta*. 1996. **1289**: 31–40

Huttlin, E.L., Jedrychowski, M.P., Elias, J.E., Goswami, T., Rad, R., Beausoleil, S.A., Villén, J., Haas, W., Sowa, M.E. and Gygi, S.P. A tissue-specific atlas of mouse protein phosphorylation and expression. *Cell*. 2010. **143**: 1174–89

Huxley, A.F. and Niedergerke, R. Structural Changes in Muscle During Contraction: Interference Microscopy of Living Muscle Fibres. *Nature.* 1954. **173**: 971–973

Huxley, H. and Hanson, J. Changes in the cross-striations of muscle during contraction and stretch and their structural interpretation. *Nature.* 1954. **173**: 973–976

Ikemoto, N., and Yamamoto, T. Regulation of calcium release by interdomain interaction within ryanodine receptors. *Front Biosci*. 2002. **7**: d671-683

Ikemoto, T., Iino, M. and Endo, M. Enhancing effect of calmodulin on Ca^{2+}-induced Ca^{2+} release in the sarcoplasmic reticulum of rabbit skeletal muscle fibres. *J Physiol*, 1995, **487**: 573–582

Jiang, D., Chen, W., Xiao, J., Wang, R., Kong, H., Jones, P.P., Zhang, L., Fruen, B. and Chen, S.R.W. Reduced threshold for luminal Ca2+ activation of RyR1 underlies a causal mechanism of porcine malignant hyperthermia. *J Biol Chem.* 2008. **283**: 20813-20

Jiang, D., Wang, R., Xiao, B., Kong, H., Hunt, D. J., Choi, P., Zhang, L., and Chen, S. R. W. *Circ. Res.* 2005. **97**: 1173–81

Jiang, D., Xiao, B., Yang, D., Wang, R., Choi, P., Zhang, L., Cheng, H., and Chen, S. R. W. *Proc Natl Acad Sci USA* .2004. **101**: 13062–7

Jungbluth, H., Müller, C.R., Halliger-Keller, B., Brockington, M., Brown, S.C., Feng, L., Chattopadhyay, A., Mercuri, E., Manzur, A.Y., Ferreiro, A., Laing, N.G., Davis, M.R., Roper, H.P., Dubowitz, V., Bydder, G., Sewry, C.A. and Muntoni, F. Autosomal recessive inheritance of RYR1 mutations in a congenital myopathy with cores. *Neurology.* 2002. 59:284–7

Jungbluth, H., Zhou, H., Hartley, L., Halliger-Keller, B., Messina, S., Longman, C., Brockington, M., Robb, SA, Straub, V., Voit, T. Swash, M., Ferreiro, A., Bydder, G., Sewry, C.A., Müller, C. and Muntoni F. Minicore myopathy with ophthalmoplegia caused by mutations in the ryanodine receptor type 1 gene. *Neurology.* 2005. **65**: 1930-5

Juranic, N., Macura, S., Simeonov, M.V., Jones, K.A., Penheiter, A.R., Hock, T.J. and Streiff, J.H. Halothane binds to druggable sites in calcium-calmodulin: Solution structure of halothane-CaM C-terminal domain. *To be published*. PDB ID: 2KUH

Juranic, N., Macura, S., Simeonov, M.V., Jones, K.A., Penheiter, A.R., Hock, T.J. and Streiff, J.H. Halothane binds to druggable sites in calcium-calmodulin: Solution structure of halothane-CaM N-terminal domain. *To be published*. PDB ID: 2KUG

Kabsch, W. Xds. *Acta Crystallogr*. *D Biol. Crystallogr*. 2010. **66**: 125-32

Kaftan, E., Marks, A.R. and Ehrlich, B.E. Effects of rapamycin on ryanodine receptor/Ca2+ release channels from cardiac muscle. *Circ. Res.* 1996. **78**: 990–7

Kazemian, P., Gollob, M.H., Pantano, A. and Oudit, G.Y. A novel mutation in the RYR2 gene leading to catecholaminergic polymorphic ventricular tachycardia and paroxysmal atrial fibrillation: dose-dependent arrhythmia-event suppression by β-blocker therapy. *Can J Cardiol.* 2011. **27**: 870.e7-10

Keating, K.E., Giblin, L., Lynch, P.J., Quane, K.A., Lehane, M., Heffron, J.J. and McCarthy, T.V. Detection of a novel mutation in the ryanodine receptor gene in an Irish malignant hyperthermia pedigree: correlation of the IVCT response with the affected and unaffected haplotypes. *J Med Genet.* 1997. **34**: 291-6

Kelley, L.A. and Sternberg, M.J.E. Protein structure prediction on the web: a case study using the Phyre serve. *Nature Protocols.* 2009. **4**: 363-71

Kim, D.H., Ohnishi, S.T. and Ikemoto, N. Kinetic studies of calcium release from sarcoplasmic reticulum in vitro. *J. Biol. Chem*. 1983. **258**: 9662–8

Kimlicka, L. and Van Petegem F. Ryanodine Receptor Mutation Database. Unpublished

Kimlicka, L. and Van Petegem, F. 2011. The structural biology of ryanodine receptors. *Sci China Life Sci.* **54**: 712–724

Kobayashi, S., Bannister, M.L., Gangopadhyay, J.P., Hamada, T., Parness, J. and Ikemoto, N. Dantrolene stabilizes domain interactions within the ryanodine receptor. *J Biol Chem.* 2005. **280**: 6580-7

Kohn, W.D., Mant, C.T. and Hodges, RS. Alpha-helical protein assembly motifs. *J Biol Chem.* 1997. **272**: 2583-6

Kolb, M.E., Horne, M.L. and Martz, R. Dantrolene in human malignant hyperthermia. *Anesthesiology*. 1982. **56**: 254–62

Kraeva, N., Riazi, S., Loke, J., Frodis, W., Crossan, M.L., Nolan, K., Kraev, A. and MacLennan, D.H. Ryanodine receptor type 1 gene mutations found in the Canadian malignant hyperthermia population. *Can J Anaesth.* 2011. **58**: 504-13

Kraus-Friedmann, N. and Feng, L. Reduction of ryanodine binding and cytosolic Ca2+ levels in liver by the immunosuppressant FK506. *Biochem. Pharmacol.* 1994. **48**: 2157–62

Krause, T., Gerbershagen, M.U., Fiege, M., Weishorn, R. and Wappler, F. Dantrolene – a review of its pharmacology, therapeutic use and new developments. *Anaesthesia*. 2004 **59**: 364–373

Kuntz, I.D., Blaney, J.M., Oatley, S.J., Langridge, R. and Ferrin, T.E. A geometric approach to macromolecule-ligand interactions. *J. Mol. Biol.* 1982 **161**: 269-88

Landschulz, W.H., Johnson, P.F. and McKnight, S.L. The leucine zipper: a hypothetical structure common to a new class of DNA binding proteins. *Science.* 1988. **240**: 1759-64

Laver, D.R., Baynes, T.M., Dulhunty, A.F. Magnesium inhibition of ryanodine-receptor calcium channels: evidence for two independent mechanisms. *J Membr Biol.* 1997. **156**: 213-29

Lebon, G., Warne, T., Edwards, P.C., Bennett, K., Langmead, C.J., Leslie, A.G. and Tate, C.G. Agonist-bound adenosine A2A receptor structures reveal common features of GPCR activation. *Nature*. 2011. **474**: 521-5

Lee, H., Kim, D.C., Lee, J.H., Cho, Y.G., Lee, H.S., Choi, S.I. and Kim, D.S. Molecular genetic analysis of the ryanodine receptor gene (RYR1) in Korean malignant hyperthermia families. *Korean J Lab Med.* 2010. **30**: 702-10

Levano, S., Vukcevic, M., Singer, M., Matter, A., Treves, S., Urwyler, A. and Girard, T. Increasing the number of diagnostic mutations in malignant hyperthermia. *Hum Mutat.* 2009. **30**: 590-8

Lin, C. C., Baek, K. and Lu, Z. Apo and InsP3-bound crystal structures of the ligand-binding domain of an InsP3 receptor. *Nat. Struct. Mol. Biol.* 2011. **18**: 1172–74

Liu, Z., Wang, R., Tian, X., Zhong, X., Gangopadhyay, J., Cole, R., Ikemoto, N., Chen, S. R., and Wagenknecht, T. Dynamic, inter-subunit interactions between the N-terminal and central mutation regions of cardiac ryanodine receptor. *J Cell Sci*. 2010. **123**: 1775-1784

Liu, Z., Zhang, J., Sharma, M.R., Li, P., Chen, S.R. and Wagenknecht, T. Three-dimensional reconstruction of the recombinant type 3 ryanodine receptor and localization of its amino terminus. *Proc. Natl Acad. Sci.* 2001, USA **98**: 6104–6109

Lobo, P.A. and Van Petegem, F. Crystal structures of the N-terminal domains of cardiac and skeletal muscle ryanodine receptors: insights into disease mutations. *Structure*. 2009, **17** 1505–1514

Lobo, P.A., Kimlicka, L., Tung, C.C., Van Petegem, F. The deletion of exon 3 in the cardiac ryanodine receptor is rescued by β-strand switching. *Structure.* 2011. **19**: 790–8

Loke, J. and MacLennan. D.H. Malignant hyperthermia and central core disease: disorders of Ca^{2+} release channels. *Am J Med.* 1998. **104**: 470–86

Loke, J.C., Kraev, N., Sharma, P., Du, G., Patel, L., Kraev, A. and MacLennan DH. Detection of a novel ryanodine receptor subtype 1 mutation (R328W) in a malignant

hyperthermia family by sequencing of a leukocyte transcript. *Anesthesiology.* 2003. **99**: 297-302

Ludtke S.J., Tran T.P., Ngo Q.T., Moiseenkova-Bell V.Y., Chiu W. and Serysheva I.I. Flexible architecture of IP3R1 by cryo-EM. *Structure.* 2011, **19**:1192–1199

Ludtke, S.J., Serysheva, I.I., Hamilton, S.L. and Chiu, W. The pore structure of the closed RyR1 channel. *Structure*, 2005, **13**: 1203–1211

Lukacs, C.M., Oikonomakos, N.G., Crowther, R.L., Hong, L.N., Kammlott, R.U., Levin, W., Li, S., Liu, C.M., Lucas-McGady, D., Pietranico, S. and Reik, L. The crystal structure of human muscle glycogen phosphorylase a with bound glucose and AMP: an intermediate conformation with T-state and R-state features. *Proteins.* 2006. **63**: 1123-6

Lupas, A. Coiled coils: new structures and new functions. *Trends Biochem Sci.* 1996. **21**: 375-82

Ma, J., Bhat, M.B., and Zhao, J. Rectification of skeletal muscle ryanodine receptor mediated by FK506 binding protein. *Biophys J*. 1995. **69**: 2398–2404

Mackey, M.D. and Melville, J.L. Better than random? The chemotype enrichment problem. *J Chem Inf Model.* 2009. **49**: 1154-62

Maclennan, D.H., Abu-Abed M., Kang C. Structure-function relationships in Ca^{2+} cycling proteins. *J Mol Cell Cardiol.* 2002. **34**: 897–918

Marx, S.O., Reiken, S., Hisamatsu, Y., Gaburjakova, M., Gaburjakova, J., Yang, Y.M., Rosemblit, N. and Marks, A.R. Phosphorylation-dependent regulation of ryanodine receptors: a novel role for leucine/isoleucine zippers. *J Cell Biol.* 2001. **153**: 699-708.

Marx, S.O., Reiken, S., Hisamatsu, Y., Jayaraman, T., Burkhoff, D., Rosemblit, N. and Marks, A.R. PKA phosphorylation dissociates FKBP12.6 from the calcium release

channel (Ryanodine receptor): defective regulation in failing hearts. *Cell.* 2000 **101** :365–76

Maximciuc, A.A., Putkey, J.A., Shamoo, Y. and MacKenzie, K.R. Complex of Calmodulin with a Ryanodine Receptor Target Reveals a Novel, Flexible Binding Mode. *Structure*. 2006. **14**: 1547–1556

Maxwell, J.T., Domeier, T.L. and Blatter, L.A. Dantrolene prevents arrhythmogenic Ca2+ release in heart failure. *Am J Physiol Heart Circ Physiol.* 2012. **302**: H953-63

Mayrleitner, M., Chandler, R., Schindler, H. and Fleischer S. Phosphorylation with protein kinases modulates calcium loading of terminal cisternae of sarcoplasmic reticulum from skeletal muscle. *Cell Calcium.* 1995. **18**: 197–206

McCarthy, T.V., Quane, K.A. and Lynch, P.J. Ryanodine receptor mutations in malignant hyperthermia and central core disease. *Hum Mutat.* 2000. **15**: 410–7

Medeiros-Domingo, A., Bhuiyan, Z.A., Tester, D.J., Hofman, N., Bikker, H., van Tintelen, J.P., Mannens M.M., Wilde, A.A. and Ackerman M.J. The RYR2-encoded ryanodine receptor/calcium release channel in patients diagnosed previously with either catecholaminergic polymorphic ventricular tachycardia or genotype negative, exercise-induced long QT syndrome: a comprehensive open reading frame mutational analysis. *J Am Coll Cardiol.* 2009. **54**: 2065-74

Meissner, G. Adenine nucleotide stimulation of Ca2+-induced Ca2+ release in sarcoplasmic reticulum. *J. Biol. Chem.* 1984. **259**: 2365–2374

Meissner, G. Ryanodine activation and inhibition of the Ca^{2+} release channel of sarcoplasmic reticulum. *J Biol Chem*. 1986. **261**: 6300–6306

Meissner, G., Darling, E. and Eveleth, J. Kinetics of rapid Ca^{2+} release by sarcoplasmic reticulum. Effects of Ca^{2+}, Mg^{2+}, and adenine nucleotides. *Biochemistry.* 1986. **25**: 236–244

Melzer, W., Herrmann-Frank, A. and Lüttgau, H.C. The role of Ca $^{2+}$ ions in excitation-contraction coupling of skeletal muscle fibres. *Biochim Biophys Acta*. 1995. **1241**: 59–116

Menegazzi, P., Larini, F., Treves, S., Guerrini, R., Quadroni, M. and Zorzato, F. Identification and characterization of three calmodulin binding sites of the skeletal muscle ryanodine receptor. Biochemistry. 1994. **33**: 9078–9084

Miledi, R., Parker, I. and Zhu, P.H. Extracellular ions and excitation-contraction coupling in frog twitch muscle fibres. *Journal of Physiology*, 1984. **351**: 687-710

Minor, W., Cymborowski, M., Otwinowski, Z. and Chruszcz, M. HKL-3000: the integration of data reduction and structure solution - from diffraction images to an initial model in minutes. *Acta Cryst*. 2006. **D62**: 859-66

Monnier, N., Kozak-Ribbens, G., Krivosic-Horber, R., Nivoche, Y., Qi, D., Kraev, N., Loke, J., Sharma, P., Tegazzin, V., Figarella-Branger, D., Roméro, N., Mezin, P., Bendahan, D., Payen J.F., Depret, T., Maclennan, D.H. and Lunardi, J. Correlations between genotype and pharmacological, histological, functional, and clinical phenotypes in malignant hyperthermia susceptibility. *Hum Mutat.* 2005. **26**:413-25

Monnier, N., Romero, N.B., Lerale, J., Landrieu, P., Nivoche, Y., Fardeau, M. and Lunardi, J. Familial and sporadic forms of central core disease are associated with mutations in the C-terminal domain of the skeletal muscle ryanodine receptor. *Hum Mol Genet.* 2001. **10**: 2581-92

Moore, C.P., Rodney, G., Zhang, J.Z., Santacruz-Tolozak, L., Strasburg, G. and Hamilton, S.L. Apocalmodulin and Ca^{2+} calmodulin bind to the same region on the skeletal muscle Ca^{2+} release channel. *Biochemistry.* 1999. **38**: 8532–8537

Morii, H. and Tonomura, Y. The gating behavior of a channel for Ca2+-induced Ca2+ release in fragmented sarcoplasmic reticulum. *J. Biochem*. 1983. **93**: 1271–1285

Morris, G. M., Huey, R., Lindstrom, W., Sanner, M. F., Belew, R. K., Goodsell, D. S. and Olson, A. J. AutoDock4 and AutoDockTools4: automated docking with selective receptor flexiblity. *J. Computational Chemistry*. 2009. **16**: 2785-91

Murshudov, G.N., Vagin, A.A. and Dodson, E.J., Refinement of macromolecular structures by the maximum-likelihood method. *Acta Crystallogr. D Biol. Crystallogr.* 1997. **53**: 240–55

Nagasaki, K. and Kasai, M. Fast release of calcium from sarcoplasmic reticulum vesicles monitored by chlortetracycline fluorescence. *J. Biochem.* **94**: 1101–1109

Nelson, T. E., Lin, M., Zapata-Sudo, G. and Sudo, R. T. Dantrolene sodium can increase or attenuate activity of skeletal muscle ryanodine receptor calcium release channel. *Anesthesiology.* 1996. **84**: 1368–79

Newton C.L., Mignery, G.A. and Südhof, T.C. Co-expression in vertebrate tissues and cell lines of multiple inositol 1,4,5-trisphosphate ($InsP_3$) receptors with distinct affinities for $InsP_3$. *J Biol Chem.* 1994. **269**: 28613-9

Nof, E., Belhassen, B., Arad, M., Bhuiyan, Z.A., Antzelevitch, C., Rosso, R., Fogelman, R., Luria, D., El-Ani, D., Mannens, M.M., Viskin, S., Eldar, M., Wilde, A.A. and Glikson, M. Postpacing abnormal repolarization in catecholaminergic polymorphic ventricular tachycardia associated with a mutation in the cardiac ryanodine receptor gene. *Heart Rhythm.* 2011. **8**: 1546-52

Oda, T., Yano, M., Yamamoto, T., Tokuhisa, T., Okuda, S., Doi, M., Ohkusa, T., Ikeda, Y., Kobayashi, S., Ikemoto, N., and Matsuzaki, M. Defective regulation of interdomain interactions within the ryanodine receptor plays a key role in the pathogenesis of heart failure. *Circulation*. 2005. **111**: 3400-3410

Ogawa Y., Harafuji H. Osmolarity-dependent characteristics of [3H]ryanodine binding to sarcoplasmic reticulum. *J. Biochem.* 1990. **107**: 894–898

Oikonomakos, N.G., Schnier, J.B., Zographos, S.E., Skamnaki, V.T., Tsitsanou, K.E. and Johnson, L.N. Flavopiridol inhibits glycogen phosphorylase by binding at the inhibitor site. *J Biol Chem.* 2000. **275**: 34566-73

Otsu, K., Willard, H.F., Khanna, V.K., Zorzato, F., Green, N.M. and MacLennan, D.H. Molecular cloning of cDNA encoding the Ca^{2+} release channel (ryanodine receptor) of rabbit cardiac muscle sarcoplasmic reticulum. *J Biol Chem*, 1990, **265**: 13472–13483

Palnitkar, S.S., Bin, B., Jimenez, L.S., Morimoto, H., Williams, P.G., Paul-Pletzer, K. and Parness, J. [3 H]Azidodantrolene: synthesis and use in identifi cation of a putative skeletal muscle dantrolene binding site in sarcoplasmic reticulum. *J Med Chem.* 1999. 42:1872–1880

Palnitkar, S.S., Mickelson, J.R., Louis, C.F. and Parness, J. Pharmacological distinction between dantrolene and ryanodine binding sites: evidence from normal and malignant hyperthermia-susceptible porcine skeletal muscle. *Biochem J.* 1997. **326**: 847-52

Pamukcoglu, T. Sudden death due to malignant hyperthermia. *Am J Forensic Med Pathol*. 1988. **9**: 161–162

Park, H., Park, I.Y., Kim, E., Youn, B., Fields, K., Dunker, A.K. and Kang, C. Comparing skeletal and cardiac calsequestrin structures and their calcium binding: a proposed mechanism for coupled calcium binding and protein polymerization. *J Biol Chem.* 2004. **279**: 18026-33

Parness, J. and Palnitkar, S.S. Identification of dantrolene binding sites in porcine skeletal muscle sarcoplasmic reticulum. *J Biol Chem.* 1995. **270**: 18465–18472

Paul-Pletzer, K., Palnitkar, S.S., Jimenez L.S., Morimoto H. and Parness, J. The skeletal muscle ryanodine receptor identified as a molecular target of [^{3}H]azidodantrolene by photoaffinity labeling *Biochemistry*. 2001. **40**: 531–542

Paul-Pletzer, K., Yamamoto, T., Bhat, M.B., Ma, J., Ikemoto, N., Jimenez, L.S., Morimoto, H., Williams, P.G. and Parness, J. Identification of a dantrolene-binding sequence on the skeletal muscle ryanodine receptor. *J Biol Chem*, 2002, **277**: 34918–34923

Paul-Pletzer, K., Yamamoto, T., Ikemoto, N., Jimenez, L.S., Morimoto, H., Williams, P.G., Ma, J. and Parness, J. Probing a putative dantrolene-binding site on the cardiac ryanodine receptor. *Biochem J*, 2005, **387**: 905–909

Pessah, I.N., Waterhouse, A.L. and Casida, J.E. The calcium-ryanodine receptor complex of skeletal and cardiac muscle. *Biochem. Biophys. Res. Commun*. 1985. **128**: 449–56

Pettersen, E.F., Goddard, T.D., Huang, C.C., Couch, G.S., Greenblatt, D.M., Meng, E.C. and Ferrin, T.E. UCSF Chimera - a visualization system for exploratory research and analysis. *J Comput Chem.* 2004. **25** :1605-12.

Postma, A.V., Denjoy, I., Kamblock, J., Alders, M., Lupoglazoff, JM, Vaksmann, G., Dubosq-Bidot, L., Sebillon, P., Mannens, M., Guicheney, P. and Wilde, A.A. Catecholaminergic polymorphic ventricular tachycardia: RYR2 mutations, bradycardia, and follow up of the patients. *J Med Genet.* 2005. 42: 863-70

Priori, S.G., Napolitano, C., Tiso, N., Memmi, M., Vignati, G., Bloise, R., Sorrentino, V. and Danieli, G.A. Mutations in the cardiac ryanodine receptor gene (hRyR2) underlie catecholaminergic polymorphic ventricular tachycardia. *Circulation.* 2001. **103**: 196-200

Quane, K.A., Healy, J.M., Keating, K.E., Manning, B.M., Couch, F.J., Palmucci, L.M., Doriguzzi, C., Fagerlund, T.H., Berg, K., Ording H., Bendixen, D., Mortier, W., Linz, U., Muller, C.R. and McCarthy, T.V. Mutations in the ryanodine receptor gene in central core disease and malignant hyperthermia. *Nat Genet.* 1993. **5**: 51–5

Quane, K.A., Keating, K.E., Healy, JM, Manning, B.M., Krivosic-Horber, R., Krivosic, I., Monnier, N., Lunardi, J. and McCarthy, T.V. Mutation screening of the RYR1 gene in

malignant hyperthermia: detection of a novel Tyr to Ser mutation in a pedigree with associated central cores. *Genomics.* 1994. **23**: 236-9

Rao, F.V., Andersen, O.A., Vora, K.A., Demartino, J.A. and Van Aalten, D.M.F. Methylxanthine drugs are chitinase inhibitors: investigation of inhibition and binding modes. *Chem Biol.* 2005. **12**: 973-80

Reiken, S., Lacampagne, A., Zhou, H., Kherani, A., Lehnart, S.E., Ward, C., Huang, F., Gaburjakova, M., Gaburjakova, J., Rosemblit, N., Warren, M.S., He, K-l., Yi, G-h., Wang, J., Burkhoff, D., Vassort, G. and Marks, A.R. PKA phosphorylation activates the calcium release channel (ryanodine receptor) in skeletal muscle: defective regulation in heart failure. *J Cell Biol.* 2003. **160** :919–28

Revel, J.P. The sarcoplasmic reticulum of the bat cricothroid muscle. *J Cell Biol*, 1962, **12**: 571–588

Rios, E. and Brum, G. Involvement of dihydropyridine receptors in excitation-contraction coupling in skeletal muscle. *Nature.*1987. **325**: 717–720

Robinson, R., Carpenter, D., Shaw, M.A., Halsall, J. and Hopkins, P. Mutations in RYR1 in malignant hyperthermia and central core disease. *Hum Mutat.* 2006. **27**: 977-89

Rodney, G.G,. Williams, B.Y., Strasburg, G.M., Beckingham, K. and Hamilton, S.L. Regulation of RYR1 activity by Ca^{2+} and calmodulin. *Biochem*. 2000. **39**: 7807–7812

Romero, N.B., Monnier, N., Viollet, L., Cortey, A., Chevallay, M., Leroy, J.P., Lunardi, J. and Fardeau, M. Dominant and recessive central core disease associated with RYR1 mutations and fetal akinesia. *Brain.* 2003. **126**: 2341-9

Rosenberg, H., Davis, M., James, D., Pollock, N. and Stowell, K. Malignant hyperthermia. *Orphanet J Rare Dis.* 2007. **2**: 21

Rousseau, E., Ladine, J., Liu, Q.Y. and Meissner, G. Activation of the Ca2+ release channel of skeletal muscle sarcoplasmic reticulum by caffeine and related compounds. *Arch. Biochem. Biophys.* 1988. **267**: 75–86

Saito, A., Inui, M., Radermacher, M., Frank, J. and Fleischer, S. Ultrastructure of the calcium release channel of sarcoplasmic reticulum. *J Cell Biol*, 1988, **107**: 211–219

Saito, A., Seiler, S., Chu, A. and Fleischer, S. Preparation and morphology of sarcoplasmic reticulum terminal cisternae from rabbit skeletal muscle. *J Cell Biol*. 1984, **99**: 875–885

Sambuughin, N., Holley, H., Muldoon, S., Brandom, B.W., de Bantel, A.M., Tobin, J.R., Nelson, T.E. and Goldfarb, L.G. Screening of the entire ryanodine receptor type 1 coding region for sequence variants associated with malignant hyperthermia susceptibility in the north american population. *Anesthesiology.* 2005. **102**: 515-21

Samsó, M. and Wagenknecht, T. Apocalmodulin and Ca^{2+}-Calmodulin Bind to Neighboring Locations on the Ryanodine Receptor. *J Biol Chem.* 2002 **277**: 1349–1353.

Samsó, M., Feng, W., Pessah, I.N. and Allen, P.D. Coordinated movement of cytoplasmic and transmembrane domains of RyR1 upon gating. *PLoS Biol*, 2009, **7**: e85

Samsó, M., Wagenknecht, T. and Allen P.D. Internal structure and visualization of transmembrane domains of the RyR1 calcium release channel by cryo-EM. *Nat Struct Mol Biol*, 2005, **12**: 539–544

Sandow, A. Excitation-contraction coupling in muscular response. *Yale J Biol Med*. 1952. **25**: 176-201

Seo, M.D., Velamakanni, S., Ishiyama, N., Stathopulos, P.B., Rossi, A.M., Khan, S.A., Dale, P., Li, C., Ames, J.B., Ikura, M., and Taylor, C.W. Structural and functional conservation of key domains in InsP3 and ryanodine receptors. *Nature.* 2012. **483**: 108–12

Serysheva, I.I., Bare, D.J., Ludtke, S.J., Kettlun, C.S., Chiu, W. and Mignery, G.A. Structure of the type 1 inositol 1, 4, 5-trisphosphate receptor revealed by electron cryomicroscopy. *J Biol Chem,* 2003. **24:** 21319-22

Serysheva, I.I., Hamilton, S.L., Chiu, W. and Ludtke, S.J., Structure of Ca^{2+} release channel at 14 Å resolution. *J Mol Biol.* 2005, **345**: 427-431

Serysheva, I.I., Ludtke, S.J., Baker, M.L., Cong, Y., Topf, M., Eramian, D., Sali, A., Hamilton, S.L. and Chiu, W. *Proc Natl Acad Sci USA*, 2008, **105**: 9610–9615

Serysheva, I.I., Orlova, E.V., Chiu, W., Sherman, M.B., Hamilton, S.L., and Van Heel, M. Electron cryomicroscopy and angular reconstitution used to visualize the skeletal muscle calcium release channel. *Nat Struct Biol*, 1995, **2**: 18–24

Sharma, P., Ishiyama, N., Nair, U., Li, W., Dong, A., Miyake, T., Wilson, A., Ryan, T., MacLennan, D.H., Kislinger, T., Ikura, M., Dhe-Paganon, S. and Gramolini, A.O. Structural determination of the phosphorylation domain of the ryanodine receptor. *FEBS J.* 2012, doi: 10.1111/j.1742-4658.2012.08755.x

Smith, J.S., Rousseau, E. and Meissner, G. Calmodulin modulation of single sarcoplasmic reticulum Ca-release channels from cardiac and skeletal muscle. *Circ Res.* 1989. **64**: 352–359

Snyder, H.R. Jr, Davis, C.S., Bickerton, R.K. and Halliday, R.P. 1-[(5-arylfurfurylidene) amino]-hydantoins. A new class of muscle relaxants. *J Med Chem.* 1967. **10**: 807–10

Sorrentino, V. and Volpe, P. Ryanodine receptors: How many, where and why? *Trends Pharmacol Sci*, 1993, **14**: 98–103

Stephenson, D.G., Lamb, G.D. and Stephenson, G.M. Events of the excitation-contractionrelaxation (E-C-R) cycle in fast- and slow-twitch mammalian muscle fi bres relevant to muscle fatigue. *Acta Physiol Scand.* 1998. **162** :229–245

Storoni, L.C., McCoy, A.J. and Read, R.J. Likelihood-enhanced fast rotation functions. *Acta Cryst*. 2004. **D60**: 432-8

Streiff, J.H., Juranic, N.O., Macura, S.I., Warner, D.O., Jones, K.A. and Perkins, WJ. Saturation transfer difference nuclear magnetic resonance spectroscopy as a method for screening proteins for anesthetic binding. *Mol Pharmacol*. 2004. **66**: 929-35

Sudo, R.T., Carmo, P.L., Trachez, M.M. and Zapata-Sudo, G. Effects of azumolene on normal and malignant hyperthermia-susceptible skeletal muscle. *Basic Clin Pharmacol Toxicol.* 2008. **102**: 308–16

Suko, J., Maurer-Fogy, I., Plank, B., Bertel, O., Wyskovsky, W., Hohenegger, M. and Hellmann, G. Phosphorylation of serine 2843 in ryanodine receptor-calcium release channel of skeletal muscle by cAMP-, cGMP- and CaM-dependent protein kinase. *Biochim. Biophys. Acta*. 1993. **1175**: 193–206

Szentesi, P., Collet, C., Sárközi, S., Szegedi, C., Jona, I., Jacquemond, V., Kovács, L. and Csernoch, L. Effects of dantrolene on steps of excitation-contraction coupling in mammalian skeletal muscle fibers. *J Gen Physiol.* 2001. **118**: 355-75

Takeshima, H., Nishimura, S., Matsumoto, T., Ishida, H., Kangawa, K., Minamino, N., Matsuo, H., Ueda, M., Hanaoka, M. and Hirose, T. Primary structure and expression from complementary DNA of skeletal muscle ryanodine receptor. *Nature,* 1989, **339**: 439–445

Tammaro, A., Bracco, A., Cozzolino, S., Esposito, M., Di Martino, A., Savoia, G., Zeuli, L., Piluso, G., Aurino, S. and Nigro, V. Scanning for mutations of the ryanodine receptor (RYR1) gene by denaturing HPLC: detection of three novel malignant hyperthermia alleles. *Clin Chem.* 2003. **49**: 761-8

Tanabe, T., Beam, K.G., Adams, B.A., Niidome, T. and Numa, S. Regions of the skeletal muscle dihydropyridine receptor critical for excitation-contraction coupling. *Nature*. 1990. **346**: 567–569

Tanabe, T., Beam, K.G., Powell, J.A. and Numa, S. Restoration of excitation-contraction coupling and slow calcium current in dysgenic muscle by dihydropyridine receptor complementary DNA. *Nature.* 1988. **336**: 134–139

Tester, D.J., Arya, P., Will, M., Haglund, C.M., Farley, A.L., Makielski, J.C. and Ackerman, M.J. Genotypic heterogeneity and phenotypic mimicry among unrelated patients referred for catecholaminergic polymorphic ventricular tachycardia genetic testing. *Heart Rhythm.* 2006. **3**: 800-5

Tester, D.J., Kopplin, L.J., Will, M.L. and Ackerman, M.J. Spectrum and prevalence of cardiac ryanodine receptor (RyR2) mutations in a cohort of unrelated patients referred explicitly for long QT syndrome genetic testing. *Heart Rhythm.* 2005. **2**: 1099-105

Tester, D.J., Spoon, D.B., Valdivia, H.H., Makielski, J.C. and Ackerman, M.J. Targeted mutational analysis of the RyR2-encoded cardiac ryanodine receptor in sudden unexplained death: a molecular autopsy of 49 medical examiner/coroner's cases. *Mayo Clin Proc.* 2004. **79**: 1380-4

Timerman, A.P., Onoue, H., Xin, H-B., Barg, S., Copello, J., Wiederrecht, G. and Fleischer, S. Selective Binding of FKBP12.6 by the Cardiac Ryanodine Receptor. *J Biol Chem.* 1996. **271**: 20385–20391

Tong, J., McCarthy, T.V. and MacLennan, D.H. Measurement of resting cytosolic Ca^{2+} concentrations and Ca^{2+} store size in HEK-293 cells transfected with malignant hyperthermia or central core disease mutant Ca^{2+} release channels. J Biol Chem. 1999. **274**: 693–702

Tripathy, A., Resch, W., Xu, L.E., Valdivia, H.H. and Meissner, G. Imperatoxin A induces subconductance states in Ca^{2+} release channels (ryanodine receptors) of cardiac and skeletal muscle. *J Gen Physiol.* 1998. **111**: 679–90

Tripathy, A., Xu, L., Mann, G. and Meissner, G. Calmodulin activation and inhibition of skeletal muscle Ca^{2+} release channel (ryanodine receptor). *Biophy J*. 1995. **69**: 106–119

Tung, C-C., Lobo, P.A., Kimlicka, L., Van Petegem, F. The amino-terminal disease hotspot of ryanodine receptors forms a cytoplasmic vestibule**.** *Nature*, 2010, **468**: 585–588

Van Petegem, F. Ryanodine receptors: structure and function. *J Biol Chem.* 2012. **287**: 31624-32.

Van Petegem, F., Clark, K.A., Chatelain, F.C. and Minor, D.L. Jr. Structure of a complex between a voltage-gated calcium channel beta-subunit and an alpha-subunit domain. *Nature*. 2004. **429**: 671–5

Van Winkle, W.B. Calcium release from skeletal muscle sarcoplasmic reticulum: site of action of dantrolene sodium? *Science.* 1976. **193**: 1130–1131

Wagenknecht, T., Berkowitz, J., Grassucci, R., Timerman, A.P. and Fleischer, S. Localization of calmodulin binding sites on the ryanodine receptor from skeletal muscle by electron microscopy. *Biophys J.* 1994. **67**: 2286–2295

Wagenknecht, T., Radermacher, M., Grassucci, R., Berkowitz, J., Xin, H-B. and Fleischer, S. Locations of Calmodulin and FK506-binding Protein on the Three-dimensional Architecture of the Skeletal Muscle Ryanodine Receptor. *J Biol Chem.* 1997. **272**: 32463–32471

Wang, J. and Best, PM. Inactivation of the sarcoplasmic reticulum calcium channel by protein kinase. *Nature*. 1992. **359**: 739–741

Wang, R., Chen, W., Cai, S., Zhang, J., Bolstad, J., Wagenknecht, T., Liu, Z. and Chen, S.R.W. Localization of an NH2-terminal disease-causing mutation hot spot to the 'clamp' region in the three-dimensional structure of the cardiac ryanodine receptor. *J. Biol. Chem.* 2007 **282**: 17785–17793

Wang, R., Zhong, X., Meng, X., Koop, A., Tian, X., Jones, P.P., Fruen, B.R., Wagenknecht, T., Liu, Z. and Chen, S.R.W. Localization of the dantrolene binding sequence near the FK506-binding protein-binding site in the three-dimensional structure of the ryanodine receptor. *J Biol Chem*, 2011, **286**: 12202–12212

Wehrens, X.H., Lehnart, S.E., Huang, F., Vest, J.A., Reiken, S.R., Mohler, P.J., Sun, J., Guatimosim, S., Song, L.S., Rosemblit, N., D'Armiento, J.M., Napolitano, C., Memmi, M., Priori, S.G., Lederer, W.J. and Marks, A.R. FKBP12.6 deficiency and defective calcium release channel (ryanodine receptor) function linked to exercise-induced sudden cardiac death. *Cell.* 2003. **113**: 829–40

Wilson, M.A. and Brunger, A.T. The 1.0 A crystal structure of Ca(2+)-bound calmodulin: an analysis of disorder and implications for functionally relevant plasticity. *J Mol Biol.* 2000 **301**: 1237-56

Wojcikiewicz, R.J. Type I, II, and III inositol 1,4,5-trisphosphate receptors are unequally susceptible to down-regulation and are expressed in markedly different proportions in different cell types. *J Biol Chem.* 1995 **270**: 11678–83

Wriggers, W. and Chacón, P. Modeling tricks and fitting techniques for multiresolution structures. *Structure.* 2001, **9**: 779–788

Wright, N.T., Prosser, B.L., Varney, K.M., Zimmer, D.B., Schneider, M.F. and Weber, D.J. S100A1 and calmodulin compete for the same binding site on ryanodine receptor. *J Biol Chem*, 2008, **283**: 26676–26683

Wu, S., Ibarra, M.C., Malicdan, M.C., Murayama, K., Ichihara, Y., Kikuchi, H., Nonaka, I., Noguchi, S., Hayashi, Y.K. and Nishino, I. Central core disease is due to RYR1 mutations in more than 90% of patients. *Brain.* 2006. **129**: 1470-80

Xiong, L., Zhang, J-Z., He, R., and Hamilton, S.L. A Ca^{2+}-Binding Domain in RyR1 that Interacts with the Calmodulin Binding Site and Modulates Channel Activity. *Biophys J.* **90**: 173-182

Yang, H.C., Reedy, M.M., Burke, C.L. and Strasburg, G.M. Calmodulin interaction with the skeletal muscle sarcoplasmic reticulum calcium channel protein. *Biochemistry*. 1994. **33**: 518–25

Yang, J., Gan, Z., Lou, Z., Tao, N., Mi, Q., Liang, L., Sun, Y., Guo, Y., Huang, X., Zou, C., Rao, Z., Meng, Z. and Zhang, K.Q. Crystal structure and mutagenesis analysis of chitinase CrChi1 from the nematophagous fungus Clonostachys rosea in complex with the inhibitor caffeine. *Microbiology.* 2010. **156**: 3566-74

Yeh, H.M., Tsai, M.C., Su, Y.N., Shen, R.C., Hwang, J.J., Sun, W.Z. and Lai, L.P. Denaturing high performance liquid chromatography screening of ryanodine receptor type 1 gene in patients with malignant hyperthermia in Taiwan and identification of a novel mutation (Y522C). *Anesth Analg.* 2005. **101**: 1401-6

Yoshikawa, F., Morita, M., Monkawa, T., Michikawa, T., Furuichi, T. and Mikoshiba, K. Mutational analysis of the ligand binding site of the inositol 1,4,5-trisphosphate receptor. *J. Biol. Chem.* 1996. 271: 18277–84

Yuchi, Z., Lau, K. and Van Petegem, F. Disease mutations in the ryanodine receptor central region: crystal structures of a phosphorylation hot spot domain. *Structure.* 2012, **20**: 1201-11

Zhang, Y., Chen, H.S., Khanna, V.K., De Leon, S., Phillips, M.S., Schappert, K., Britt, B.A., Browell, A.K. and MacLennan, D.H. A mutation in the human ryanodine receptor gene associated with central core disease. *Nat Genet.* 1993. **5**: 46–50

Zhao, F., Li, P., Chen, S. R., Louis, C. F., and Fruen, B. R. Dantrolene Inhibition of Ryanodine Receptor Ca^{2+}Release Channels – Molecular Mechanism and Isoform Selectivity. *J. Biol. Chem.* 2001. **276**: 13810–16

Zhou, Q., Wang, Q.L., Meng, X., Shu, Y., Jiang, T., Wagenknecht, T., Yin, C.C., Sui, S.F. and Liu, Z. Structural and functional characterization of ryanodine receptor-natrin toxin interaction. *Biophys J.* 2008. **95**: 4289–99

Zorzato, F., Fujii, J., Otsu, K., Phillips, M., Green, N.M., Lai, F.A., Meissner, G. and MacLennan, D.H. Molecular cloning of cDNA encoding human and rabbit forms of the Ca^{2+} release channel (ryanodine receptor) of skeletal muscle sarcoplasmic reticulum. *J Biol Chem*. 1990. **265**: 2244–56